Engineering a Repeats-in-Toxin Scaffold for Stimulus-Responsive Biotechnology Applications

Kevin P. Dooley

Submitted in partial fulfillment of the

requirements for the degree of

Doctor of Philosophy

in the Graduate School of Arts and Sciences

COLUMBIA UNIVERSITY

2014

Abstract

Engineering a Repeats-in-Toxin Scaffold for Stimulus-Responsive Biotechnology Applications

Kevin P. Dooley

Protein scaffolds are described as polypeptide frameworks with well-defined tertiary structures that are tolerable to mutagenesis or insertions. These scaffolds have gained significant interest from researchers and clinicians as they have challenged immunoglobulin domains as the preferred protein to address critical problems in biomedical engineering and biotechnology. While engineered antibodies and antibody fragments have been immensely successful, their complex structure, costly production and purification requirements, and large size preclude them from a host of applications. Small, stable proteins devoid of disulfide bond networks that express well recombinantly in prokaryotic systems offer viable alternatives to immunoglobulins.

Repeat proteins are characterized structurally by tandem repeats of a consensus motif. These proteins are used in nature to mediate a variety of protein-protein interactions and are appealing scaffolds to bioengineers because of their predictable secondary structures. Several repeat scaffolds have been identified and successfully engineered for *in vivo* imaging and therapeutic applications. We have identified the repeats-in-toxin (RTX) protein as a potential antibody mimetic and interesting scaffold for protein engineering studies. RTX domains are commonly associated with extracellular proteins secreted through the type 1 secretion system in Gram-negative bacteria. They are composed of tandem repeats of a nonamer calcium binding sequence capped by N and

C-termianl flanking regions. These proteins are conformationally dynamic and will fold from an intrinsically disordered state to a compact β-roll secondary structure in response to increasing calcium concentration. We aim to explore the RTX domain as an alternative protein scaffold and exploit the intrinsic conformational response to calcium as a mechanism to mediate molecular interactions.

In our first study, we rationally engineer the RTX domain as a calcium-responsive physical cross-linker for hydrogel formation. Protein based materials are favorable for many biomedical applications because of their biocompatibility, tunable mechanical properties, and predictable erosion rates. We have designed a hydrophobic interface on the surface of the RTX domain that is present only in the calcium-bound β-roll conformation. In the absence of calcium, the peptide returns to its disordered state, delocalizing the hydrophobic patch and in turn mitigating the driving force for self-assembly. We show that these mutant RTX domains, with the aid of additional protein cross-linkers, self-assemble into cross-linked macromolecular hydrogel networks, only in the presence of calcium.

To expand on this study, we further engineered the RTX domain to contain hydrophobic surfaces on both sides of the folded β-roll simultaneously. By doing this, we doubled the cross-linking capacity of the mutant RTX. This translates to a higher oligomerization state and lower protein concentration required for self-assembly. We also show the double mutant can function as a stand-alone cross-linking domain, eliminating the need for extraneous self-assembling proteins. This designed RTX mutant provides a new platform for stimulus-responsive cross-linking and self-assembly.

In our next line of work, we created several synthetic RTX peptides based on a consensus design approach. Such an approach relies on identifying the minimal requirements for a single repeating unit, and concatenating the unit to achieve a desired protein interface. We identified the consensus nonameric unit for the RTX domain and generated several constructs of varying lengths using this sequence. However, it was discovered that these designed RTX peptides undergo a reversible phase change in response to calcium. Rather than abandon these synthetic peptides, we looked to use them as calcium-responsive protein purification tags. By appending a consensus RTX domain to a protein of interest, we were able to rapidly and efficiently purify fusions out of cell lysate by precipitation cycling. We were also able to separate the tag from the protein of interest by including a protease recognition site between the two. This system offers an alternative to time consuming and expensive chromatographic techniques for recombinant protein purification.

In our final study, we evaluated the RTX domain as a scaffold for evolving molecular recognition. We planned to use the calcium-responsive structural rearrangement as a switch to turn an evolved binding interface "on" and "off". One face of the folded β-roll structure was randomized on the genetic level and the resultant protein constructs were selected against a target protein using ribosome display technology. A consensus binding sequence emerged after several rounds of biopanning and was thoroughly characterized. The evolved β-roll bound the target protein with low micromolar affinity. Although this weak attraction was not suitable for efficiently capturing the target protein in a packed column application, this work provides a platform for evolving the RTX protein for molecular recognition. Several strategies are discussed to achieve

higher affinity binders.

Overall, this dissertation explores the RTX domain as an alternative stimulus-responsive scaffold for use in a variety of biotechnology applications. We have successfully developed new protein based platforms based on rationally designed or combinatorailly selected RTX proteins for calcium-responsive biomaterials, non-chromatographic protein purification, and calcium-dependent molecular recognition.

Contents

List of Figures

List of Tables

Acknowledgements

I'd like to take this opportunity to thank those whose help and support have made this work possible. First, I'd like to thank my advisor and mentor for the last 5 years, Dr. Scott Banta. Your patience, timely advice and steadfast optimism have made this process a rewarding and enjoyable one despite your contempt for the New York Yankees.

Thank you to my committee members Drs. Alan West, Vanessa Ortiz, Raymond Tu, and Lance Kam. I appreciate you all taking the time out of your schedules to serve on my committee. I'd like to thank you in advance for your mercy.

To all the members of the Banta Lab, past and present, I'd like to thank you all for your engaging scientific discussions and companionship. I would like to thank Drs. Asli Sahin, Elliot Campbell and Oren Shur for your mentorship and guidance while I was getting acclimated to graduate school and life in the lab. I would particularly like to thank my beer pong partner Dr. Tushar Patel for helping me maintain my sanity and keeping me up to date on all things Fantasy Football. Thank you as well to my army of undergraduate researchers for making my life easier, especially Raymond Bellon, Joohee Jung, and Victoria Sun.

Thank you to my girlfriend Kristen for reminding me there is more to life than toiling away in the lab.

And finally, thank you to my parents, Jack and Carol, and my siblings, Mike and

Lauren, for your love and support during my time here. I couldn't have made it this far without you. You guys are awesome.

Chapter 1

Introduction

Excerpts from this chapter have been previously published as, "Replacing Antibodies: Engineering New Binding Proteins" with coauthors Kevin Dooley, Oren Shur & Scott Banta appearing in Annual Review of Biomedical Engineering, volume 15, pages 93-113.

1.1 Protein Engineering

Naturally evolved proteins composed of the twenty common amino acids are responsible for enabling the cellular processes which make life possible. Their staggering array of functions includes molecular transport, signaling, ligand recognition, catalysis, and self-assembly. The multitude and specificity of these interactions is attributed to intricate three dimensional folding and diverse structural architectures of protein domains. Secondary and tertiary structural motifs fold in such ways to create binding pockets, catalytic active sites, and charged surfaces that are central to protein function.

The inherent relationship between sequence, structure, and function is at the heart of protein engineering. Classically, the field has been applied on two main fronts. First, to identify residues involved with a protein's catalytic activity, thermostability, binding capacity, or other property of interest [21, 106, 117]. By mutating positions on the DNA level thought to be important for these properties and evaluating the resultant protein construct, critical residues and interactions can be identified. Secondly, and more interestingly, protein engineers have applied these same principles in hopes of generating mutant proteins with enhanced or entirely novel functions. The field has flourished with the advent of combinatorial biochemistry, high-throughput screening, and advances in genomic/proteomic technologies. The expanding protein engineering toolbox allows for the efficient and precise manipulation of natural or synthetic DNA. And further, mutant

DNA libraries with diversities of ~10^{12} variants are routinely prepared using degenerate codons and oligonucleotides. Coupling this with prokaryotic expression in *Escherichia coli* or other systems has led to cost-effective production of folded, functional protein libraries containing previously unexplored molecules.

Over the last few decades, protein engineering has garnered much interest in the biomedical and biotechnology arenas. There is a constant demand for new protein-based tools for therapeutics, *in vivo* imaging, drug delivery, clinical diagnostics, and bioseparations. Engineers rely on naturally occurring protein domains, or scaffolds, as starting points to create new, functional proteins for these applications. The term scaffold has been used to describe polypeptide frameworks with well-defined secondary and tertiary structures that are amenable to mutations or insertions. Sufficient space must be available in the scaffold to introduce mutations without compromising the stability of the three-dimensional protein structure, similar to the hypervariable complementarity determining regions (CDR) in antibodies. These peptide loops contain the highest density of diversity, both structurally and sequentially, and generally do not interfere with the folding of the antibody structure.

Antibodies are undoubtedly the most successfully engineered class of proteins in the last 20 years. In 2010, the 25 actively marketed FDA approved monoclonal antibodies generated $43 billion USD in sales [42]. Since the immune system of higher organisms is nature's paradigm for selecting highly specific binding proteins, immunoglobulin domains were a logical choice to begin engineering efforts. Antibodies have been shown to bind a diverse repertoire of targets, from large, multi-domain proteins to small molecules. However several limitations make antibodies an impractical solution

to many biomedical problems.

The most common problem associated with antibodies is their large, complex assemblies. They are 150 kDa multi-domain glycoproteins that are structurally reliant on disulfide bridges, which cannot form in the reducing cytosol of microbial hosts. Consequently, expression must be directed to the periplasmic space of prokaryotes, which leads to poor yield. Mammalian cell cultures are also commonly used, but are mired with time consuming and costly production requirements. More recently, recombinantly expressed antibody fragments have been successfully engineered to bind a multitude of targets [60]. Although smaller in size, antibody fragments can still suffer from some of the same limitations as full-length immunoglobulin (Ig) domains. As such, small, thermostable, single-domain proteins devoid of disulfide bonds and glycosylation are attractive alternatives. They should be able to express and fold rapidly in the cytoplasm of bacterial systems while avoiding aggregation and proteolytic cleavage. Low molecular weight proteins are also more manageable in terms of display technologies for directed evolution experiments. Several protein scaffolds that meet these criteria have been identified, allowing for researchers to choose an appropriate framework for their engineering interests. These scaffolds have been reviewed in detail [11, 17, 51, 58, 75, 88, 107].

1.2 Repeat Protein Scaffolds

Nature frequently uses repeating structural motifs to mediate a host of protein-protein interactions. In fact, the immune systems of jawless invertebrates rely on leucine-rich repeat (LRR) domains as opposed to Ig-based proteins for immunological response

[2,3,33,66,89,90]. The crystal structure for one such domain is provided in Figure 1.1a. Because these repeat proteins are naturally involved with selection of high affinity variants in some organisms, they are thought to be suitable scaffolds for engineering applications. Repeat proteins are modular domains that consist of tandem repeats of a 10-50 amino acid sequence. The modularity allows for concatenation of the repeating building block, which translates to a tunable surface for engineering purposes. Synthetic constructs can also be generated through consensus design. This allows for uniformity across the designed protein, making it easier to add, delete or alter repeats and can also result in increased stability and expression levels, all of which are desired traits for protein scaffolds [20]. Consensus designs for leucine-rich repeats, tetratricopepties, and HEAT repeat proteins have all been reported [78, 109, 118].

Another interesting modular scaffold is the ankyrin repeat (AR) protein, shown in Figure 1.1b. Ubiquitous in nature, they are responsible for mediating a broad range of protein interactions and have been reported in cytosolic, membrane-bound, and secreted forms [67]. Structurally, they are comprised of a β-turn followed by 2 anti-parallel α-helices and an unstructured loop, leading into the next repeat unit [67]. They express well in microbial hosts, and have a high degree of solubility and stability. Functionally designed ankyrin repeat proteins (DARPins) selected from consensus combinatorial libraries have been shown to bind to a variety of targets with picomolar affinity, including kinases and membrane receptors associated with malignant tissue [5, 6, 38, 131].

Elastin-like peptides (ELP) are repetitive, artificial polypeptides modeled after the recurring primary sequence of the hydrophobic domain in tropoelastin [77]. While ELPs are not technically a repeat protein scaffold per se, their successful implemen-

tation into several biomedical systems makes them worth mentioning in this section. They are composed of repeating blocks of the peptide motif $(VPGXG)_n$ where X is the guest residue (any amino acid besides proline) and n is the number of repeating units. These pentapeptide repeats exhibit a reversible inverse temperature transition resulting in the formation of an insoluble coacervate phase at temperatures above their transition temperature. This phase transition has been exploited for a variety of interesting applications in biomaterials development, targeted drug delivery, and wound healing strategies. By fusing hydrophilic and hydrophobic ELP blocks together, Chilkoti and coworkers have developed thermally triggered self-assembling spherical micelles [37,55]. These micelles have been conjugated with targeting peptides and small molecule anticancer drugs for therapeutic treatment strategies [15, 27, 36]. Koria et al. have used these particles as vehicles to deliver bioactive proteins to highly proteolytic epidermal wound sites thereby enhancing the wound-healing cascade in diabetic mouse models [69]. ELP domains have also been used as protein purification tags for efficient separation of recombinantly expressed proteins from host cell proteins [54]. The inverse temperature transition is used to specifically precipitate ELP fusions from cell lysate resulting in pure protein of interest. The ELP response to an external stimulus provides a layer of control over the engineered system, which can prove advantageous for many applications.

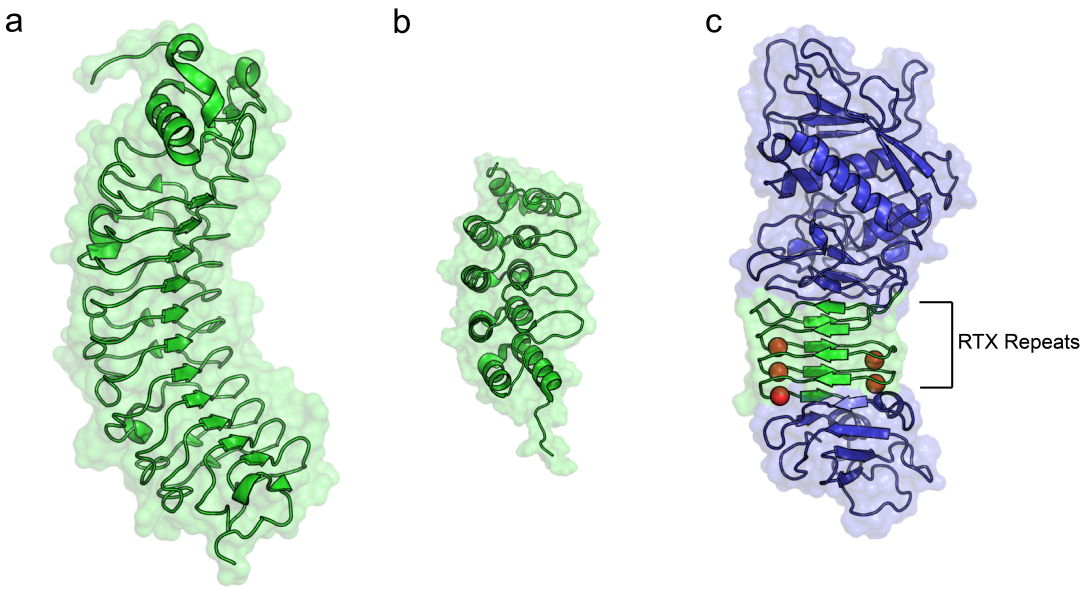

Figure 1.1: Repeat scaffolds. Panel (a) depicts a leucine rich repeat (LRR) protein with an elongated stretch of β-sheet rich repeats responsible for complexing with antigens (PDB 3ZYN). Panel (b) shows a designed ankyrin repeat protein (DARPin) (PDB 4DUI). The projecting loops and α-helical repeating units have been evolved to bind a variety of targets. A metallo protease from *S. marcescens* (PDB 1SAT) in panel (c) shows the repeats-in-toxin motif in green. Note the similarites in structure between the folded RTX domain and the LLR binding interface.

1.3 The Repeats-in-Toxin (RTX) Domain

There are a number desirable traits for a potential protein scaffold depending on the engineering goals, some of which have been outlined above. One such protein backbone that meets several of these criteria is the repeats-in-toxin (RTX) domain. RTX domains

are typically found at the C-terminus of virulence factors and extracellular lipases or proteases secreted by Gram-negative bacteria through a designated type 1 secretion system (T1SS) [13]. The T1SS forms channels spanning the entire cellular envelope, bypassing the periplasmic space, composed of three separate domains: (i) an inner membrane domain operating as an ATP binding cassette exporter, (ii) a membrane fusion protein, and (iii) an outer membrane protein [25, 73]. A C-terminal secretion signal is recognized by this complex, and proteins are exported from the cytosol directly to the extracellular space.

RTX domains are structurally composed of a repeating nonamer calcium binding sequence of the prototype GGXGXDXUX where X can represent any amino acid and U represents an aliphatic residue, most commonly leucine [13]. These repeats are typically found in successive blocks (5-10 repeats per block) separated by flanking regions (20-50 residues). The repeating glycine/aspartate-rich motif reversibly binds calcium, which was found to be essential for protein function. At cytosolic calcium concentrations (sub-millimolar), the RTX domains behave as intrinsically disordered peptides, evidenced by extended hydrodynamic radii and the absence of hydrophobic clustering [25]. Upon secretion to the extracellular milieu, higher calcium concentrations induce RTX folding into a compact, stable, β-rich structure. Crystallographic studies on a metallo protease from *S. marcescens* (PDB 1SAT) have determined RTX domains fold into a parallel β-helix or β-roll structure, shown in Figure 1.1c. The first six residues in the canonical repeating unit (GGXGXD) compose flexible turning regions responsible for coordinating calcium ions while the last three residues (XUX) create short β-strands. Two repeating units create one full turn of the corkscrew-like structure.

Perhaps the most thoroughly investigated RTX domain has been isolated from the secreted adenylate cyclase toxin (CyaA) from *Bordetella Pertussis*, the causative agent of whooping cough [13, 25, 26, 92, 108]. CyaA is composed of an N-terminal catalytic domain and a C-terminal hemolytic domain, largely made up of RTX repeats (Figure 1.2). Interestingly, the block V cluster of glycine/aspartate-rich repeats along with its N and C-terminal flanking regions has been shown to fold autonomously, retaining the intrinsic calcium-induced structural rearrangement when isolated from the full length RTX domain [13]. The block V RTX protein is an interesting platform for engineering experiments as it is a relatively small (20 kDa), cysteine-free, modular protein that offers a unique calcium-dependent switching mechanism from an intrinsically disordered state to a compact, stable β-roll structure.

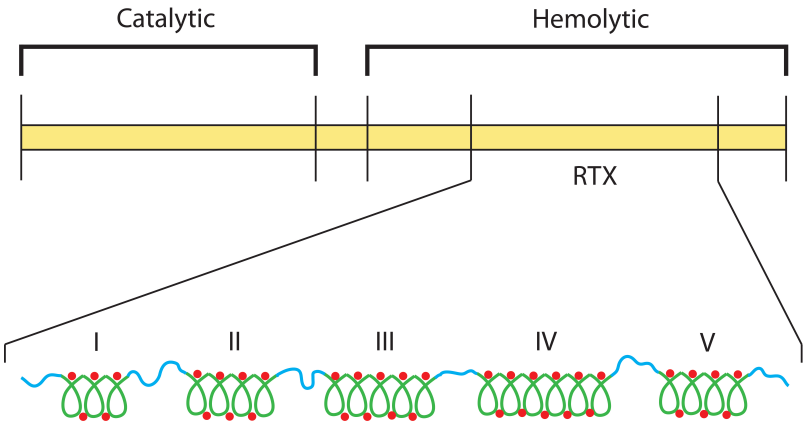

Block V

GSARD**D**VLI
GDAGANVLN
GLAGN**D**VLS
GGAGD**D**VLL
GDEGS**D**LLS
GDAGN**D**DLF
GGQGD**D**TYLFG *
VGYGH**D**TIYE *
SGGGH**D**TIR *

Figure 1.2: Adenylate cyclase toxin schematic. The adenylate cyclase toxin is composed of a C-terminal catalytic domain and an N-terminal hemolytic domain. The RTX portion of the hemolytic domain is highlighted and the primary sequence for the block V repeats is given on the right. The starred repeats represent non-native RTX repeats.

1.4 Characterizing the RTX Domain

Prior to designing functional β-roll domains for biotechnology applications, the isolated protein needed to be extensively characterized. Several properties pertaining to calcium responsiveness, surface immobilization, and modularity were investigated. First, the role of the N and C-terminal flanking regions were studied and the minimal requirements for calcium-induced folding were elucidated. Blenner and coworkers created a series of block V RTX constructs with incremental truncations to either the N or C-terminal flanking region [19]. It was discovered that only the C-terminal cap was required to achieve protein folding in the presence of calcium. Truncation of this C-terminal capping region resulted in marked losses in calcium responsiveness, whereas no significant loss was observed with the complete removal of the N-terminal flanking region. Also, the naturally occurring C-terminal flank could be replaced with globular proteins (MBP & YFP) while sustaining no loss in calcium-induced RTX folding. These results suggest that calcium-responsive folding is an intrinsic property of the glycine/aspartate-rich repeats, and a C-terminal cap is required for entropic stabilization.

The conformational behavior of the block V RTX protein was further characterized by Szilvay et al. using an *in vitro* FRET-based method [111]. Optically active proteins CFP and YFP were grafted onto the N and C-terminus of the RTX domain, respectively, replacing the native flanking groups. Addition of calcium ions to these chimeras caused an increase in FRET efficiency that was attributed to changes in the end-to-end distance of the RTX domain, indirectly reporting RTX folding. Again, it was shown that globular proteins can serve as suitable capping groups, suggesting that the native flanking regions do not play a specific role in β-roll formation.

Since the RTX domain is a repeating protein, it is important to understand its sequence modularity and concatenation tolerance in order to efficiently tune the scaffold depending on the engineering application. Shur & Banta created a set of block V RTX-based peptides ranging in size from 5 to 17 repeats in length, with and without the native C-terminal cap [104]. Additionally, the ordering of non-standard RTX repeats (*'d in Figure 1.2), typically located near the C-terminus, was examined by modifying their position in the RTX sequence. As expected, all uncapped constructs were non-responsive to calcium. Moving the non-standard repeats away from the C-terminus resulted in drastic losses in calcium affinity and cooperativity, suggesting the non-natively ordered constructs fold along an alternative pathway. However, all naturally ordered, C-terminally capped constructs folded in a similar fashion as the wild-type protein indicating the RTX domain is tolerant to concatenation. This offers a tunable β-sheet interface for a variety of engineering applications.

Lastly, immobilization of the block V RTX domain on a solid surface was investigated and the subsequent calcium binding properties were elucidated [105]. Cysteine modified RTX constructs were immobilized on gold plated quartz crystals for analysis by quartz crystal microbalance (QCM). This sensitive instrument can detect small perturbations in mass loading and has been used to analyze biomolecular interactions and conformational changes [30, 124, 125]. Shur et al. demonstrated that a solid surface can entropically stabilize uncapped RTX domains in a similar fashion as the globular proteins discussed previously, with minimal effects on calcium affinity or cooperativity. The retention of calcium-induced protein folding while immobilized on a solid surface opens the door for a host of applications, particularly in biosensor development and

smart protein purification.

1.5 Engineering the RTX Domain

Although much work has been devoted to identifying and characterizing RTX domains, few attempts have been made at engineering them for specific purposes. Lilie et al. constructed synthetic RTX domains based on a consensus sequence. However, a molecular crowding agent in addition to 100 mM calcium were required to induce calcium-responsive folding [72]. Scotter et al. demonstrated the ability of a minimally designed RTX domain to form non-amyloid-like filaments in the presence of lanthanum ions (not calcium). Filament formation was reversible using a chelating agent [101]. While these findings are scientifically interesting, no practical applications of the peptides were discussed.

In this work, we aim to explore the RTX domain as an alternative protein scaffold for use in biotechnology and biomedical systems including biomaterials development, engineered molecular recognition, and non-chromatographic bioseparations. The intrinsic calcium-induced structural rearrangement will be exploited as a peptide switching mechanism to mediate different protein-protein interactions. The residues composing the short β-strand faces will be evaluated for mutation tolerance. We hypothesize that these residues can be readily mutated because (i) crystallographically, the side chains of the residues in the 7th and 9th positions of the RTX motif project radially into the solvent and do not play an integral role in β-roll stabilization, and (ii) these positions are highly variable in naturally occurring RTX domains. This will open the door to

protein engineering techniques including rational design and directed evolution to generate mutant RTX domains with entirely novel functions. Consensus design will also be evaluated as a viable engineering strategy for RTX repeats. The specific goals of this thesis work are outlined below.

1. **Engineer the RTX domain as a calcium-responsive cross-linking domain for proteinaceous hydrogel formation.** Chapter 2 discusses the rational engineering of the RTX domain to create a leucine-rich face in the calcium-bound conformation capable of self-assembling. The RTX calcium responsiveness is used as a switch to modulate self-assembly. The resultant protein-based hydrogels are thoroughly characterized by microrheology to elucidate the mechanical properties of these new materials. Chapter 3 expands on this initial work by doubling the cross-linking potential of the leucine-rich RTX mutants. By creating cross-linking interfaces on both sides of the folded β-roll simultaneously, a higher association number can be achieved. This translates to lower protein concentrations required for self-assembly and allows the RTX domain to function as a stand-alone cross-linking domain, circumventing the need for additional cross-linking moieties.

2. **Evaluate a consensus designed RTX domain as a non-chromatographic protein purification tag.** Chapter 4 discusses the engineering of a consensus designed RTX domain. Interestingly, we found that our consensus protein undergoes a reversible phase transition in response to calcium. We have exploited this triggered precipitation mechanism to efficiently separate recombinantly expressed proteins from host cell contamination. We further engineered this system to separate the RTX tag from the expressed protein resulting in isolated, highly purified

protein of interest.

3. **Engineer the RTX domain as an allosterically regulated molecular recognition element.** In Chapter 5, we use directed evolution to select for RTX molecular recognition against a target protein, lysozyme. A library of RTX mutants is assembled and selected for via an optimized ribosome display method. Binding affinity, thermodynamics, and allosteric regulation are extensively characterized using biophysical techniques including isothermal titration calorimetry.

Chapter 2

Rational Engineering of an RTX Domain for Calcium-Responsive Self-Assembly

Project Collaborators: Kevin Dooley, Yang Hee Kim, Hoang Liu, Raymond Tu, & Scott Banta

A version of this chapter entitled, "Engineering of an Environmentally Responsive Beta Roll Peptide for Use as a Calcium-Dependent Cross-Linking Domain for Peptide Hydrogel Formation" appeared in Biomacromolecules volume 13, issue 6, pages 1758-17. KD prepared DNA constructs, expressed and purified all proteins, performed all CD, FRET, bis-ANS fluorescence spectroscopy, microrheology experiments and analysis.

2.1 Abstract

We have created a set of rationally designed peptides that form calcium-dependent hydrogels based on the beta roll (β-roll) peptide domain. In the absence of calcium, the β-roll domain is intrinsically disordered. Upon addition of calcium, the peptide forms a β-helix secondary structure. We have designed two variations of our β-roll domain. First, we have mutated one face of the β-roll domain to contain leucine residues, so that the calcium-dependent structural formation leads to dimerization through hydrophobic interactions. Second, an α-helical leucine zipper domain was appended to the engineered β-roll domain as an additional means of forming intermolecular cross-links. This full peptide construct forms a hydrogel only in calcium-rich environments. The resulting structural and mechanical properties of the supramolecular assemblies were compared to the wild type domain using several biophysical techniques including circular dichroism, FRET, bis-ANS binding and microrheology. The calcium responsiveness and rheological properties of the leucine β-roll containing construct confirm the potential of this allosterically-regulated scaffold to serve as a cross-linking domain for

stimulus-responsive biomaterials development.

2.2 Introduction

The development of smart materials and hydrogels has opened to the door to a host of potential applications in such fields as drug delivery, tissue engineering and microfluidics [28,41,43,57,68,71,87,96]. Hydrogels are composed of water-soluble monomers that are physically or covalently cross-linked to form three dimensional polymer networks. This cross-linking can often be controlled by the incorporation of stimulus-responsive proteins or peptides into the monomeric building block. Stimuli such as pH, temperature, or ionic strength can be used to regulate the assembly of hydrogel networks. Several examples of protein domains that facilitate environmentally responsive gelation have been described, including elastin-like peptides, calmodulin, and α-helical leucine zipper domains [12, 41, 115].

Alpha-helical leucine zippers are a common structural motif found in DNA binding proteins. The name is derived from the periodic repeat of leucine residues that protrude outward and align along a side of the helix creating a hydrophobic driving force to form "zipped" coiled-coil bundles. These domains have been extensively characterized and have proven useful in developing stimulus-responsive hydrogels as they assemble and dissociate in response to changes in temperature and pH [64, 128]. Previously, we have appended these domains to enzymes and other globular proteins to create bi-functionalized hydrogel constructs [76, 120, 121].

In this work, we present a new domain suitable for creating physical cross-links

and a hydrogel network. We used a β-roll peptide scaffold taken from the block V repeats-in-toxin (RTX) domain of adenylate cyclase from *Bordetella pertussis*. The β-roll motif is a modular repeated sequence that has been shown to be intrinsically disordered in the absence of calcium [13,25]. In calcium-rich environments, the peptide forms a β-helix consisting of two short parallel β-sheet faces separated by turns. A highly conserved aspartic acid residue in each turn is responsible for calcium binding [8]. A C-terminal capping group responsible for entropic stabilization is required for conformational response to calcium. We have previously characterized the calcium responsiveness and capping requirements of the native β-roll domain [19,105,111]. Each β-strand in the folded β-roll domain contains two amino acids that protrude radially from the scaffold and are exposed to the solvent. We hypothesize that mutating the protruding residues on one face to leucine side chains will create a hydrophobic surface suitable for cross-linking in response to calcium binding (Figure 2.1).

Thus, we have rationally designed an allosterically-regulated β-roll motif that should form calcium-dependent cross-links suitable for hydrogel formation. Hydrogel networks modulated by calcium-induced conformational change differ from conventional approaches that rely heavily on pH and temperature swings to destabilize intermolecular cross-links. Allosteric regulation allows for the precise tuning of gel formation and strength by simply adjusting the calcium concentration, making these gels suitable for applications in systems that do not permit fluctuations in temperature or pH.

In order to assemble a macromolecular hydrogel network, we have fused an α-helical leucine zipper domain (H) to the N-terminus of the leucine β-roll (Leuβ) through a soluble linker region (S). Both the H and S domains have been previously character-

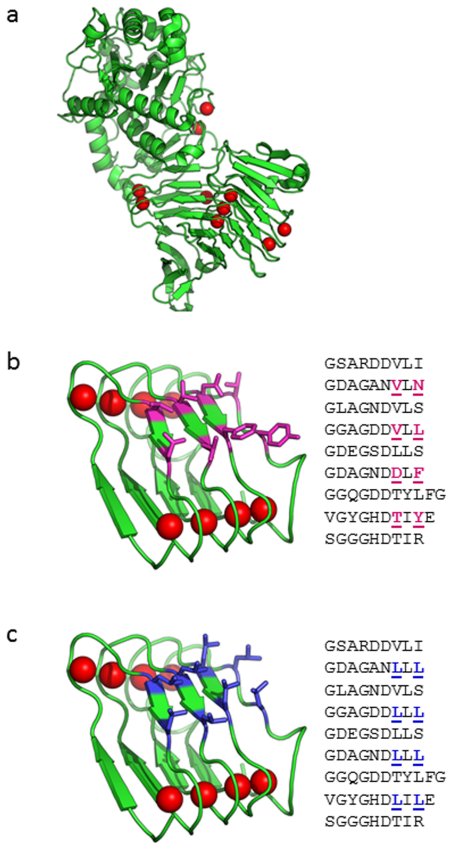

Figure 2.1: β-roll structures. (a) Crystal structure of an extracellular lipase from *Pseudomonas sp.* MIS38 (PDB 2Z8X) containing a β-roll domain. The folded β-roll domain can be seen in the lower right with the bound calcium ions in red. The structure of this folded β-roll was used as a template to model the block V β-roll domain of adenylate cyclase from *B. pertussis*. Homology models were generated using SWISS-MODEL which are shown in (b) and (c) (Swiss Institute of Bioinformatics). The positions of the bound calcium ions were approximated manually. (b) Model of the WT adenylate cyclase β-roll peptide used in this work along with its primary sequence. The surface exposed residues in the folded conformation are highlighted in magenta with the residues underlined in the sequence. Calcium ions are shown in red. (c) Model of the mutant leucine β-roll engineered in this work along with its primary sequence. The leucine mutations to the WT β-roll are shown in blue and underlined in the sequence.

ized [102, 103, 128]. In the absence of calcium, the β-roll should remain disordered while the leucine zippers can form tetrameric coiled-coil bundles. The lack of interaction between the disordered β-roll domains should prohibit the formation of a hydrogel. Upon addition of calcium, the β-roll should undergo a conformational change forming the leucine-rich face. The hypothesized cross-linking between β-roll domains along with the formation of the leucine zipper bundles should provide the physical interactions necessary to form a hydrogel (Figure 2.2). Gel formation and strength will be modulated using the calcium-dependent allosteric control that is intrinsic to the peptide sequence. Through circular dichroism (CD) spectroscopy, bis-ANS binding, and terbium binding, we show that the leucine mutations have minimal effect on the response of the peptide to calcium. After appending the H and S domains to the wild type (WTβ) and engineered leucine β-roll (forming HS-WTβ and HS-Leuβ respectively), rheological analysis confirms the hydrogel formation is a result of the leucine mutations as the HS-WTβ does not self-assemble in calcium-rich environments.

2.3 Materials & Methods

2.3.1 Materials

The maltose binding protein (MBP) expression kit and all enzymes were purchased from New England Biolabs (Ipswich, MA). Isopropyl β-D-1-thiogalactopyranoside (IPTG) was obtained from Promega (Madison, WI). HaltTM protease inhibitor cocktail was purchased from Fisher Scientific (Waltham, MA). Amicon centrifugal filters were purchased from Millipore (Billerica, MA). Native PAGE gels, running buffer, protein lad-

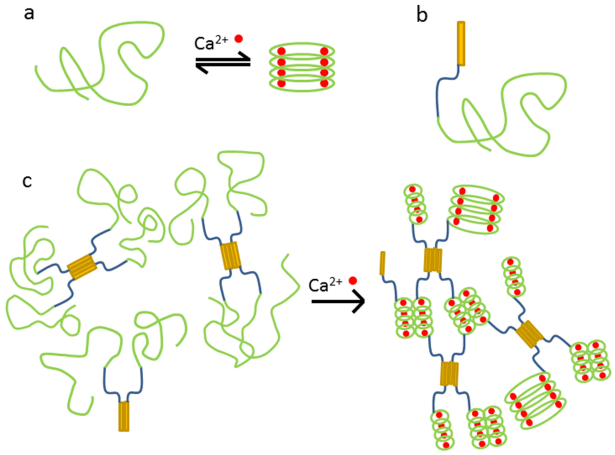

Figure 2.2: Leuβ hydrogel formation. (a) Calcium-induced conformational change of the β-roll. In the absence of calcium, the β-roll remains disordered. Upon addition of calcium, the β-roll undergoes a reversible structural change forming the corkscrew-like structure. The β-roll is depicted face forward. Calcium ions are shown in red. (b) Hydrogel monomeric building block. The α-helical leucine zipper domain (H) is shown in yellow with the soluble linker domain (S) in blue. The mutant leucine β-roll with the C-terminal capping region are shown in green. (c) Hydrogel transition. Prior to the addition of calcium, the helical domains can form tetrameric bundles, but the β-roll domains remain unstructured. When calcium is added, the folded β-roll domains expose the leucine rich faces, enabling cross-linking and hydrogel network formation. Some folded β-rolls are depicted from a side view, showing how two leucine faces could cross-link.

der, and SimplyBlue SafeStain were obtained from Life Technologies (Grand Island, NY). All chemicals and other reagents were purchased from Sigma-Aldrich (St. Louis, MO) unless otherwise specified.

2.3.2 Cloning into pMAL and pQE9 Vectors

Both WTβ and Leuβ proteins were expressed using a modified pMAL vector. The intein domain from pET-EI/OPH, a gift from Dr. David Wood (Ohio State University, OH), was cloned into the pMAL vector [46]. The WT β-roll and the C-terminal capping region were amplified out of pDLE9-CyaA, a gift from Dr. Daniel Ladant (Institut Pasteur, Paris, France), using PCR primers with KpnI and HindIII restriction sites for ligation into the pMAL-intein vector [13]. The mutant β-roll was constructed by inserting the appropriate leucine codons into two overlapping oligonucleotides encoding for the entire β-roll sequence. The oligonucleotides were annealed and extended to produce the full-length double stranded leucine β-roll. The C-terminal capping domain was added by overlap extension PCR. KpnI and HindIII sites were added to the capped leucine β-roll before ligation into pMAL-intein. Both HS-WTβ and HS-Leuβ were expressed using a modified pQE9AC10Acys vector, a gift from Dr. David Tirrell (California Institute of Technology, CA) [102]. In this work, AC10Acys is termed H-S-H. Both β-roll genes were amplified by PCR using primers with SphI and SpeI restrictions sites for subsequent cloning into pQE9, which was previously modified to remove the C-terminal H domain. pMAL vectors were transformed into OmniMAX (Invitrogen) and pQE9 vectors were transformed into SG13009 (QIAGEN) *E.coli* strains for expression. A schematic of the constructs is provided in Figure 2.3. All oligonucleotide sequences can be found in the

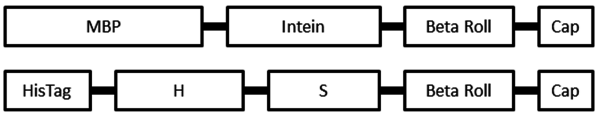

Figure 2.3: Schematic of β-roll constructs. WTβ and Leuβ were expressed as fusions to maltose binding protein (MBP) and purified by intein cleavage. HS-WTβ and HS-Leuβ were expressed using the pQE9 vector and purified using polyhistadine tags. H represents an α-helical leucine zipper domain and S represents a randomly coiled linker domain. The blocks are not drawn to scale.

publication listed at the beginning of this chapter.

2.3.3 Expression and Purification of WT and Leucine β-rolls

The WTβ and Leuβ constructs were expressed identically in LB media containing 2 g/L D-glucose. 1 L cultures (supplemented with 100 µg/mL ampicillin) were inoculated from an overnight culture of the appropriate pMAL-intein vector. The 1 L cultures were incubated at 37 °C with shaking until an $OD_{600} = 0.6$ is reached. Protein expression was induced by the addition of IPTG to a final concentration of 0.3 mM. Expression was carried out for 2 h at 37 °C with shaking. Cells were pelleted at 3,000 x g for 15 min and the supernatant was discarded. The cell pellets were resuspended in 25 mL MBP column buffer (20 mM Tris-HCl, 200 mM NaCl, 1 mM EDTA, pH 7.4) containing Halt protease inhibitor cocktail. Cells were lysed by sonication with a microtip sonicator for 6 min on ice (Misonix Sonicator 3000). The lysate was clarified by centrifugation at 15,000 x g for 30 min after which the pellet was discarded. The supernatant was diluted 5-fold with MBP column buffer and loaded onto amylose resin columns, according to the manufacturer's protocol (New England Biolabs). The columns were washed, capped, and filled with 8 mL of intein cleaving buffer (137 mM NaCl, 2.7 mM KCl, 8.1 mM

Na_2HPO_4, 1.76 mM KH_2PO_4, 40 mM bis-Tris, 2 mM EDTA, pH 6.2) for incubation at 37 °C for 12-16 h. Cleaved β-roll was eluted with 50 mL of MBP column buffer, concentrated in 10 kDa MWCO Amicon centrifugal filters, and buffer exchanged with 20 mM bis-Tris, 25 mM NaCl, pH 6.0. The samples were run over a 16/10 QFF ion-exchange column (GE Healthcare) using an $AKTA_{FPLC}$ (GE Healthcare). Separation between MBP fusions and cleaved β-roll was achieved using an NaCl gradient from 25 mM to 500 mM over 20 column volumes. β-roll fractions were collected and desalted prior to SDS-PAGE. Sample concentrations were determined by absorption at 280 nm (Spectramax M2, Molecular Devices) using calculated extinction coefficients (WTβ, ε_{280} = 17,780 $M^{-1}cm^{-1}$; Leuβ, ε_{280} = 16,500 $M^{-1}cm^{-1}$). Typical yields ranged from 3-7 mg of pure protein per L culture.

2.3.4 Expression and Purification of HS Constructs

Both HS-WTβ and HS-Leuβ constructs were expressed identically and purified using immobilized metal affinity chromatography and a polyhistidine tag. 1 L cultures of Terrific Broth (TB) were supplemented with 50 µg/mL kanamycin and 200 µg/mL ampicillin prior to inoculation from an overnight culture of the appropriate vector. Protein expression was induced by the addition of IPTG to a final concentration of 0.5 mM after an OD_{600} = 0.6 is reached. Expression was carried out for 5 h at 37 °C with shaking. Cells were pelleted and resuspended in 25 mL of HisA buffer (20 mM Tris-HCl, 150 mM NaCl, 40 mM imidazole, pH 7.5) supplemented with Halt protease inhibitor cocktail. Cells were harvested and lysed as described previously. Samples were loaded on to a 5 mL nickel charged HisTrap FF column (GE Healthcare) equilibrated

in HisA. Unbound protein was eluted with 10 column volumes of HisA, and the his-tagged construct was eluted with HisB buffer (20 mM Tris-HCl, 150 mM NaCl, 500 mM imidazole, pH 7.5) using a linear gradient to 100% HisB over 20 column volumes. Fractions containing the desired protein were collected and confirmed by SDS-PAGE. Samples were desalted and concentrated by ultrafiltration using 30 kDa MWCO Amicon centrifugal filters. Increased purity can be achieved by size exclusion chromatography. Typical yields ranged from 20-30 mg of pure protein per L culture.

2.3.5 Circular Dichroism Spectroscopy

CD spectroscopy was performed as described previously [19]. Briefly, 100 μM samples were loaded into a 0.01 cm pathlength quartz cuvette and analyzed on a J-815 CD spectrometer (Jasco, Easton, MD) equipped with a Peltier junction temperature controller. All measurements were performed in triplicate in 50 mM Tris pH 7.5 at 25 °C. Titration data were fit using SigmaPlot (Systat Software, San Jose, CA) nonlinear regression software.

2.3.6 bis-ANS Binding Fluorescence Spectroscopy

250 nM protein samples were loaded into a 1 cm pathlength cuvette and equilibrated with 0 or 50 mM calcium prior to the addition of 1 μg/mL bis-ANS. Changes in fluorescence emission were measured from 420 nm to 600 nm using a FMO-427S monochromator (Jasco, Easton, MD). Excitation was at 390 nm. All measurements were performed in triplicate in 50 mM Tris pH 7.5 at 25 °C.

2.3.7 Fluorescence Resonance Energy Transfer (FRET)

1 μM protein samples were titrated with terbium chloride. Following excitation of the sample at 282 nm, changes in fluorescence emission from bound terbium ions were monitored at 545 nm. All experiments were performed in 96 well plates in 20 mM PIPES pH 6.8, 120 mM NaCl, 10 mM KCl. Terbium was incubated with the protein samples for 30 min at 25 ℃ prior to reading. All data were fit using SigmaPlot nonlinear regression software.

2.3.8 Native Polyacrylamide Gel Electrophoresis (PAGE)

2 μg samples of Leuβ and WTβ were run on 4-16% Bis-Tris 1.0 mm gels. The voltage was held constant at 150 V and the run time was set to 105 min. For runs completed with calcium, 5 mM $CaCl_2$ was added to the running buffer. The gels were stained with SimplyBlue SafeStain according to the manufacturer's protocol.

2.3.9 Hydrogel Preparation

Hydrogel constructs were allowed to self-assemble by reconstituting lyophilized protein with small volumes of water as previously described [120]. HS-WTβ and HS-Leuβ concentrations were determined by UV absorbance at 280 nm using the extinction coefficients ε_{280} = 24,750 $M^{-1}cm^{-1}$ and ε_{280} = 23,470 $M^{-1}cm^{-1}$ respectively. 1.5 mg of protein was diluted in 250 μL of 5 mM Tris-HCl pH 7.5 with the appropriate salt concentration. Samples were frozen overnight at -80 ℃ and lyophilized the following day. The lyophilized protein was rehydrated with 25 μL of Millipore water yielding 6

wt% samples. Mechanical mixing, vortexing, and centrifugation were used to insure all of the protein is rehydrated. The samples were centrifuged for 5 min at 13,000 x g to remove any air bubbles and allowed to set.

2.3.10 Microrheology

Microrheology was used to analyze the mechanical properties of a viscoelastic fluid by following the motion of micrometer sized spherical particles embedded in the sample. In this study, passive microrheology was used, which relies on the intrinsic Brownian motion of the particles caused by small thermal fluctuations [29, 80]. The particles' mean square displacements (MSD) can be calculated experimentally and are related to the mechanical properties of the fluid through a generalized Stokes-Einstein equation:

$$\left\{\Delta\check{r}^2\left(s\right)\right\} = \frac{dk_BT}{3\pi as\breve{G}(s)} \tag{2.1}$$

where $\{\Delta\check{r}^2(s)\}$ is the time averaged Laplace transform of the particles' MSD, d is the dimensionality of the track (2 for this work), k_B is the Boltzmann constant, T is the temperature, a is the radius of the tracer particle, s is the Laplace frequency, and $\breve{G}(s)$ is the frequency dependent Laplace representation of the complex modulus. This is composed of both the elastic (G') and viscous (G") moduli [81,128]. 1 μm fluorescently labeled tracer particles were added when reconstituting the lyophilized protein. The samples were mixed thoroughly, loaded onto a glass microscope slide between two strips of Parafilm and sealed with a glass coverslip. Particle motion was observed using a Nikon Eclipse 50i microscope with a 40X objective. 300 frames of video were recorded per run at an exposure time of 33ms with a Nikon HRD076 camera. Three separate

videos were taken per sample to ensure a good statistical average. Readings were made in the middle of each sample so that edge effects can be neglected. Image stacks were created using ImageJ and analyzed using Interactive Data Language (IDL) software. The particle trajectories and rheological properties of each sample were calculated using algorithms created by Crocker et al. [32].

2.4 Results

2.4.1 Leucine β-roll Characterization

A β-roll domain from the adenylate cyclase protein from *B. pertussis* was rationally mutated to contain a leucine-rich face, and the mutant peptide was expressed, purified and characterized. Experiments were conducted to compare the mutant construct to the WTβ to ensure the mutations did not disrupt the response of the peptide to calcium. CD spectroscopy, bis-ANS dye binding, and terbium binding experiments all suggested that the mutated β-roll exhibits a similar calcium-induced conformational change and calcium binding affinity as compared to the wild type peptide. In the absence of calcium, both Leuβ and WTβ CD spectra exhibited a large negative peak at 198 nm indicative of randomly coiled polypeptide. Upon addition of 50 mM calcium, both constructs showed a similar increase in β-sheet secondary structure with a negative peak emerging at 218 nm (Figure 2.4a-b). These results are consistent with what has been reported previously [19]. A calcium titration was performed by monitoring the change in CD signal at 218 nm (Figure 2.4e). Both data were fit to the Hill equation yielding nearly identical calcium binding affinities and binding cooperativity (Table 2.1). Bis-ANS

Construct	K_d(mM)	n_H	R^2
WTβ	0.91 ± 0.02	2.91 ± 0.2	0.993
Leuβ	0.87 ± 0.02	2.97 ± 0.2	0.996

Table 2.1: Summary of calcium binding affinity and Hill coefficients for the WTβ and Leuβ constructs.

binding was used to further probe structural changes in response to calcium. Bis-ANS binds to surface exposed hydrophobic patches resulting in an increase in fluorescence signal in calcium-rich environments [19, 112]. Both WTβ and Leuβ fluorescence signals were measured in the presence and absence of 50 mM calcium (Figure 2.4c-d). The slightly elevated signal in Figure 2.4d was a result of the additional hydrophobic residues in the Leuβ.

Fluorescence resonance energy transfer (FRET) experiments were performed to confirm the CD and bis-ANS binding data. Terbium, a lanthanide atom, was titrated into β-roll samples. The emission from bound terbium ions in close proximity to excited tyrosine residues was measured spectrophotometrically [61, 130]. It is important to note that while terbium is often used as a calcium analog, it does not directly indicate calcium binding. However, when analyzed in coordination with the CD and bis-ANS data, terbium binding does corroborate the claim that both constructs bind calcium in a similar manner. The terbium titrations for the WTβ and Leuβ yield K_d values of 97 ± 4 μM and 91 ± 4 μM, respectively (Figure 2.4f).

WT and leucine constructs were analyzed by native PAGE to confirm the oligimerization state of the mutant β-roll in the presence of calcium. Both samples migrated similarly through the native gel in the absence of calcium (Figure 2.9). Upon addition of 5 mM calcium to the running buffer, there was a clear difference in migration between

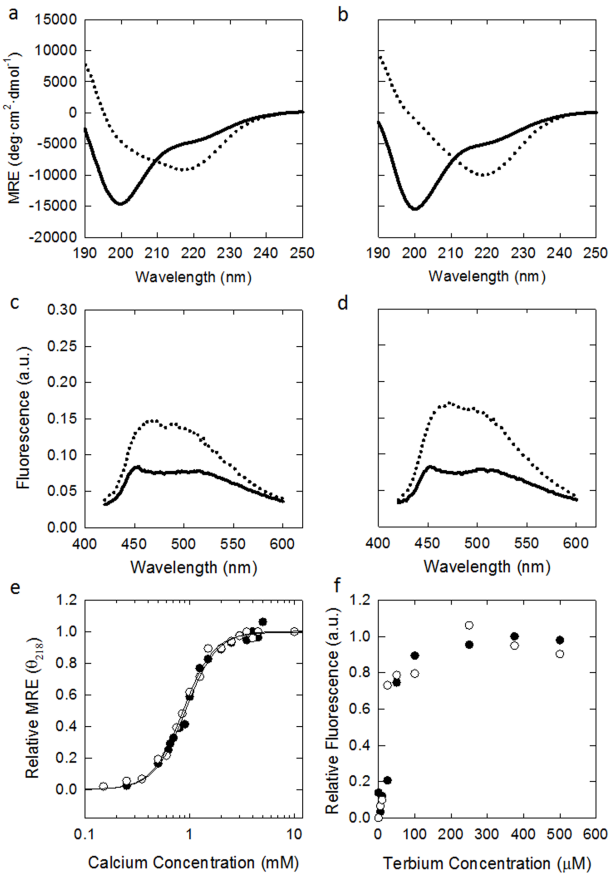

Figure 2.4: WTβ and Leuβ calcium responsiveness and characterization. (a) WTβ and (b) Leuβ CD spectra in the presence (●●●) and absence (—) of 50 mM calcium showing similar responses. These results are consistent with bis-ANS binding results for WTβ and Leuβ shown in (c) and (d), respectively. The higher bis-ANS signal observed for the leucine construct is due to the increased number of nonpolar residues. The CD calcium titration (e) shows nearly identical curves for both WTβ (●) and Leuβ (○). The data are fit to the Hill equation and the parameters are summarized in Table 2.1. Terbium binding results are shown in (e) for the WTβ (●) and Leuβ (○) constructs. Both show very similar responses.

the WTβ and Leuβ. The Leuβ appeared to run larger, suggesting the formation of an oligomer, most likely caused by the cross-linking of the leucine rich faces. While these gels are not entirely quantitative, they do suggest an apparent difference in size, only in the presence of calcium.

2.4.2 HS-Leucine β-roll Characterization

An α-helical leucine zipper domain (H) along with a randomly coiled soluble domain (S) was fused to the N-terminus of the leucine and WT β-rolls. Similar characterization experiments were performed in order to determine if these domains have any effect on calcium-induced structural change. The CD spectra showed changes in response to calcium, but the signal was dominated by the largely helical content of the H domain (Figure 2.8). Bis-ANS binding experiments showed no discernible difference between the HS-WTβ and HS-Leuβ proteins (Figure 2.5a-b). It is important to note that the fluorescence signals were much higher in this case due to bis-ANS binding to the H and S domains. However, the relative change in peak intensity upon addition of calcium was conserved among all 4 constructs (2.5x higher). The terbium titrations for HS-WTβ and HS-Leuβ (Figure 2.5c) yielded K_d values of 93 ± 3 μM and 86 ± 2 μM respectively.

2.4.3 HS-Leucine β-roll Microrheology

Mechanical properties of HS-WTβ and HS-Leuβ samples were characterized using microrheology. The Brownian motion of small particles imbedded into the sample was recorded using video microscopy, and the average mean square displacements (MSD) of the particles were calculated as a function of time. The MSD of the tracer particles

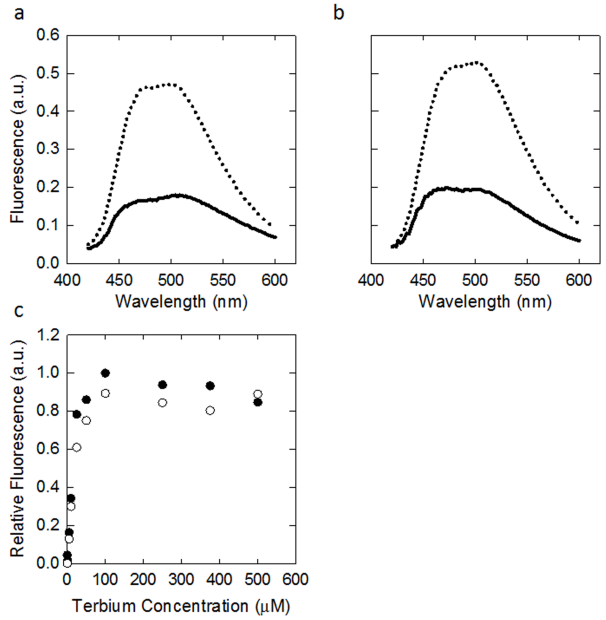

Figure 2.5: HS-WTβ and HS-Leuβ calcium responsiveness and characterization. (a) HS-WTβ and (b) HS-Leuβ bis-ANS binding spectra in the presence (•••) and absence (—) of 50 mM calcium. This data is consistent with the bis-ANS data presented in Figure 2.4, with the increases in baseline fluorescence due to binding to H and S domains. Terbium binding titrations are shown in (c) for the HS-WTβ (●) and HS-Leuβ (○) constructs. CD spectra are included in the Supplemental Information.

allows one to quantify the mechanical properties of the fluid where they are embedded [81, 128]. Once the MSD is obtained, the frequency dependent viscous and elastic moduli of a sample can be calculated using the modified Stokes-Einstein equation given above. Both constructs demonstrate concentration-dependent gelation. Initial experiments showed that at protein concentrations below 5 wt%, the samples remained viscous with and without calcium. Conversely, at weight percentages above 10%, the samples were completely elastic (Data not shown). At weight percentages of 6%, we observed a calcium-dependent phase transition and behavior at this concentration was further explored.

6 wt% samples of HS-WTβ and HS-Leuβ were prepared as described above. After tracer particles were imbedded in the samples, video microscopy was used to record the motion of the particles. The trajectories and mechanical properties were calculated using IDL software. The viscous (G") and elastic (G') moduli of HS-WTβ and HS-Leuβ as a function of frequency are shown in Figure 2.6. Both WT and leucine constructs appeared to be viscous liquids in buffer (Figure 2.6a-b) and in the presence of 50 mM magnesium (Figure 2.6c-d). However, while the WTβ construct remained viscous in 50 mM calcium (Figure 2.6e), the leucine construct formed a hydrogel (Figure 2.6f). To supplement this data, a calcium titration was performed with 6 wt% HS-Leuβ samples. The calcium concentration was varied from 0-10 mM and the resultant rheological plots were given in Figure 2.7. Large shifts in the elastic and viscous moduli were observed at 500 μM calcium with a crossover frequency of about 3 s^{-1}. As the calcium concentration is increased, the crossover frequency continued to decrease. At 10 mM calcium, the sample was elastic in the frequency range we explored.

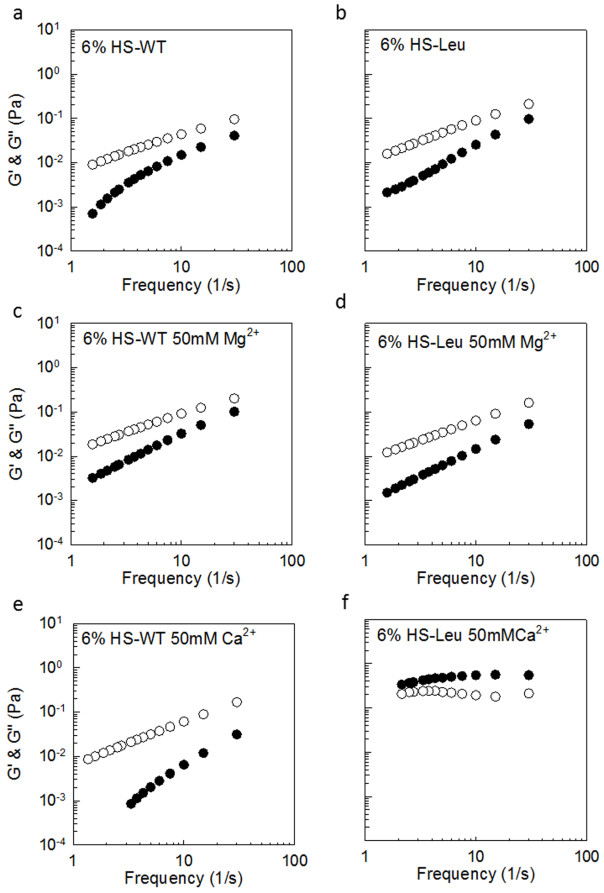

Figure 2.6: HS-WTβ and HS-Leuβ roll microrheology. Viscous (○) and elastic (●) moduli have been calculated for 6wt% HS-WTβ and HS-Leuβ samples. Both constructs appear mostly viscous in buffer (a-b) and in 50 mM magnesium (c-d). The HS-WTβ remains viscous in 50 mM calcium as well (e). The HS-Leuβ sample shows a shift in mechanical properties after the addition of calcium, gaining elasticity as compared to the HS-WTβ control. MSD vs. τ plots are included in the Supplemental Information for all microrheology experiments.

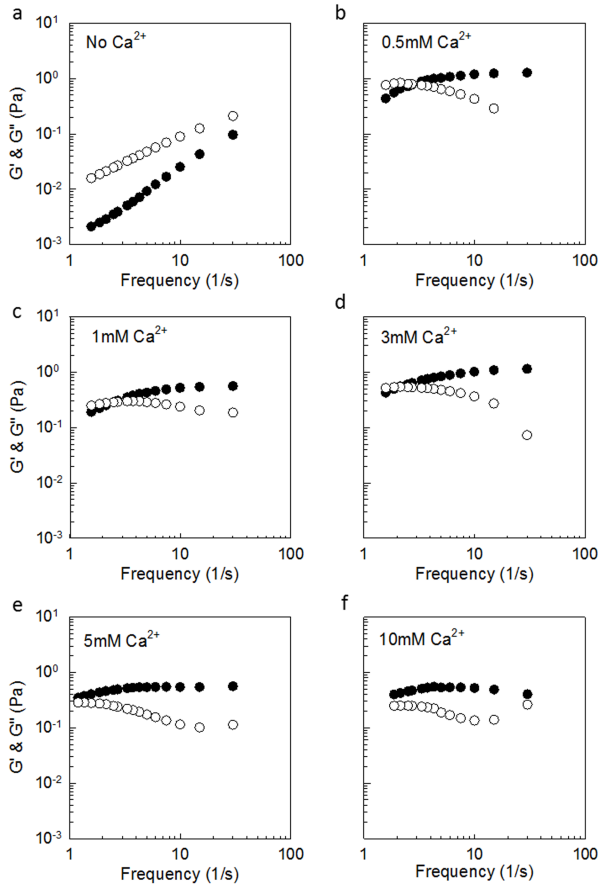

Figure 2.7: HS-Leuβ microrheology calcium titration. Viscous (○) and elastic (●) moduli have been calculated for 6 wt% HS-Leuβ samples at various calcium concentrations showing the transition from viscous liquid to hydrogel. MSD vs. τ plots are included in the Supplemental Information for all microrheology experiments.

2.5 Discussion

Several biophysical techniques were used in this work to probe the calcium binding, structural confirmation, and mechanical properties of the WTβ and Leuβ peptide constructs. We showed that the leucine mutations made to the WT β-roll resulted in no change in calcium responsiveness or binding affinity; similar conformational changes were observed in the mutant β-roll as shown by CD and bis-ANS binding. This was expected as the residues selected for mutation most likely do not participate in calcium binding [8]. Assuming the β-roll adopts a structure similar to those derived crystallographically in other RTX containing proteins, the amino acid side chains that were mutated project radially outwards, away from the hydrophobic core minimizing any potential steric effects. Further, native PAGE data indicated a calcium-dependent difference in migration between the mutant and WT proteins, likely caused by leucine β-roll cross-linking. This premise was elucidated through the rheological experiments after cloning both constructs into the pQE9 vector.

Appending the H and S domains to the N-termini of the WT and leucine β-roll also resulted in minimal effects on response to calcium as shown by the bis-ANS and terbium binding data. This was consistent with our previous results showing that the native N-terminal capping group of the β-roll domain does not play an important role in protein folding [19]. Although the CD spectra of the constructs containing the H and S domains were dominated by the highly helical H domain, there appeared to be conformational changes following the addition of calcium.

The microrheology data presented substantial differences in viscoelastic properties between the HS-WTβ and HS-Leuβ peptides in the presence of calcium. At 6 wt%,

both constructs exhibited viscous character in buffer and in buffer supplemented with 50 mM magnesium. The magnesium control showed that ionic effects did not influence the changes in mechanical properties of both samples. When calcium was added to the HS-WTβ protein, the sample remained viscous. Here, we suspect that the WT β-roll is fully folded, as indicated by the CD data. However, this calcium-induced structural response does not promote the formation of a hydrogel network as the WTβ domains do not interact. Upon addition of calcium to the HS-Leuβ, we observed a significant change in rheological properties. The sample appeared to be elastic, showing frequency independent viscous and elastic moduli. At 50 mM calcium, we expected the leucine β-roll to be completely folded, and the engineered hydrophobic leucine face should be exposed to the solvent. This hydrophobic face promotes cross-linking of the β-roll domains. The calcium-dependent physical cross-linking coupled with the coiled-coil bundles formed by the leucine zipper domains provides enough interaction to alter the mechanical properties of the sample and create a hydrogel network. It may also be possible for the leucine zipper domains to interact with the leucine β-roll domains, and this would introduce a different mode of cross-linking within the hydrogels.

The transition from viscous liquid to hydrogel shown in Figure 2.7 is consistent with the Leuβ CD titration in Figure 2.4, where we observed the transition from disordered to structured peptide between 0.5-3.0 mM calcium. At concentrations higher than 3 mM the β-roll was completely folded. A strong parallel can be drawn with the rheology data in Figure 2.7. The sample was found to transition from a viscous liquid to a hydrogel between 0.5-5 mM calcium. By 10 mM, the hydrogel was completely formed as the β-roll domains should have been completely folded, maximizing the cross-linking.

Most stimulus-responsive hydrogels described in the literature use cross-link forming scaffolds and then a trigger is found to destabilize the binding interaction. For example, the leucine zipper-based hydrogels are destabilized by changes in pH as this interferes with the alpha helix formation. And the elastin-like peptide based hydrogels take advantage of the unique inverse temperature transition to destabilize the hydrogel. We have taken a different approach in this work, where we have chosen a scaffold that undergoes a specific and unique conformational transition from an intrinsically disordered structure to the folded β-roll domain in response to calcium. The β-roll domain is not normally involved in biomolecular recognition or self-assembly, so this feature was engineered into the scaffold to control self-assembly by calcium addition. Eliminating the reliance on temperature and pH swings to modulate self-assembly may allow for the use of these hydrogels in more biologically relevant environments, where changes in temperature or pH are not tolerated.

Although the gels produced in this proof-of-concept work have relatively low elastic moduli, the leucine β-roll can be optimized in future work to create stronger hydrogels for different applications. Since the β-roll is a modular repeat protein, the number of repeats and composition of the repeating unit can be easily altered to extend the size and makeup of the hydrophobic domain. In addition, alternative cross-linking strategies could be incorporated such as the inclusion of specific ionic interactions as has been explored for the leucine zipper domains. Also, the β-roll has a second face amenable to mutation, which could be used to create leucine-rich surfaces on both sides of the β-roll domain.

2.6 Conclusions

In this work, we presented a rationally engineered peptide that can be used to create allosterically-controlled hydrogel networks. Leucine mutations were inserted into the β-roll peptide scaffold to create a hydrophobic surface suitable for cross-linking, which is exposed only after calcium binding. An α-helical leucine zipper domain with a randomly coiled linker were attached to the N-terminus of the beta roll to provide additional physical cross-linking. Hydrogels formed only in calcium-rich environments where the folded leucine β-roll domains provided the necessary hydrophobic interface. The WTβ remained a viscous liquid regardless of the calcium concentration.

2.7 Supplemental Information

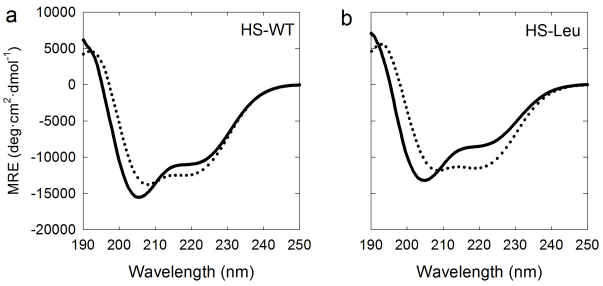

Figure 2.8: HS-WTβ and HS-Leuβ CD spectra. HS-WTβ (a) and HS-Leuβ (b) were analyzed by CD spectroscopy with (●●●) and without (—) 10 mM calcium. The spectra are dominated by the helical domain indicated by the positive peaks at 192 nm and negative peaks around 205 nm. An obvious shift in secondary structure is observed after the addition of calcium due to beta roll folding. All measurements were taken in triplicate in 50 mM Tris pH 7.5 at 25 °C.

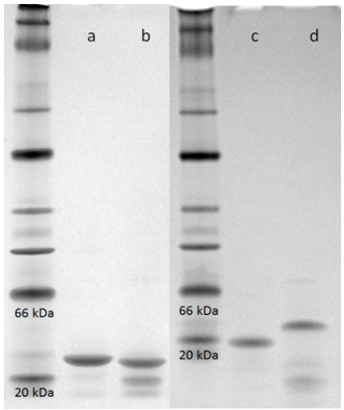

Figure 2.9: WTβ and Leuβ native PAGE. WTβ (a) and Leuβ (b) domains were run on 4-16% bis-Tris native gels (Invitrogen). WTβ (c) and Leuβ (d) fractions were then run in buffer supplemented with 5 mM calcium. Purity of the samples was ensured by SDS-PAGE. While these results are not precisely quantitative, there is a clear perturbation in migration observed following calcium addition.

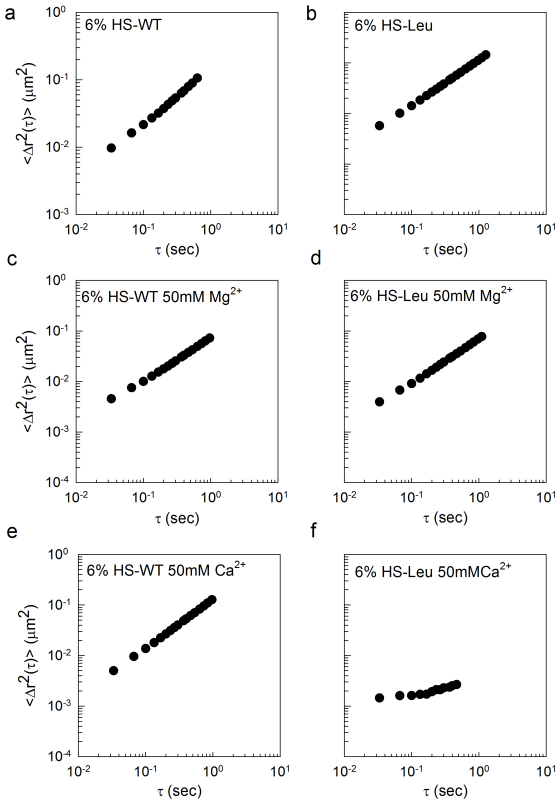

Figure 2.10: The calculated mean square displacements for HS-WTβ and HS-Leuβ are given with respect to lag time in buffer (a-b), 50 mM magnesium (c-d), and 50 mM calcium (e-f), respectively.

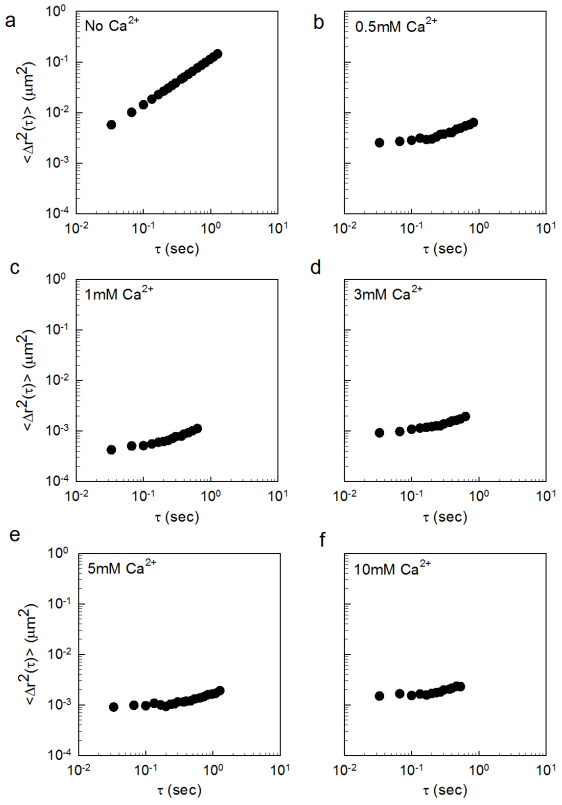

Figure 2.11: The calculated mean square displacements for HS-Leuβ samples are given with respect to lag time at various calcium concentrations.

Chapter 3

Doubling the Cross-Linking Potential of a Rationally Engineered RTX Domain for Calcium-Responsive Self-Assembly

Project Collaborators: Kevin Dooley, Beyza Bulutoglu, & Scott Banta

A version of this chapter entitled, "Doubling the cross-linking potential of a rationally-designed beta roll peptide for calcium-dependent proteinaceous hydrogel formation" has been submitted to Biomacromolecules. KD prepared DNA constructs, expressed and purified all proteins, performed all FRET, bis-ANS fluorescence spectroscopy, microrheology experiments and analysis.

3.1 Abstract

We have rationally engineered a stimulus-responsive cross-linking domain based on a repeats-in-toxin (RTX) peptide to enable the triggered formation of supramolecular hydrogel networks. The peptide isolated from the RTX domain is intrinsically disordered in the absence of calcium. In calcium-rich environments, the peptide folds into a beta roll (β-roll) secondary structure composed to two parallel β-sheet faces. Previously, we mutated one of the faces to contain solvent exposed leucine side chains which are localized only in the calcium-bound β-roll conformation. We demonstrated the ability of this mutant peptide to self-assemble into hydrogels in the presence of calcium with the aid of additional peptide-based cross-linking moieties. Here, we have expanded this approach by engineering both β-roll faces to contain leucine resides thereby doubling the cross-linking potential for each monomeric building block. These leucine-rich surfaces impart a hydrophobic driving force for self-assembly. Extensive characterization was performed on this double-faced mutant to ensure the retention of calcium affinity and subsequent structural rearrangement similar to that of the wild type domain. We genetically fused an α-helical leucine zipper capable of forming tetrameric coiled-coil

bundles to the peptide and the resulting chimeric protein self-assembles into a hydrogel only in calcium-rich environments. To further investigate the cross-linking potential of the mutant β-roll, we constructed concatemers of the β-roll with maltose binding protein (MBP), without the leucine zipper domains. These concatemers show a similar sol-gel transition in response to calcium. Several biophysical techniques were used to probe the structural and mechanical properties of the mutant β-roll domain and the resulting supramolecular networks including circular dichroism, fluorescence resonance energy transfer, bis-ANS binding, and microrheology. These results demonstrate that the engineered β-roll peptides can mediate calcium-dependent cross-linking for protein hydrogel formation without the need for additional cross-linking moieties.

3.2 Introduction

Protein-based biopolymer hydrogels composed of three-dimensionally cross-linked macroscopic networks have been widely investigated for a host of applications in the biomedical field because of their biocompatibility, predictable erosion rates, and tunable viscoelastic properties [12, 52, 62, 65, 110]. Proteins or peptides with the ability to respond "intelligently" to external stimuli such as pH, temperature, ionic strength or light are often incorporated into monomeric polymer building blocks to trigger or disrupt self-assembly through a variety of mechanisms. Calmodulin, elastin-like polypeptides, and α-helical leucine zipper domains have been used to actuate hydrogel formation in response to environmental cues, leading to successful implementation into microfluidic systems, biosensors, and vehicles for controlled release [7, 12, 23, 41, 62, 119].

We have previously reported a rationally designed peptide based on the beta roll (β-roll) domain that functions as a stimulus-responsive cross-linker for calcium-dependent hydrogel formation [35]. The β-roll scaffold was taken from the block V repeats-in-toxin (RTX) domain of adenylate cyclase from *Bordetella pertussis* [13]. It is a modular, repeating polypeptide that undergoes a reversible structural rearrangement in response to calcium. The peptide is intrinsically disordered in the absence of calcium and folds into a β-roll in calcium-rich environments consisting of two parallel β-sheet faces separated by flexible turn regions (Figure 3.1a) [13, 25]. Conserved aspartic acid residues in the turn regions are responsible for coordinating calcium ions in each turn. Only a C-terminal capping group is required for calcium-induced folding of the polypeptides [19, 111].

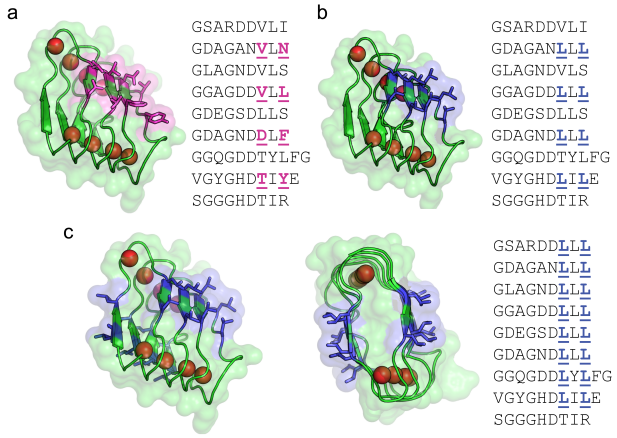

Figure 3.1: Homology models for WT and mutant β-roll domains with primary sequences. Homology models for WTβ (a), Leuβ (b), and DLeuβ (c) domains were generated with SWISS-MODEL (Swiss Institute of Bioinformatics) using a β-roll containing lipase as a template (PDB 2Z8X). The side chains of the surface exposed residues are highlighted and underlined in the sequences. All images were rendered in PyMOL.

Each β-sheet face in the folded conformation contains eight resides with solvent ex-

posed side chains that project radially away from the hydrophobic core. In our previous study, we mutated one β-sheet face to contain leucine residues at these eight positions (Figure 3.1b). We fused the mutant leucine β-roll (Leuβ) to a self-assembling α-helical leucine zipper domain (H) and a randomly coiled hydrophilic linker (S) which is included to provide flexibility and prevent aggregation. Both H and S domains have been extensively characterized previously [102, 103, 128]. Without calcium, the helices form tetrameric coiled-coil bundles, but the β-roll domains remain unstructured, delocalizing the leucine-rich patches and prohibiting HS-Leuβ supramolecular self-assembly. After calcium binding, the β-roll folds and the leucine-rich faces are exposed creating a hydrophobic driving force for oligomerization (Figure 3.2a). The resulting calcium-responsive hydrogel networks have been characterized using a variety of techniques [35].

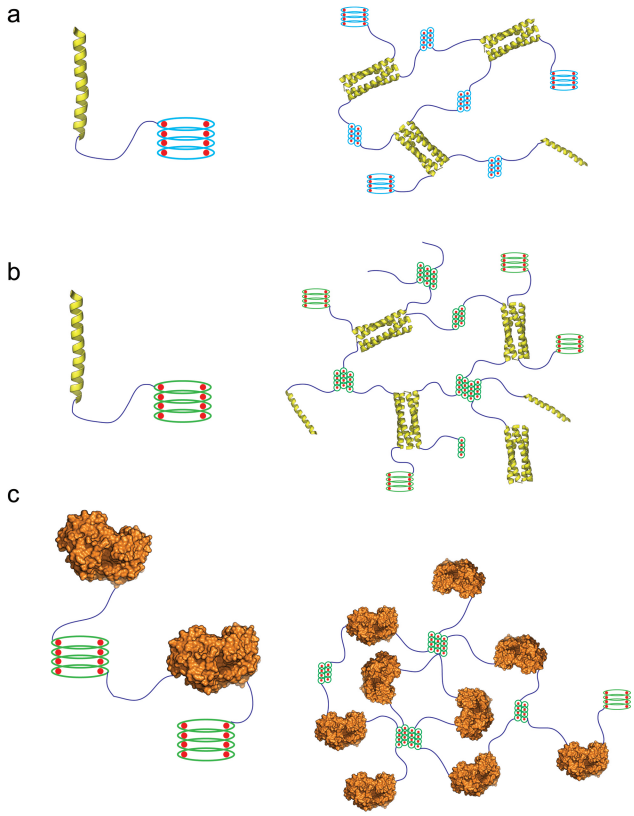

Figure 3.2: Monomeric polymer building blocks and assembled hydrogel networks. All cartoons represent β-roll domains in the folded conformation after calcium (red) binding. (a) HS-Leuβ monomer composed of an α-helical leucine zipper (yellow), a randomly coiled linker (purple), and the mutant Leuβ (light blue). The assembled network depicts an association number of 2 for Leuβ. (b) HS-DLeuβ monomer composed of an α-helix, linker, and DLeuβ mutant (green). Association numbers of $\geq$2 are depicted. (c) MBP-DLeuβ-MBP-DLeuβ monomer. The DLeuβ can achieve higher oligomerization states and does not require cross-linking provided by the helical bundles. Alpha-helices and MBP were rendered in PyMOL using PDB files 1GCL and 1YTV respectively.

In this study, we have expanded this approach by further engineering the Leuβ peptide to increases its cross-linking potential. The folded β-roll domain consists of two β-sheet faces, each with eight solvent exposed residues. We have now rationally engi-

neered a "double-faced" leucine β-roll peptide (DLeuβ) such that all sixteen positions are leucines (Figure 3.1c). This should enable cross-linking on both sides of the folded construct simultaneously, thereby increasing the potential oligomerization state (Figure 3.2b). Previously, Leuβ domains were approximated to have an association number of 2 (Figure 3.2a), which required significant protein concentrations (60 mg/mL) and additional cross-linking moieties to assemble into supramolecular networks. We hypothesize that DLeuβ will self-assemble at lower weight percentages as concentration dependent sol-gel transition and oligomerization state of the cross-linking domain are directly related [128]. Further, DLeuβ should be able to induce calcium-dependent self-assembly without the additional cross-linking provided by the α-helical leucine zippers (Figure 3.2c). Circular dichroism (CD), fluorescence resonance energy transfer (FRET) and bis-ANS binding were used to ensure DLeuβ folds in a similar manner as the wild type β-roll (WTβ) and Leuβ in response to calcium. The mechanical properties of HS-DLeuβ were analyzed using a microrheology technique and compared to results obtained previously for HS-WTβ and HS-Leuβ [35]. Finally, the utility of the DLeuβ as a stand-alone cross-linking domain was assessed by creating fusions to maltose binding protein (MBP) and analyzing the resulting hydrogel networks (Figure 3.2c).

3.3 Materials & Methods

3.3.1 Materials

Amylose resin, the MBP expression kit, and all enzymes for DNA cloning were purchased from New England Biolabs (Ipswich, MA). Isopropyl β-D-1-thiogalactopyranoside

(IPTG) and ampicillin sodium salt were purchased from Gold Biotechnology (St. Louis, MO). Amicon centrifugal filters were purchased from Millipore (Billerica, MA). All materials for polyacrylamide gel electrophoresis (PAGE) experiments as well as 1 μm Nile Red FluoSpheres for particle tracking were purchased from Life Technologies (Grand Island, NY). All oligonucleotides were purchased from Integrated DNA Technologies (Coralville, IA). BL21 *E. coli* cells were purchased from Bioline (Taunton, MA). All other reagents were purchased from Sigma-Aldrich (Sr. Louis, MO) unless otherwise stated.

3.3.2 Cloning into the pMAL expression plasmid

Cloning and expression of the WTβ and Leuβ constructs have been described in the previous chapter. The DLeuβ peptide was assembled by annealing and extending two overlapping oligonucleotides encoding for the entire gene. The C-terminal cap of the β-roll domain was amplified from the pDLE-9-cyaA plasmid, a gift from Dr. Daniel Ladant (Institut Pasteur, Paris, France), and appended to the DLeuβ gene by overlap extension PCR [13]. KpnI and HindIII restriction sites were added for ligation into a modified pMAL plasmid containing a self-cleaving intein, a gift from Dr. David Wood (Ohio State University, Columbus, OH) [46]. DLeuβ was also cloned into the same pMAL-intein backbone modified with an α-helical domain (H) and a soluble linker (S) from the pQE9AC10Acys plasmid, a gift from Dr. David Tirrell (California Institute of Technology, Pasadena, CA) [102]. The resultant constructs, pMAL-intein-DLeuβ and pMAL-intein-HS-DLeuβ were transformed into BL21 *E. coli* cells for expression. Concatemers of MBP and DLeuβ (Figure 3.2c) were cloned into the pMAL-c4e vector

backbone. DLeuβ with the C-terminal cap was amplified out of pMAL-intein-DLeuβ construct and cloned using EcoRI and BamHI restriction sites. MBP was amplified from the pMAL-c4e construct and inserted after DLeuβ-Cap via BamHI and SalI restriction sites. Lastly, the second DLeuβ-Cap was amplified and cloned using SalI and HindIII restriction sites, resulting in the final construct: pMAL-MBP-DLeuβ-MBP-DLeuβ. All oligonucleotide sequences can be found in the publication listed at the beginning of this chapter.

3.3.3 Expression & Purification of DLeu Constructs

All DLeuβ constructs were expressed identically in Terrific Broth (TB) supplemented with 100 µg/mL ampicillin and 2 g/L D-glucose. Saturated 10 mL overnight cultures containing the appropriate transformed cells were diluted in 1 L of sterilized TB and grown at 37 °C and shaken at 220 RPM. Once the optical density (OD) at 600 nm reached 0.6, protein expression was induced with IPTG to a final concentration of 0.3 mM. Expression was carried out for either 5 h at 37 °C or 16 h at 25 °C after which cells were harvested via centrifugation at 5,000 x g for 10 min. Cell pellets were resuspended in 50 mL MBP column buffer (20 mM Tris-HCl, 200 mM NaCl, 1 mM EDTA, pH 7.4) per L of culture. Expressed protein was liberated from the cells by microtip sonication for 6 min on ice (Sonicator 3000, QSonica, Newtown, CT). Cell debris and insoluble protein were collected via centrifugation at 15,000 x g for 30 min and discarded. Soluble protein was diluted five-fold in MBP column buffer and loaded onto equilibrated amylose resin drip columns. The columns were washed to remove any nonspecifically bound protein. MBP-DLeuβ concatemers were eluted with maltose and further purified on

a Superdex HiLoad 16/60 size exclusion chromatography column (GE Healthcare). Columns containing proteins with the intein domain were saturated with intein cleaving buffer (137 mM NaCl, 2.7 mM KCl, 8.1 mM Na_2HPO_4, 1.76 mM KH_2PO_4, 40 mM bis-Tris, 2 mM EDTA, pH 6.2), capped, and incubated at 37 °C for 12-16 h. Cleaved fusion proteins were eluted with 50mL of MBP column buffer and concentrated using either 10 or 30 kDa MWCO centrifugal filter devices. The samples were buffer exchanged into 20 mM bis-Tris, 25 mM NaCl, pH 6.0 and loaded onto a 16/10 Q FF ion exchange column (GE Healthcare). Target proteins were eluted using a linear NaCl gradient from 25 mM to 500 mM over 20 column volumes. Protein size and purity were confirmed by SDS-PAGE. Protein concentration was determined by absorbance at 280 nm using calculated extinction coefficients available in the Supplemental Information. Purified protein fractions were pooled, concentrated and buffer exchanged into the appropriate assay buffer.

3.3.4 Circular Dichroism Spectroscopy

100 µM β-roll samples were loaded into a 0.1 mm path length quartz cuvette and analyzed on a J-815 CD spectrometer (Jasco, Easton, MD). The temperature was held constant at 25 °C by a Peltier junction temperature controller. Samples were incubated in the presence or absence of $CaCl_2$ prior to analysis. All experiments were performed in triplicate in 50 mM Tris pH 7.4. Titration data were fit to the Hill equation using SigmaPlot (Systat Software, San Jose, CA) nonlinear regression software.

3.3.5 Bis-ANS Dye Binding

1 μM β-roll samples were prepared in 50 mM Tris pH 7.4 in the presence and absence of 50 mM $CaCl_2$ prior to the addition of 5 μg/mL bis-ANS dye. Samples were loaded into a 1 cm path length UV cuvette and analyzed on a SpectraMax M2 cuvette reader (Molecular Devices, Sunnyvale, CA). Fluorescence emission was monitored from 420 nm to 600 nm following excitation at 390 nm. All measurements were performed in triplicate.

3.3.6 Fluorescence Resonance Energy Transfer (FRET)

1 μM β-roll samples were prepared in 20 mM PIPES buffer pH 6.8 supplemented with 120 mM NaCl and 10 mM KCl. A terbium (III) chloride stock solution was prepared in the same buffer. β-roll samples were titrated with increasing amounts of terbium in 96 well microtiter plates and incubated at 25 °C for 30 min prior to analysis. Tyrosine residues in the β-roll domain were excited at 282 nm and the fluorescence emission from bound terbium ions was monitored at 545 nm. All data were collected in triplicate.

3.3.7 Hydrogel Preparation

All β-roll samples were prepared in a similar manner. 500 μL of diluted protein samples were lyophilized in 5 mM Tris pH 7.4 supplemented with $CaCl_2$ or $MgCl_2$. Self-assembly was initiated by reconstituting the lyophilized protein in 1/10 the original volume resulting in 4-6 wt% (40-60 mg/mL) protein in 50 mM Tris pH 7.4. Mechanical mixing, vortexing, and centrifugation were used to ensure all of the lyophilized protein was

rehydrated. Samples were allowed to set at room temperature for 30 min prior to analysis.

3.3.8 Microrheology

Microrheology experiments were performed as previously described with minor modifications [35]. When rehydrating lyophilized protein for particle tracking experiments, ddH_2O was supplemented with 1 μm FluoSpheres conjugated with Nile Red. The samples were mixed, loaded onto a glass slide and sealed with a coverslip. Particle motion was tracked using an Olympus IX81 motorized inverted microscope with a 40 X objective. A high-speed Hamamatsu C9300 digital camera was used to record particle motion at an exposure time of 33 ms. 300 frames of video were recorded at 30 frames per second for each run. 3 runs were recorded per sample to ensure a good statistical average. All runs were recorded on a ThorLabs air table to eliminate ambient vibrational noise. All videos were analyzed using MetaMorph software and converted to TIFF stacks in ImageJ [1]. Particle tracking and rheological analysis were completed in Interactive Data Language (IDL) software using algorithms created by Crocker et al. [32].

3.4 Results

3.4.1 DLeuβ Characterization

The rationally designed "double-faced" leucine β-roll was expressed, purified, and characterized by CD, bis-ANS dye binding, and terbium binding assays to assess its response

to calcium and self-assembly capability. We have previously characterized the WTβ and Leuβ using these same techniques [35]. 100 μM samples of purified protein were analyzed by CD in the presence and absence of 10 mM $CaCl_2$. The resulting spectra are shown in Figure 3.3a-c for WTβ, Leuβ, and DLeuβ constructs, respectively. All three proteins demonstrated similar conformational changes in response to calcium. In calcium-free environments, the spectra exhibited large negative peaks at 198 nm, which is indicative of randomly coiled peptide. Significant changes in secondary structure were observed in 10 mM $CaCl_2$ for all β-roll domains. A random coil to β-sheet transition was evidenced by the emergence a negative peak at 218 nm and is consistent with previous reports [19]. Calcium-induced folding parameters were also similar for all three constructs. A titration was performed by monitoring CD signal at 218 nm over a range of $CaCl_2$ concentrations (Figure 3.3c). The data were fit to the Hill equation and the resulting calcium binding parameters are summarized in Table 3.1. Leuβ and DLeuβ bound calcium with affinities similar to the wild type peptide and all constructs exhibited cooperative binding with Hill coefficients (nH) greater than 1. Bis-ANS is a commonly used molecular probe that binds to protein surfaces through hydrophobic interactions causing in an increase in fluorescence [56]. It can be used to detect changes structure and has been previously used to examine the conformational transition of β-roll peptides [19, 35]. Purified DLeuβ was incubated with bis-ANS in the presence and absence of calcium and the resulting emission spectra are available in the Supplemental Information. Significant increases in fluorescence were observed in the calcium-rich samples indicating a disordered to folded transition.

Construct	K_D *(mM)*	n_H	R^2
WTβ	0.91 ± 0.02	2.3 ± 0.1	0.997
Leuβ	0.82 ± 0.01	3.1 ± 0.1	0.998
DLeuβ	1.18 ± 0.02	4.6 ± 0.3	0.998

Table 3.1: Calcium binding properties for WT, Leuβ, and DLeuβ peptides.

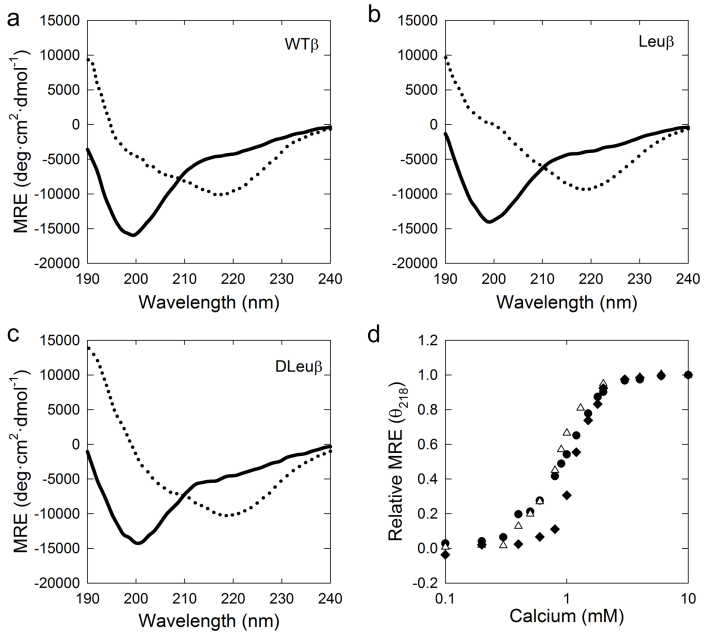

Figure 3.3: β-roll CD characterization. Mean residue ellipticity (MRE) were plotted over a range of wavelengths for WTβ (a), Leuβ (b), and DLeuβ (c) in the presence (• • •) and absence (—) of 10 mM $CaCl_2$. (d) Relative MRE at 218 nm for WTβ (●), Leuβ (Δ), and DLeuβ (♦) plotted over a range of calcium concentrations. All data were collected in triplicate in 50 mM Tris pH 7.4. Titration data were fit to the Hill equation using non-linear regression software and the resulting parameters are summarized in Table 3.1.

Terbium, a fluorescent calcium analog, was shown previously to trigger β-roll folding [19, 35]. In the folded conformation, bound terbium ions are in close proximity to a tyrosine residue in the 7th repeat of the β-roll. Excitation of the tyrosine residue results

in a fluorescence emission from the terbium ion proportional to the distance between the two [4]. A terbium titration was performed while monitoring this fluorescence emission and the resulting plot is available in the Supplemental Information. While this does not directly report calcium-induced folding, it is consistent with the CD and bis-ANS data suggesting that the DLeuβ mutant retains its intrinsic stimulus-responsive conformational behavior.

3.4.2 HS-DLeuβ Microrheology

An α-helical leucine zipper domain (H) and an unstructured hydrophilic linker (S) were appended to the N-terminus of the DLeuβ (Figure 3.2b). We previously demonstrated that this N-terminal fusion does not interfere with β-roll folding in response to calcium [35]. Self-assembly into non-covalently cross-linked supramolecular networks was analyzed by passive microrheology. Average mean square displacements (MSD) of 1 μm fluorescent particles embedded into the samples were calculated over a range of frequencies. Additionally, viscous and elastic moduli were extracted from the particle motion videos using an inverse Laplace transform method based on the generalized Stokes-Einstein equation [32]. Initial experiments were conducted at 6 wt%, the concentration at which HS-Leuβ self-assembles in calcium-rich environments. It should also be noted that 6 wt% HS-WTβ was shown to remain viscous regardless of the calcium concentration [35]. The results from these experiments are provided in Figure 3.4. HS-DLeuβ remained viscous in 50 mM $MgCl_2$ at 6 wt% (Figure 3.4a) and assembled into an a hydrogel network in the presence of 50 mM $CaCl_2$ (Figure 3.4b). All MSD vs. τ plots are available for all rheological experiments in the Supplemental Information.

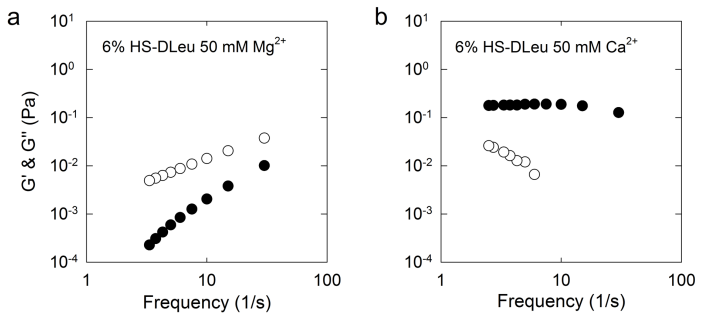

Figure 3.4: HS-DLeuβ microrheology results at 6 wt% (60 mg/mL). Viscous (○) and elastic moduli (●) were plotted over a range of frequencies in the presence of 50 mM $MgCl_2$ (a) or $CaCl_2$ (b). All mean square displacement (MSD) vs. τ plots are available in the Supplemental Information.

The rheology experiments were repeated at lower weight percentages to explore the lower critical protein concentration required for HS-DLeuβ self-assembly. The results at 4 wt% are shown in Figure 3.5a-e. Again, the HS-WTβ construct remained viscous in both magnesium (Figure 3.5a) and calcium (Figure 3.5b) rich solutions. HS-Leuβ appeared viscous in magnesium (Figure 3.5c) and remained largely viscous in calcium (Figure 3.5d) exhibiting a crossover frequency of approximately 12 sec^{-1}. HS-DLeuβ remained viscous in magnesium (Figure 3.5e) and self-assembled into a hydrogel in the presence of calcium (Figure 3.5f), similar to that observed at 6 wt%.

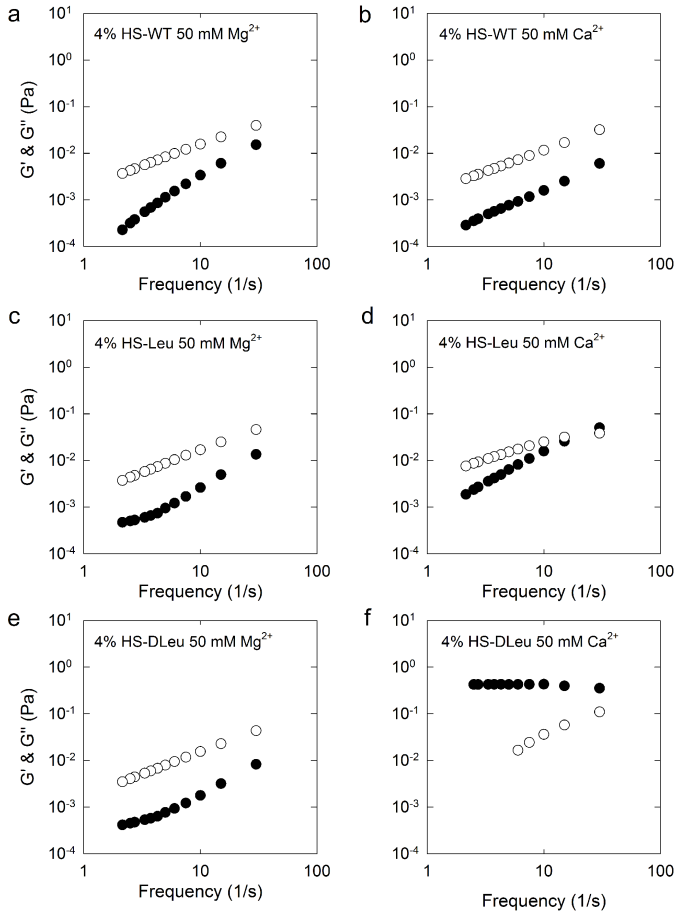

Figure 3.5: HS-WTβ (a,b), HS-Leuβ (c,d), and HS-DLeuβ (e,f) microrheology results at 4 wt% (40 mg/mL). Viscous (○) and elastic moduli (●) were plotted over a range of frequencies in the presence of 50 mM $MgCl_2$ (a,c,e) or $CaCl_2$ (c,d,f). All mean square displacement (MSD) vs. τ plots are available in the Supplemental Information.

3.4.3 MBP-DLeuβ Concatemer Microrheology

In order to assess the utility of DLeuβ as a stand-alone cross-linking domain, we genetically constructed concatemers of DLeuβ and MBP. The monomeric block is shown in Figure 3.2c. In this case, the linkers are either composed of a poly-asparagine linker

at the C-terminus of MBP or the unstructured capping group at the C-terminus of DLeuβ. Significantly higher weight percentages were required (21.3 wt%) to maintain the same molar cross-linking content used in the 6 wt% HS-β-roll experiments. Rheological analysis was performed as described above and the results are provided in Figure 3.6. A viscoelastic to elastic transition was observed when moving from magnesium rich (Figure 3.6a) to calcium-rich (Figure 3.6b) samples. Rheological analyses were also performed on samples with identical cross-linking content as the 4 wt% HS-β-roll experiments (14.2 wt%), and similar results were obtained. Samples prepared in the absence of calcium remained viscoelastic (Figure 3.6c) while samples prepared in 50 mM calcium self-assembled into elastic networks in the frequency range explored (Figure 3.6d).

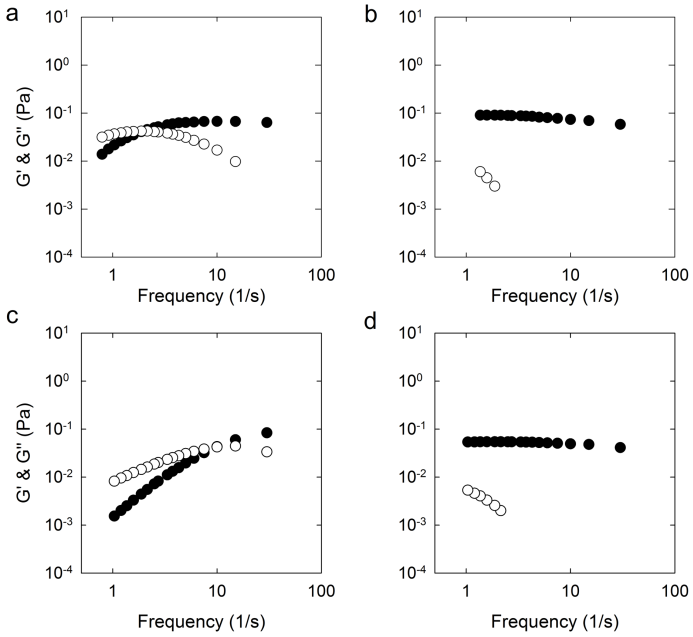

Figure 3.6: MBP-DLeuβ concatemer microrheology results. Samples were ran at equivalent cross-linking content as 6 wt% (a, b) and 4 wt% (c, d) experiments described previously. Total protein weight percentages are 21.3% (a, b) and 14.2% (c, d). Viscous (○) and elastic moduli (●) were plotted over a range of frequencies in the presence of 50 mM $MgCl_2$ (a, c) or 50 mM $CaCl_2$ (b, d). All mean square displacement (MSD) vs. τ plots are available in the Supplemental Information.

3.5 Discussion

In this work, we have rationally engineered a stimulus-responsive cross-linking peptide by exploiting the calcium-induced conformational change intrinsic to the β-roll domain. Unlike other environmentally responsive cross-linkers that rely on large swings in temperature or pH to destabilize cross-linking interactions, the Leuβ and DLeuβ require only small amounts of calcium to trigger self-assembly, providing a much gentler mechanism. Additionally, viscoelastic properties can be allosterically regulated by simply

adjusting the calcium concentration. Several biophysical techniques were used to investigate the structural responses of the mutant peptides to calcium, the lower critical protein concentration required for self-assembly, and the mechanical properties of the resulting supramolecular networks. We have shown previously that mutating one face of the β-roll peptide (Leuβ) has minimal impact on the affinity for calcium or the structural rearrangement induced upon calcium binding [35]. By mutating both faces to contain leucine residues (DLeuβ), we have substantially increased the solvent exposed hydrophobic surface area of the folded construct. Despite the significant increase in hydrophobicity, little effect on calcium responsiveness or protein solubility was observed for DLeuβ. Similar CD spectra were obtained in the presence and absence of 10 mM calcium for WTβ, Leuβ, and DLeuβ constructs (Figure 3.3a-c) indicating a disordered to β-sheet transition. Titrations yielded similar affinities for calcium (approximately 1 mM), however larger variations in the Hill coefficients were observed. Interestingly, both mutants bind calcium with a higher cooperativity than WTβ (Table 3.1). The data suggested that higher calcium concentrations were required to initiate folding, especially for the double mutant, most likely caused by the increased hydrophobicity of surface exposed side chains in the folded confirmation. Bis-ANS dye binding experiments were used supplement the CD data and ensure the DLeuβ mutant retained the calcium binding properties intrinsic to the WTβ domain. Significant increases in fluorescence emission were detected in calcium-rich solutions as compared to spectra obtained in the absence of calcium (Figure 3.7b, SI). This increase in fluorescence can be attributed to an increase in hydrophobic surface area amenable to dye binding caused by calcium-induced folding. These results are in agreement with previously reported

data for WTβ and Leuβ [19, 35]. Terbium binding assays were also conducted to further ensure the performance of the DLeuβ mutant. Figure 3.7a (SI) shows increases in fluorescence emissions as terbium concentrations are increased from 0-500 μM. Near identical responses were observed for WTβ and Leuβ in Chapter 2. However, it is important to note that while terbium acts as a calcium analog, it does not directly report calcium affinity. Taken together, the CD, bis-ANS, and terbium binding data suggest that all three constructs bind calcium in a similar manner resulting in a transition from a disordered state to a spatially organized β-roll structure.

After the preliminary characterization was completed, the self-assembly capabilities of DLeuβ were assessed by two separate approaches. First we expanded our previous study by appending an α-helical leucine zipper domain (H) and a soluble linker (S) to the N-terminus of DLeuβ (Figure 3.2b). Microrheology experiments performed at 6 wt% confirmed HS-DLeuβ self-assembly into a hydrogel in 50 mM $CaCl_2$ (Figure 3.4b) while remaining a viscous in 50 mM $MgCl_2$ (Figure 3.4a), thereby verifying what we have previously observed with Leuβ. Without calcium, the helical domains can assemble into tetrameric coiled-coil bundles, but the unstructured β-roll domains prohibit the formation of a macromolecular network. In 50 mM $CaCl_2$, we expect the β-roll domains to be fully folded thus localizing the leucine side chains into a structurally well-defined surface suitable for cross-linking. In our earlier work, the Leuβ peptide contained leucine residues on only one face of the folded β-helix which yielded a potential association number of 2 (Figure 3.2a). This required protein concentrations of 60 mg/mL (6 wt%) to induce self-assembly. At lower concentrations, there were not enough cross-links to sustain a macromolecular hydrogel. We hypothesized that by

designing a β-roll peptide with cross-linking interfaces on both sides of the folded construct, the association number could potentially be increased (Figure 3.2b). Association numbers higher than 2 should facilitate self-assembly at lower protein concentrations. To investigate this, we prepared 40 mg/mL (4 wt%) samples of HS-WTβ, HS-Leuβ, and HS-DLeuβ. Self-assembly was observed only for the HS-DLeuβ sample in calcium. All constructs remained viscous in the magnesium controls (Figure 3.5). Figure 3.5d suggested that the HS-Leuβ sample was viscoelastic as indicated by the crossover of the viscous and elastic moduli in the explored frequency range. However, as mentioned above, there are not enough cross-links to fully induce self-assembly into a hydrogel at 4 wt%. At protein concentrations below 4wt%, HS-DLeuβ assembled into several small elastic aggregates, but they did not constitute the entire volume, indicating fluctuations in local protein concentration (data not shown). These rheological experiments suggest that DLeuβ has a higher association number than the Leuβ construct.

To further test the utility of the DLeuβ as a stimulus-responsive cross-linking domain, we constructed concatemers of DLeuβ and MBP (Figure 3.2c), eliminating the α-helical leucine zipper domains. The microrheology results indicate similar calcium-dependent self-assembly properties as seen with the HS constructs (Figure 3.6). Both 21.3 wt% and 14.2 wt% samples in magnesium had significantly more viscoelastic character than the corresponding HS samples (Figure 3.6a, c). In order to normalize the cross-linking content between the HS and concatemer experiments, significantly higher protein concentrations were required due to the large size of MBP. However, a clear transition in mechanical properties was still observed for the concatemer samples at both weight percentages tested (Figure 3.6b, d). These results demonstrated that the DLeuβ

mutant has the ability to create enough elastically effective associations to actuate self-assembly in the presence of calcium, without depending on additional cross-linking provided by the leucine zipper domains.

The DLeuβ peptide is considerably different from other stimulus-responsive protein-associating domains used for hydrogel cross-linking. β-roll domains do not naturally participate in self-assembly or biomolecular recognition; the self-assembly capabilities were rationally designed and engineered into the stimulus-responsive domain itself. More commonly, a naturally associating domain is placed in an environment which destabilizes the cross-linking interactions such as higher pH, temperature or by addition of denaturation agents. In contrast, the DLeuβ can be easily modulated from disordered to structured and, in turn, sol to gel by simply adjusting the calcium concentration, providing a much gentler mechanism for self-assembly. This may also offer a convenient strategy to encapsulate small molecules inside a β-roll hydrogel. Target molecules can be incubated with soluble β-roll cross-linking domains after which calcium can be added to trigger macromolecular assembly, trapping small molecules inside. Catalytically active proteins can also be inserted in between β-roll cross-linking domains to create bifunctional stimulus-responsive enzymatic hydrogels. Future experiments are planned to investigate erosion rates, reversibility of self-assembly and to further elucidate the mechanical properties of the β-roll hydrogels. While the microrheology experiments clearly demonstrate a sol-gel transition, the absolute values of G' and G" are most likely distorted by the inverse Laplace transform analysis. Traditional oscillatory shear rheology over a larger time domain should provide more accurate measurements of the viscous and elastic moduli of these new materials.

3.6 Conclusions

In this work, we have described a calcium-responsive β-roll peptide with the ability to induce self-assembly into supramolecular networks. The β-roll scaffold was modified to create two hydrophobic surfaces suitable for cross-linking which are available only after calcium-induced structural rearrangement of the peptide. We have characterized the self-assembly capabilities of this domain by fusing an α-helical leucine zipper to the N-terminus and completing microrheology analysis. These chimeras were shown to self-assemble only in the presence of calcium. DLeuβ was also shown to self-assemble at lower protein concentrations than the single-faced mutant, indicating a higher association number. Furthermore, we have demonstrated the ability of the DLeuβ peptide to induce self-assembly without the additional cross-links provided by the leucine zipper by evaluating concatemers of DLeuβ and MBP. Thus we showed that Dleuβ can serve as a new cross-linking domain, capable of hydrogel formation, which can be allosterically-regulated via alteration of calcium concentrations.

3.7 Supplemental Information

Construct	Extinction Coefficient ($M^{-1}cm^{-1}$)
WTβ	17,780
Leuβ	16,500
DLeuβ	16,500
HS-WTβ	24,750
HS-Leuβ	23,470
HS-DLeuβ	23,470
MBP-DLeuβ-MBP-DLeuβ	162,440

Table 3.2: Extinction coefficients

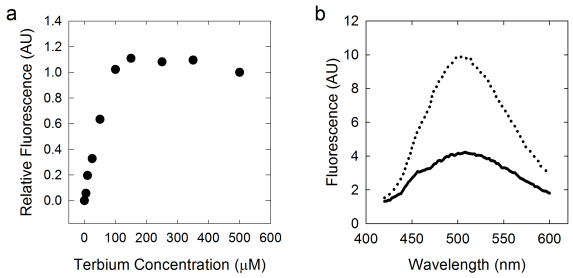

Figure 3.7: DLeuβ characterization. Terbium (a) binding results and bis-ANS (b) binding results in the presence (• • •) and absence (—) of 50 mM calcium for DLeuβ

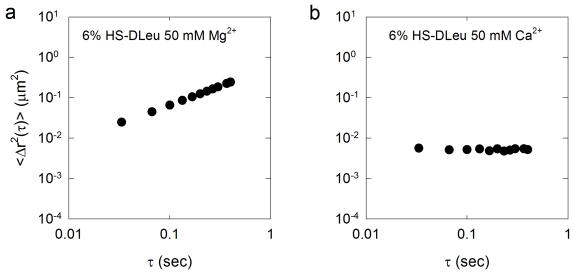

Figure 3.8: 6 wt% HS-DLeuβ MSD plots in 50 mM magnesium (a) and calcium (b)

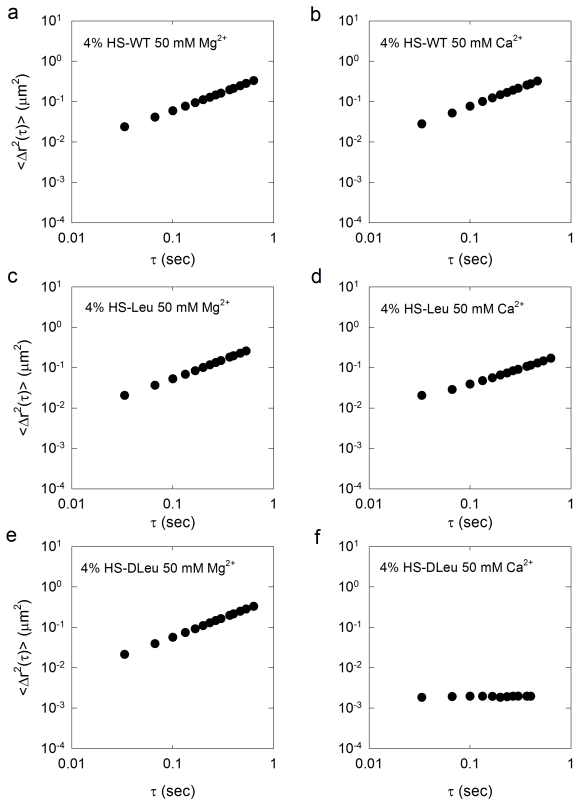

Figure 3.9: 4 wt% HS-WTβ (a,b), HS-Leuβ (c,d), and HS-DLeuβ (e,f) MSD plots in 50 mM magnesium (a,c,e) and 50 mM calcium (b,d,f)

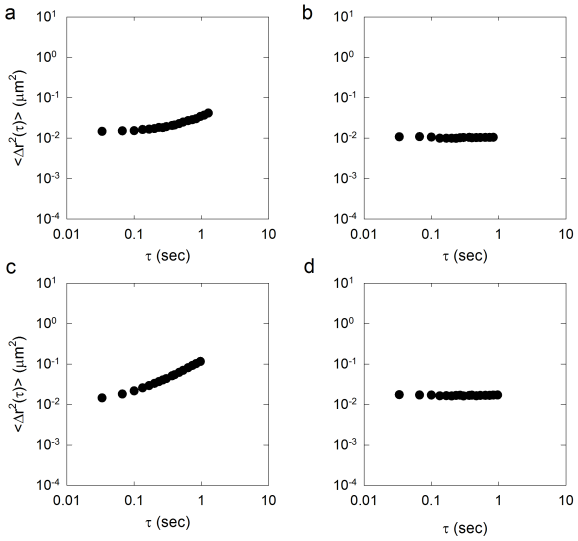

Figure 3.10: 21.3 wt% (a,b) and 14.1 wt% (c,d) MBP concatemer MSD plots in 50 mM magnesium (a,c) and calcium (b,d)

Chapter 4

A Designed RTX Domain for Calcium-Responsive Bioseparations

Project Collaborators: Kevin Dooley, Oren Shur, Matthew Baltimore, Mark Blenner & Scott Banta

A version of this chapter entitled, "A designed, phase changing RTX-based peptide for efficient bioseparations" appeared in BioTechniques volume 54, issue 4, pages 197-206. KD cloned all knockouts and AdhD constructs. KD completed all precipitation experiments, SDS-PAGE gels, and yield/activity analysis.

4.1 Abstract

Chromatography is typically the most costly and time consuming step in protein purification processes. As a result, alternative methods have been sought for bioseparations. One successful approach has been the use of stimulus-responsive tags that can reversibility precipitate out of solution. With an appropriate stimulus, target proteins can be efficiently and rapidly removed from complex solutions and purified. While effective, these tags tend to require either temperature changes or relatively harsh buffer conditions to induce precipitation. Therefore, there is a need for gentler alternatives. We have developed a synthetic peptide, based on the natural repeats-in-toxin (RTX) domain, which undergoes calcium-responsive, reversible precipitation. In this work, this tag is coupled to maltose binding protein and shown capable of efficiently purifying the fusion protein. The maltose binding protein fusion was appended to green fluorescent protein, β-lactamase and a thermostable alcohol dehydrogenase and we demonstrate that these constructs can also be purified using calcium-induced precipitation. Finally, protease cleavage downstream of the precipitating tag demonstrates that pure, active target protein can be obtained by cycling precipitations before and after cleavage. This

work presents a new stimulus-responsive precipitating tag that can be used for efficient bioseparations using gentler conditions that existing alternatives .

4.2 Introduction

Non-chromatographic purification techniques are of significant interest as chromatography is typically the most expensive step in protein purification [94]. Alternative approaches have been sought and these methods often rely on targeted precipitation of the protein. One approach is metal chelate affinity precipitation, where thermoresponsive copolymers can be used to specifically precipitate out poly-histidine tagged recombinant proteins [9, 70]. Another purely protein based approach is the use of thermoresponsive elastin-like peptides (ELPs) that precipitate with small temperature increases and consist of tandem repeats of the sequence VPGXG [83, 84]. ELPs undergo an inverse phase transition and aggregation, which is thought to be driven by the exposure of hydrophobic patches upon heating [129]. As part of a purification system, ELPs have been coupled to intein domains which have been genetically engineered into their minimal self-cleaving units [123]. When coupled, the ELP-intein system allows for a simple two stage purification scheme. In the first step, the ELP is triggered and the fusion protein is purified. Then, the intein is induced to cleave off the target protein and the ELP is again precipitated, leaving behind pure target protein [10]. While effective for many purification applications, the necessary heating of samples or the alternative use of high salt concentrations can be problematic in many situations [45]. Another protein-based non-chromatographic purification scheme developed by Ding et al. relies

on calcium-dependent precipitation of annexin B1 [34]. A self-cleaving intein has also been incorporated to remove the tag following purification.

Our interest in alternatives to chromatography is a product of discoveries made while exploring repeat scaffolds for protein engineering applications. Repeat scaffolds are of interest to protein engineers as their repetitive, predictable secondary structures make them ideal for both studying folding and engineering novel functions [31, 53]. Multiple examples exist of repeat scaffolds being engineered for biomolecular recognition, most notably the ankyrin repeats [16]. In order to improve the engineerability of these scaffolds, efforts have been made toward consensus design. Consensus design seeks to identify the core repeating peptide unit. Once this unit is identified, multiple repeats can be concatenated as necessary for the particular application. Consensus design approaches have been successfully used for a number of repeat scaffolds, including ankyrin repeats, tetratricopeptide repeats, and armadillo repeats [18, 78, 86, 91]. The ability to alter the size of a scaffold is of particular use when engineering binding, as the interface size can be tuned to the particular target.

In an effort to explore novel scaffolds for protein engineering, we have sought to identify a repeat scaffold which is also stimulus-responsive. Towards this end, we have investigated the calcium-responsive repeats-in-toxin (RTX) domain. The RTX domain is found in proteins secreted through the bacterial type 1 secretion system [59]. The domain consists of repeats of the consensus amino acid sequence GGXGXDXUX, where X is variable and U is a hydrophobic amino acid. One of the most well characterized RTX domains is the block V RTX domain from the adenylate cyclase toxin (CyaA) of *B. pertussis*. The domain is intrinsically disordered in the absence of calcium and

forms a β-roll structure (Figure 4.1a) in the presence of calcium [25]. Of note, the block V RTX domain retains its reversible calcium responsiveness even when expressed separately from the larger protein [13,19]. Previous efforts have been made to use RTX domains in protein engineering, including incorporation into mesh networks, design of synthetic RTX peptides, and hydrogel forming RTX domains [35,72,99,101].

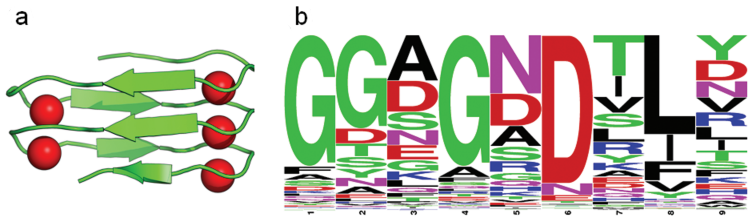

Figure 4.1: β-roll structure and sequence logo. (a) Crystal structure of β-roll domain from metalloprotease of *S. marcescens* (PDB: 1SAT). (b) Amino acid frequencies for a single β-roll repeat identifying consensus sequence GGAGNDTLY. Height of the letter corresponds to proportion of sequences containing the particular amino acid at that position. Sequence logo was generated using WebLogo.

Our original objective in this work was to design consensus RTX domains. Specifically, we identified the frequency of amino acids at each position of the nine amino acid repeat unit from a set of RTX-containing proteins (Figure 4.1b). This led to identification of the consensus sequence GGAGNDTLY. We then sought to create a library of consensus RTX constructs consisting of 5, 9, 13, or 17 repeats of the consensus unit. Upon purification of a number of these constructs, we observed that many of them precipitate in the presence of calcium. Therefore, we decided to explore the possibility for using these consensus β-roll tags (BRTs) as a tool for bioseparations, similar to the ELP system. Here, we report the use of BRTs to purify recombinant proteins. We first purify a maltose binding protein (MBP)-BRT17 fusion as a proof of principle. Then, this

MBP-BRT17 construct is fused to green fluorescent protein (GFP), which was used as a reporter during initial purification experiments. We have also fused β-lactamase and a thermostable alcohol dehydrogenase (AdhD) to demonstrate the feasibility of purifying enzymatic proteins. Finally, a specific protease site was engineered downstream of the tag to show target proteins can be fully purified by protease cleavage while retaining their activity.

4.3 Materials & Methods

4.3.1 Materials

All oligonucleotides were purchased from Integrated DNA Technologies (Coralville, IA). All enzymes for cloning experiments as well as the maltose binding protein expression system were purchased from New England Biolabs (Ipswich, MA). Isopropyl β-D-1-thiogalactopyranoside (IPTG) was obtained from Promega (Madison, WI). PAGE gels, protein ladder, and SimplyBlue SafeStain were obtained from Life Technologies (Grand Island, NY). All chemicals and other reagents were purchased from Sigma-Aldrich (St. Louis, MO) unless otherwise specified.

4.3.2 Cloning

Four different sized MBP-BRT fusions were prepared consisting of 5, 9, 13, or 17 repeats of the consensus RTX sequence (named BRT5, BRT9, BRT13, and BRT17). In order to generate the DNA fragment for BRT9, three oligonucleotides were synthesized: cons-beta-1, cons-beta-2, and cons-beta-3. 1 ng of each of these oligonucleotides was mixed

along with the primers cons1-AvaI-F and cons9-BseRI-HindIII-R. PCR was performed and a clean product was obtained and gel extracted. This fragment was digested with AvaI and HindIII and cloned into the similarly digested pMAL-c4E vector to generate pMAL-BRT9.

To generate the BRT5 construct, pMAL-BRT9 was used as a template for PCR with the primers cons1-AvaI-F and cons5-BseRI-HindIII-R. This product was digested with AvaI and HindIII and cloned into the pMAL-c4E vector producing pMAL-BRT5.

BRT13 was produced by concatenation of four additional repeats to BRT9. Concatenations were achieved using a recursive ligation technique we developed, similar to those previously described [82, 85]. This four repeat insert was amplified using primers cons1-BtsCI-F and cons4-BseRI-HindIII-R. The product was digested with BtsCI and HindIII and cloned into pMAL-BRT9 cut with BseRI and HindIII to yield pMAL-BRT13. BRT17 was produced analogously to BRT13, except that the reverse primer cons8-BseRI-HindIII-R was used instead of cons4-BseRI-HindIII-R.

The emGFP gene was amplified from Invitrogen pRSET/emGFP vector using primers GFP-BseRI-F and GFP-HindIII-R. The β-lactamase gene was amplified from the pMAL-c4E vector using primers βlac-BseRI-F and βlac-HindIII-R. AdhD was amplified out of pWUR85 using primers AdhD-BserI-F and AdhD-HindIII-R [24]. All three of these inserts were digested with BseRI and HindIII and cloned into similarly digested pMAL-BRT17 to yield pMAL-BRT17-GFP, pMAL-BRT17-βlac and pMAL-BRT17-AdhD.

The native enterokinase site in the pMAL-c4E vector, which sits between MBP and BRT17, was knocked out in the pMAL-BRT17-βlac and pMAL-BRT17-AdhD plasmids. Two rounds of site directed mutagenesis were required to change the native recogni-

tion site, DDDDK, to DDGEQ, which was shown to be resistant to cleavage. A novel enterokinase recognition site was also engineered downstream of BRT17 in these constructs to allow for purification of the untagged protein of interest. All oligonucleotide sequences can be found in the publication listed at the beginning of this chapter.

4.3.3 Expression and Purification

For expression and cloning, Invitrogen Omnimax T1 *E. coli* cells were used. 1 L cultures of TB supplemented with 100 µg/mL ampicillin and 0.2% glucose were inoculated with 10 mL of overnight culture. Cultures were grown at 37 °C with shaking at 225 RPM to an approximate OD_{600} of 0.6 and induced with 0.3 mM IPTG. Cells harboring pMAL-BRT17 and pMAL-BRT17-βlac were allowed to express for an additional 2 h and harvested. Cultures transformed with pMAL-BRT17-GFP were transferred to a shaker at 25 °C and allowed to express for an additional 16 h and then harvested as no fluorescence was observed when expressed at 37 °C. Cultures transformed with pMAL-BRT17-AdhD were allowed to express at 37 °C for an additional 16 h as previously reported [24]. Cells were harvested after expression and resuspended in 1/20 culture volume of 50 mM Tris-HCl, pH 7.4 for precipitation purification. For amylose resin purification, cells were resuspended in 1/20 culture volume of MBP column buffer (20 mM Tris-HCl, 200 mM NaCl, 1 mM EDTA, pH 7.4). In both cases, cells were subsequently lysed via sonication using 15 second pulses for a total of 150 seconds. Lysate was then clarified by centrifugation at 15,000 x g for 30 min at 4 °C. For amylose resin purification, clarified lysate was diluted with five volumes of column buffer and purified as previously described [19]. All subsequent steps were performed at room

temperature.

For precipitation purification, clarified lysate was added to a concentrated calcium stock as indicated by the calcium concentration in the data presented. For example, for precipitation of MBP-BRT17 lysate in 100 mM $CaCl_2$, 950 μL of clarified lysate was added to 50 μL of 2M $CaCl_2$ solution. The sample was promptly mixed by gentle pipetting and allowed to sit at room temperature for 2 min. The sample was then centrifuged at 16,000 x g in a microcentrifuge for 2 min. The supernatant was carefully removed and the pellet was resuspended in the same Tris buffer by gentle pipetting. The turbid solution was centrifuged and washed for four additional cycles. For the final step, the pellet was resuspended in Tris buffer with a concentration of EGTA equivalent to the original calcium concentration. Gentle pipetting was sufficient to cause the sample to redissolve as confirmed by observation and the lack of a precipitate upon subsequent centrifugation.

4.3.4 Recovery, Activity and Fluorescence Assays

Concentrations of all purified proteins were determined by 280 nm absorbance using calculated extinction coefficients. A table of all extinction coefficients is provided in the Supplemental Information. Recovery of MBP-BRT17 both by amylose resin purification and precipitation was determined using solely this method.

MBP-BRT17-GFP recoveries were estimated by comparing fluorescence emission intensity at 509 nm with excitation at 487 nm. 100-fold dilutions of both clarified lysate and purified protein were made for fluorescence measurements. Purified proteins were resuspended in the same volume as the lysate from which they were extracted, so

signals were compared directly.

For estimation of MBP-BRT17-βlac recovery, protein was added to a nitrocefin solution and the absorbance at 486 nm was tracked corresponding to the hydrolysis of nitrocefin. 500 µL of nitrocefin solution was prepared by placing three nitrocefin disks (Fluka) in 450 µL 50 mM Tris-HCl, pH 7.4 and 50 µL DMSO. In each sample well, 50 µL of this solution was mixed with 90 µL of the same Tris buffer and 10 µL of protein sample. For each sample tested, serial dilutions from 1X to 1000X were prepared from lysate and purified protein. Initial rates were determined by measuring the change in absorbance at 486 nm over the first 10% of the change in signal between the starting absorbance and the end absorbance. The same nitrocefin stock solution was used for all samples to account for variations in concentration. MBP-BRT17-AdhD recovery was also evaluated by enzymatic activity using a protocol previously described [24]. Since this alcohol dehydrogenase has been isolated from the hyperthermofile *Pyrococcus furiosus*, all samples were heat treated at 80 °C for 1 h prior to evaluating activity. All assays were performed at saturated conditions of both cofactor and substrate, 0.5 mM NAD+ and 100 mM 2,3-butanediol, respectively. Reaction mixtures containing 2,3-butanediol and protein sample in 50 mM glycine pH 8.8 were incubated at 45 °C in a 96 well UV microplate in a spectrophotometer. Reactions were initiated by the addition of NAD+. Initial rates were calculated by following the production of NADH at 340 nm. Specific activity of cleaved AdhD was calculated using an NADH extinction coefficient (ε_{340} = 6.22 mM^{-1} cm^{-1}). All spectroscopic measurements were done on a SpectraMax M2 spectrophotometer (Molecular Devices, Sunnyvale, CA).

4.4 Results & Discussion

In order to identify the consensus RTX sequence, a database of RTX containing proteins was constructed by a search of the UniProt database for hemolysin-type calcium binding domains. Individual repeats were identified and the frequency of amino acids at each of the nine repeat positions was determined (Figure 4.1b). From this result, the repeat sequence GGAGNDTLY was identified as the consensus sequence. For a few of these positions, other amino acids were found with nearly equal frequency. However, as this sequence was found to be effective for purification, further investigation on sequence variation was not performed. A variety of synthetic RTX domains of different lengths (5, 9, 13, and 17 repeats) were prepared as fusions to the C-terminus of MBP. These lengths were chosen based on the natural variability in the lengths of RTX domains. These BRT constructs were named BRT5, BRT9, BRT13, and BRT17, with numbers denoting the number of repeats. Unexpectedly, we observed that upon the addition of calcium to the purified BRT17 construct, there was significant precipitation out of solution, which was reversed upon the addition of the chelating agent, EGTA.

In order to more thoroughly characterize the observed precipitation behavior, cells were induced to express the four MBP-BRT constructs. Clarified cell lysates were prepared from these four cultures and were then titrated with calcium to assess precipitation behavior. Briefly, 1 mL of clarified cell lysate was mixed with calcium chloride solution at the indicated concentrations, clarified by centrifugation, and the mass of the pellet measured (Figure 4.2). Due to possible variations in cell growth rates and densities, all cultures were started from saturated overnight cultures and induced simultaneously. Both BRT13 and BRT17 precipitated when calcium concentrations exceeded

25 mM. Some precipitation was observed from BRT5 and BRT9 lysate, similar to what was observed with control cell lysate. Addition of an equivalent concentration of EGTA allowed the pellets to quickly dissolve again upon gentle pipetting.

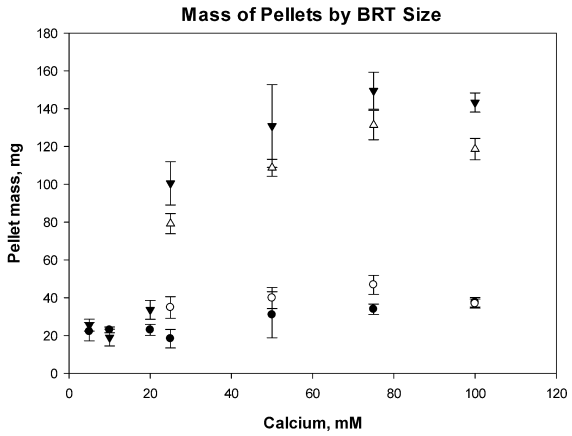

Figure 4.2: Mass of precipitated pellet versus calcium chloride concentration and BRT size. Results for MBP-BRT5(●), MBP-BRT9(○), MBP-BRT13(▼), and MBP-BRT17(△). Error bars represent standard deviations for 3 trials.

While both BRT13 and BRT17 precipitated upon calcium addition, it was observed that the BRT17 formed a pellet that was easier to clarify and was selected for further examination. Three additional constructs were prepared by fusing MBP-BRT17 to the N-terminus of GFP, β-lactamase, and AdhD, all of which are well-folded proteins. (named MBP-BRT17-GFP and MBP-BRT17-βlac, MBP-BRT17-AdhD respectively). These three proteins were fused to MBP to allow for amylose resin chromatography purification as an orthogonal comparative technique. GFP was chosen as a reporter protein for initial purification experiments to track the location of the BRT. β-lactamase and AdhD were chosen as they are well characterized enzymes with straightforward

assays to assess activity.

The folding of RTX domains into β-roll secondary structures is highly calcium-specific. Therefore, we were interested in whether or not the precipitation behavior observed was also calcium-specific. To test this, MBP-BRT17-GFP was purified on an amylose resin and diafiltered into salt-free Tris buffer. Diafiltration was necessary as proteins are purified in high salt buffer for the amylose resin and it was observed that BRT precipitation was significantly reduced in high salt. This is consistent with previous observations that RTX calcium affinity is reduced with increasing salt concentration [111]. Solutions of various salts were added to final concentrations of 100 mM. The samples were then gently mixed by pipetting, allowed to sit for 2 min, and centrifuged at 16,000 x g in a microcentrifuge for 2 min. Tubes were then inverted and the presence of a pellet at the top was indicative of precipitation (Figure 4.3). BRT precipitation was observed to be calcium-specific, with near complete precipitation of MBP-BRT17-GFP (as indicated by the remaining color in solution) in calcium and no precipitation in other salts. While this behavior does not establish the formation of a β-roll structure, it does indicate that at least one property of the β-roll is preserved in these constructs.

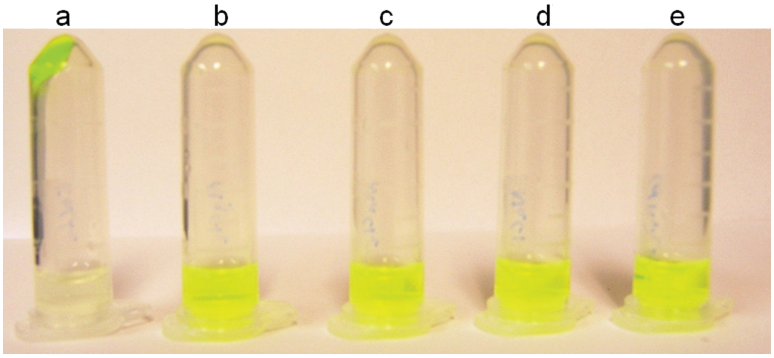

Figure 4.3: Ion specificity of BRT precipitation. Purified MBP-BRT17-GFP was mixed with 100 mM of the compound indicated, and centrifuged to collect any pellet. The tube was then inverted such that precipitated protein remained on top. The compounds were as follows: (a) $CaCl_2$, (b) $MgCl_2$, (c) $MnCl_2$, (d) NaCl, and (e) $(NH_4)_2SO_4$.

For all four constructs tested, calcium concentrations greater than 25 mM were found to cause precipitation of the fusion protein. To assess the ideal calcium concentration, all four constructs were precipitated from 1 mL of clarified cell lysate in 25, 50, 75, and 100 mM calcium chloride. Pellets were washed in salt-free Tris buffer five times. Pellets were broken up upon washing, but did not redissolve until exposed to an equivalent concentration of EGTA after the final wash. The 100 mM $CaCl_2$ samples were found to not fully redissolve, so only lower $CaCl_2$ concentrations were tested further. A slight increase in recovery was observed at 75 mM $CaCl_2$ (as compared to lower $CaCl_2$ concentrations) as confirmed by SDS-PAGE (data not shown). All four constructs were subsequently purified by precipitation with 75 mM $CaCl_2$ and SDS-PAGE gels were run after five washes (Figure 4.4). No significant difference was found with increasing number of washes, so further quantification and recovery measurements were performed on samples washed five times. To confirm scalability, the analogous protocol was also performed on 50 mL lysate, and comparable results were obtained (data not shown).

Additionally, we briefly tested the reversibility of the precipitation process. It was found that addition of calcium to the redissolved pellet in EGTA solution did yield a pellet once again. However, full pellet size was only recovered after dialysis into EGTA-free buffer.

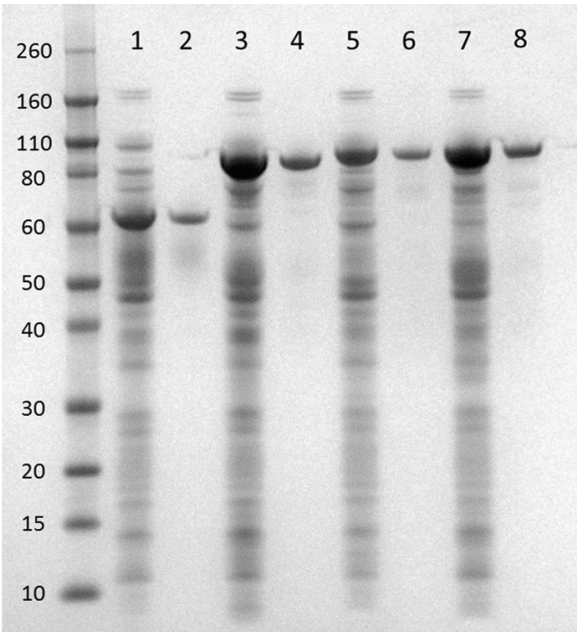

Figure 4.4: SDS-PAGE results for purification of four fusion constructs tested. Numbers are standard size in kDa. Expected molecular weights for MBP-BRT17, MBP-BRT17-GFP, MBP-BRT17-βlac, and MBP-BRT17-AdhD are 57.1, 83.4, 88.6, and 89.1 kDa, respectively. (1-2) Purification of MBP-BRT17. Lane 1 is clarified lysate, and 2 is purified fusion protein. (3-4) Same samples for purification of MBP-BRT17-GFP. (5-6) Same samples for MBP-BRT17-βlac. (7-8) Same samples for MBP-BRT17-AdhD.

We next sought to quantify the recovery and functionality of the purified proteins after precipitation. To assess recovery of MBP-BRT17, we used the theoretically determined extinction coefficient to estimate concentration by absorbance at 280 nm (57). Results from purifying the construct on an amylose resin were compared to BRT precip-

itation. For MBP-BRT17-GFP, recoveries were calculated as the percentage of fluorescence signal of purified sample compared to lysate (this was normalized against control lysate). Along with total protein recoveries estimated by UV absorbance, recoveries of both MBP-BRT17-βlac and MBP-BRT17-AdhD were estimated by comparing lysate activity to activity of these constructs after purification. MBP-BRT17-βlac recoveries were calculated using activity measured by tracking the absorbance at 486 nm for the hydrolysis of nitrocefin. MBP-BRT17-AdhD recoveries were calculated by tracking NADH formation at 340 nm in saturating conditions of both substrate and cofactor. Results of these trials are shown in Table 4.1. For MBP-BRT17, calcium precipitation recovers about double the amount of protein as compared to amylose resin purification.

	MBP-BRT17	MBP-BRT17-GFP		MBP-BRT17-βlac		MBP-BRT17-AdhD	
Calcium, mM	Fold vs. Resin	Fold vs. Resin	Fluores. Recovered	Fold vs. Resin	Activity Recovered	Fold vs. Resin	Activity Recovered
25	2.0 ± 0.1	2.8 ± 0.1	61 ± 3%	4.1 ± 0.1	1.6 ± 0.1%	1.6 ± 0.1	3.8 ± 0.5%
50	2.3 ± 0.1	3.7 ± 0.1	86 ± 6%	5.3 ± 0.2	4.0 ± 0.1%	1.7 ± 0.1	4.7 ± 0.7%
75	2.2 ± 0.2	2.8 ± 0.3	78 ± 8%	5.1 ± 0.2	3.4 ± 0.1%	2.2 ± 0.1	8.3 ± 1.4%

Table 4.1: "Fold vs. Resin" denotes protein quantity recovered relative to amylose resin for equivalent loading amount. For MBP-BRT17-GFP, MBP-BRT17-βlac, and MBP-BRT17-AdhD fluorescence and activity are the respective properties relative to clarified lysate. Errors represent standard deviations. All data were collected in triplicate.

For MBP-BRT17-GFP, we observed up to 86% recovery of fluorescence. MBP-BRT17-βlac recovery from the lysate was not as high, but was still 5-fold better than the amylose resin, yielding a significant quantity of protein. Similar results were also observed for MBP-BRT17-AdhD, although the yields were not quite as high compared

to the resin (2-fold improvement). The activities recovered in Table 4.1 are seemingly low, but still out performed the amylose resin purification. Small errors may have been introduced while assessing the fusion protein activity in crude lysate, even though we have accounted for endogenous hydrolysis (β-lactamase) and reduction (AdhD). Table 4.2 lists the absolute yield of each fusion protein in mg/mL based on UV absorption at 280 nm. All fusion proteins were shown to be purified in high yields.

Calcium, mM	MBP-BRT17	MBP-BRT17-GFP	MBP-BRT17-βlac	MBP-BRT17-AdhD
25	268 ± 11	333 ± 12	124 ± 3	198 ± 3
50	305 ± 14	434 ± 17	160 ± 7	273 ± 9
75	295 ± 26	336 ± 40	176 ± 5	214 ± 6

Table 4.2: Absolute yield of precipitated constructs given in mg/mL. Values were determined using UV absorbance at 280 nm and calculated extinction coefficients available in the Supplemental Information. All data were collected in triplicate and errors represent standard deviations.

To increase the utility of this tag, it would be beneficial to couple our system with a cleavage tag to separate the protein of interest from the BRT. The pMAL-c4E vector we used for these experiments contains a cleavable enterokinase site between the MBP and BRT. This recognition sequence was removed via site directed mutagenesis. A new enterokinase site was engineered between the BRT and the protein of interest for MBP-BRT17-βlac and MBP-BRT17-AdhD. Therefore, as a proof of principle, we took precipitation purified MBP-BRT17-βlac and MBP-BRT17-AdhD and subjected them to overnight cleavage by enterokinase digestion. Calcium can then be added directly to the cleavage reaction to precipitate MBP-BRT17, thereby separating the tag from the protein of interest following centrifugation. These results are given in Figure 4.5 for MBP-BRT17-AdhD, showing pure, soluble protein by SDS-PAGE.

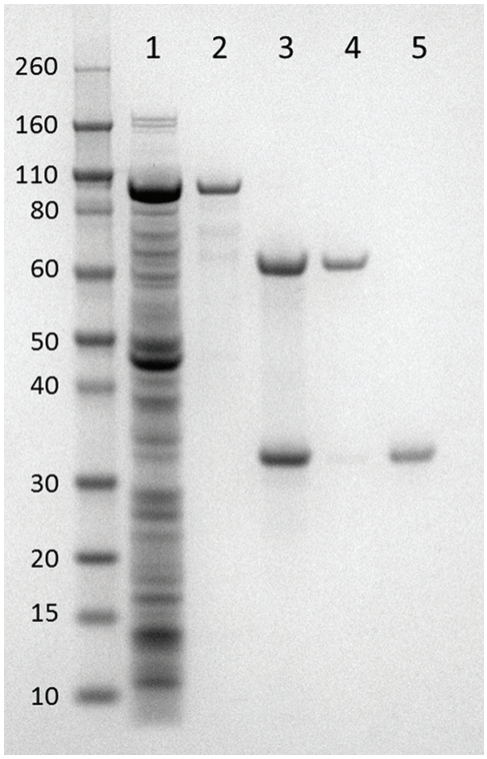

Figure 4.5: SDS-PAGE results for purification and cleavage of AdhD. Numbers are standard size in kDa. Estimated molecular weight for AdhD is 31.9 kDa. (1) Clarified MBP-BRT17-AdhD lysate. (2) Purified fusion protein. (3) Enterokinase cleavage. (4) Precipitated MBP-BRT17. (5) Soluble AdhD. 3x protein concentrations were used in lanes 3, 4, and 5.

Recoveries of $93 \pm 7\%$ were obtained by tracking UV absorbance at 280 nm, meaning 93% of the AdhD in the precipitation purified sample was recovered after cleavage and reprecipitation of the tag. Specific activity of the purified enzyme was also calculated to be 20.2 ± 1.3 min^{-1}, which is similar to what has been previously reported, indicating this system has little to no effect on protein structure or function [24]. However, in the case of MBP-BRT17-βlac, the cleaved β-lactamase remained in the insoluble fraction following enterokinase cleavage and calcium precipitation. Upon further investigation

it was found that β-lactamase will precipitate in high calcium concentrations. As a control experiment, we purchased recombinant β-lactamase and observed similar behavior. In 75 mM calcium, an insoluble pellet was formed upon centrifugation. Activity assays confirmed a significant amount of active protein in the insoluble fraction (data not shown). This illustrates a caveat of the BRT system. Proteins that naturally precipitate in calcium solutions cannot be efficiently separated from the BRT. For future improvement of this system, the protease used could be fused to the precipitating BRT or a self-cleaving intein could be incorporated. Fusing the protease to the BRT would enable its removal from the target protein in the final precipitation. A self-cleaving intein would fulfill a similar function. It should also be noted that the BRT can precipitate without being fused to MBP, suggesting MBP is not essential for this system, however MBP may be useful to improve protein expression levels.

It is not completely clear why these consensus RTX constructs are able to function as a bioseparations tag. We do observe a correlation between length and precipitation (Figure 4.2), so size certainly plays a role. However, there has not been extensive work in studying the role of number of repeats on RTX behavior. We recently studied the impact of altering the number of native RTX repeats in the block V CyaA RTX domain of *B. pertussis* but no significant size effect was observed and, further, a C-terminal capping was required for calcium responsiveness [104]. As for past efforts at synthetic RTX domains, the synthetic domains created by Scotter et al. consisted of 4 RTX repeats and those prepared by Lilie et al. consisted of 8 repeats [72, 101]. The peptides create by Lilie et al. were weakly calcium-responsive, while those of Scotter et al. were only lanthanum responsive and formed partially insoluble filaments in the

presence of lanthanum. In general, it is fairly well established that beta sheets are prone to aggregation and nature uses various strategies to ensure solubility, so perhaps BRTs are a balance between this tendency and the calcium responsiveness of the β-roll [98]. Further investigation will be required to better elucidate the mechanism of BRT functionality, but their use as a tool for protein purification is clear.

4.5 Conclusions

The technique described here offers a new stimulus-responsive phase-changing peptide that could be useful in a range of applications similar to those for which ELPs have been used, such as recombinant protein purification or in the creation of "smart" biomaterials. This tag possesses certain advantages over ELPs and annexin B1 since precipitation is simpler to achieve and the BRT is significantly smaller. Additionally, BRT17 precipitates in as little as 25 mM calcium chloride at room temperature compared with larger ionic strength and higher temperature increases required for ELP precipitation. Precipitation also occurs instantaneously, whereas annexin B1 based systems require a 2 h incubation period at 4°C. Overall, BRTs offer a new tool for rapid purification of recombinant proteins. The protocol described here can be performed to obtain purified fusion protein from lysate in only a few minutes. Further optimization of the BRT system should enable the use of specific proteases to purify target proteins and further improve the precipitation and resolubilization process, greatly enhancing the ability to rapidly purify recombinant proteins.

4.6 Supplemental Information

Construct	ε_{280}, $M^{-1}cm^{-1}$
MBP-BRT17	91,680
MBP-BRT17-GFP	113,695
MBP-BRT17-βlac	119,765
MBP-BRT17-AdhD	144,175
AdhD	52,370

Table 4.3: Extinction coefficients

Chapter 5

Engineering the RTX Domain for Calcium-Dependent Molecular Recognition

Project Collaborators: Kevin Dooley, Oren Shur, Raymond Bellon, Geza Szilvay, Mark Blenner & Scott Banta

A version of this chapter is being prepared for publication. KD prepared DNA library, completed all ribosome display experiments, and B1β characterization.

5.1 Abstract

Typically, antibody and antibody fragments have filled the demand for new molecular recognition elements required for clinical diagnostic exams, protein-based biosensors, therapeutic treatment strategies, and a host of other applications in biomedical engineering and biotechnology. However, non-immunoglobulin protein scaffolds recently emerged as viable alternatives which improve on many of the roadblocks faced by antibodies while maintaining similar degrees of affinity and specificity. We identified the repeats-in-toxin (RTX) domain as one such scaffold. These domains are conformationally dynamic and intrinsically disordered in the absence of calcium. Calcium-rich environments induce a reversible structural rearrangement to a compact, stable β-roll structure. We plan to use this calcium triggered conformational change as a peptide switch to modulate a designed binding interface thereby generating an allosterically regulated binding domain. The β-roll provides a flat, stacked β-sheet surface amenable to mutations. We designed a β-roll library by randomized 8 surface exposed residues on this β-sheet face. As a proof-of-concept work, we evolved a mutant RTX domain with low micromolar affinity for a model protein, lysozyme, via ribosome display. The binding affinity and energetic profile were evaluated by isothermal titration calorimetry. We

also evaluated the practical utility and stimulus-responsive behavior of the mutant RTX domain by attempting to capture the target protein in a calcium-rich packed column.

5.2 Introduction

Advances in combinatorial protein engineering techniques and high throughput screening have allowed researchers to explore alternatives to full-length immunoglobulin (Ig) domains to address critical problems in biomedicine and biotechnology. Several non-Ig based proteins have been engineered for applications in large-scale affinity chromatography, *in vivo* imaging, diagnostic screening, biosensor development, and cancer therapy with several constructs progressing into clinical trials [14, 126, 127]. Traditionally, antibodies have filled the demand for new, engineered molecular recognition elements. As nature's preferred method for immunological response, antibodies possess the ability to bind to a staggering array of antigens. The affinity and specificity to which antibodies bind their targets is predicated on the selection of an optimal binding interface from a large, diverse library. This process has been successfully mimicked in the laboratory giving rise to FDA approved engineered antibodies for therapeutic applications, responsible for generating billions in revenue annually [42].

However, this paradigm has been challenged in recent years by an emergent class of protein scaffolds. Small, single domain proteins devoid of disulfide bonds are becoming increasingly popular as starting frameworks for engineering molecular recognition. These scaffolds maintain the potential to achieve similar levels of affinity and specificity as full length antibodies while improving on many of the drawbacks discussed

in Chapter 1 including large size, post-translational modification requirements, and low levels of recombinant expression. In-depth reviews on several of these domains are available [11, 17, 51, 58, 75, 88, 107]. One such scaffold that fits these criteria is the calcium-responsive RTX protein. In previous chapters, the RTX domain was evaluated as a physical cross-linker in stimulus-responsive biomaterials development and as a protein purification tag. Here we aim to investigate the RTX domain as a potential scaffold for engineering molecular recognition. Moreover, we aim to use the peptide's calcium-induced structural rearrangement to modulate an engineered binding interface to explore a calcium-specific "capture and release" strategy for chromatographic purification.

Antibodies are commonly used in immunoaffinity applications to capture analytes of interest with achievable affinities in the nano- to picomolar range [44, 100]. Commercially available products, including sepharose beads and agarose resins, conjugated with engineered antibodies are marketed for purification of host cell proteins such as DNA/RNA polymerases, growth factors, and ligases (Sigma-Aldrich, Neoclone). Since immunoglobulins bind their targets with such high affinities, a critical challenge lies in creating effective strategies to release the captured target from the antibody. Typically, protein denaturants or large swings in pH are required to destabilize the antibody-antigen complex and recover the target molecule [63, 114]. These extreme conditions can often irreversibly damage both the target and the immobilized antibody causing a drop in functional analyte recovery and an abbreviated column lifetime [22]. Here we propose to evolve the RTX domain to bind a target protein with similar affinity and specificity as immunoglobulin domains while in the calcium-bound β-roll conformation.

By removing the calcium from the system, the engineered binding face will lose its structure thereby releasing the target molecule. Combining the molecular recognition advantages of antibodies with a simple release mechanism will offer an attractive system for chromatographic purification as well as other biotechnology applications.

5.2.1 Directed Evolution

There are several methods available to protein engineers for generating biomolecules with novel functions for research and clinical applications including computational and rational design. The most common method used to produce new molecular recognition elements is directed evolution. Modeled after the natural evolutionary process, directed evolution is based on applying selective pressure to a protein library in order to isolate a variant with a desired phenotype (affinity, catalytic activity, stability, etc.). This cyclic process is outlined in Figure 5.1. After identifying the RTX domain as a potential scaffold, a library of mutant RTX proteins was constructed. The folded RTX domain is composed of two parallel β-rich faces separated by flexible turn regions. This stacked β-sheet face is structurally similar to the binding interface of leucine rich repeat proteins, which naturally participate in biomolecular recognition. The side chains of the 7th and 9th residues in the glycine/aspartate rich repeating sequence (GGXGXD**X**U**X**) are solvent exposed and highly variable in naturally occurring RTX domains. The library was built by using overlapping oligonucleotides such that the 7th and 9th position in every other repeat was randomized. By doing this, the mutated positions form a contiguous surface in the calcium-bound β-roll conformation. The library construction process is outlined in Figure 5.2.

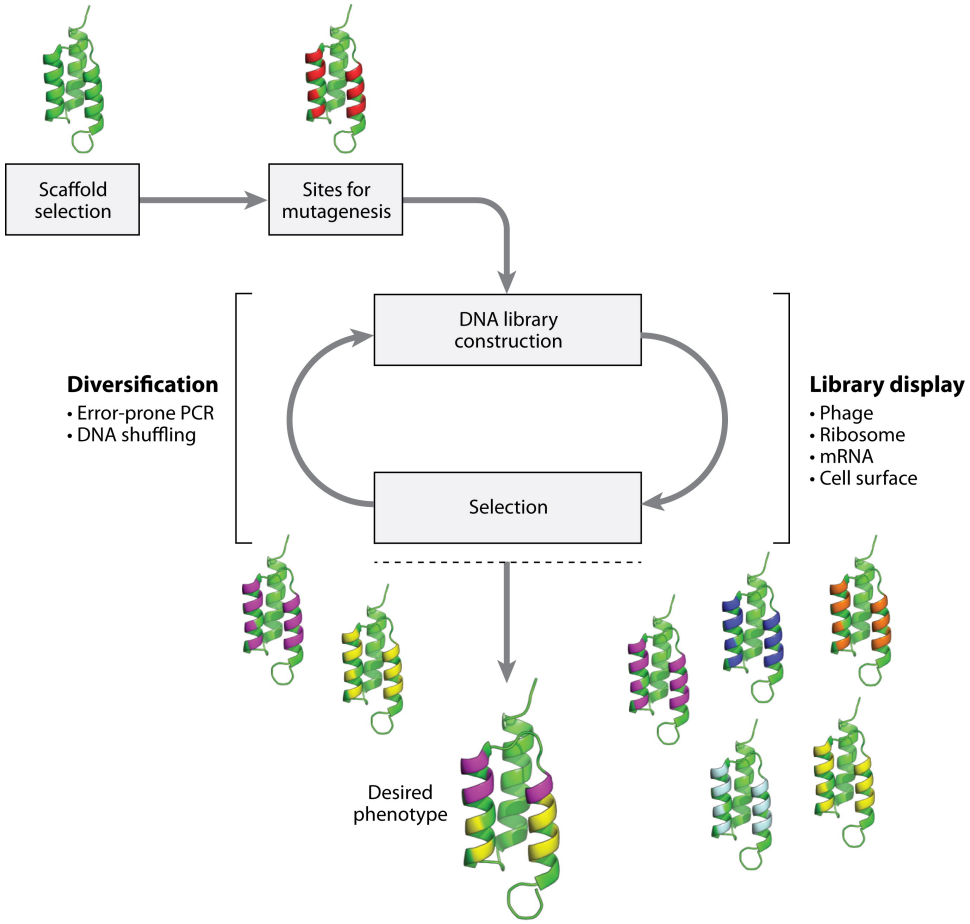

Figure 5.1: Directed evolution cycle for isolating new binding proteins. A suitable scaffold is selected and sites for mutagenesis are identified. A library of mutants is constructed at the DNA level and selected at the protein level using a library display technology. Library diversity can be added back to the system through error-prone PCR, DNA shuffling or some other mutagenesis technique. The cyclic process is repeated until the desired phenotype is achieved.

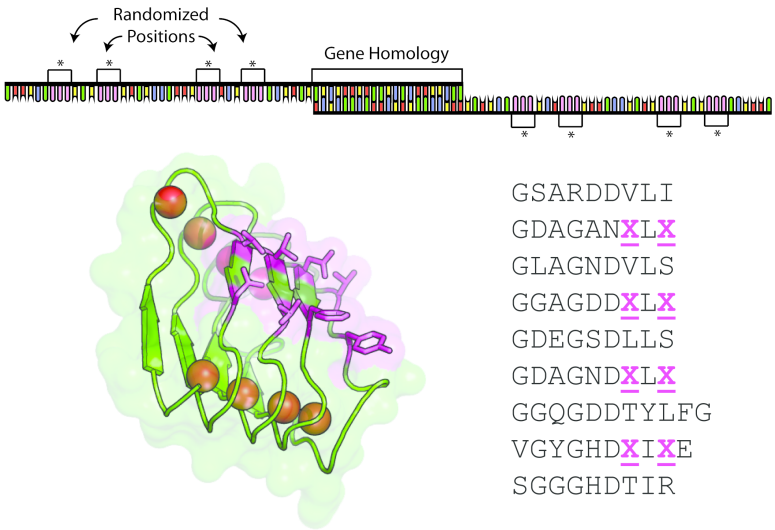

Figure 5.2: RTX library construction. Two long oligonucleotides coding for the entire β-roll gene were used to create the RTX library. Eight randomized positions were created by inserting NNK codons at the indicated positions. The oligonucleotides were annealed and extended. The resulting randomized protein is shown in the folded conformation with the bound calcium ions shown in red and the randomized surface shown in pink. The primary sequence is shown with the randomized positions underlined.

Once a library is constructed on the DNA level, the cognate translated protein constructs must be evaluated for the desired phenotype. A linkage is required between the translated mutant proteins and the genetic information that codes for them. This genotype-phenotype linkage can be achieved through a variety of available display technologies and is critical for any directed evolution experiment. Some common methods include compartmentalizing DNA inside a carrier vehicle such as bacteriophage (phage display) or *E. coli*/*S. cerevisiae* (cell surface display) while displaying the translated protein on the outside of the carrier. Other methods directly (mRNA display) or indirectly (ribosome display) link the genetic material to the associated protein through covalent bonds. All of these technologies are well documented and some are sold commercially in kits [39, 40, 49, 74, 95, 97, 113, 116].

5.2.2 Ribosome Display

For this work, we elected to use ribosome display to select for molecular recognition against a model protein, lysozyme. This technology offers several advantages over some of the more conventional techniques like phage or cell surface display. It is a completely *in vitro* method that allows for more diverse libraries to be selected against [93]. DNA libraries are not restricted by inefficient transformation into *E. coli* or yeast for expression. Instead, the libraries are produced in their protein form using purified cell extracts containing all of the required machinery for transcription and translation. A description of the ribosome display process is given in Figure 5.3 and has been outlined previously [39, 40, 93]. The RTX library is first cloned into the ribosome display vector (pRDV) which provides a T7 promoter and a ribosome binding site. The gene for an

unstructured portion of the endogenous *E. coli* tolA protein lies directly downstream of the RTX library in pRDV. The sole function of this protein, in this context, is to act as a spacer and allow the translated protein of interest to exit the ribosomal tunnel. The library and spacer are amplified by PCR using primers which anneal outside of the promoter and in the middle of the tolA spacer. It is important to note here that the amplicon does not include a stop codon. The amplified library is transcribed *in vitro* producing an mRNA strand coding for the RTX mutant and the tolA spacer. 5' and 3' stem loops help stabilize and protect the mRNA strand from ribonuclease degradation. The mRNA strands are then translated in the presence of *E. coli* extracts. Since there is no stop codon present, the protein remains covalently attached to the tRNA inside the ribosome, with the tolA spacer allowing the protein of interest to fold outside of the tunnel in solution.

Ternary complexes composed of the ribosomal subunits, mRNA strand, and nascent folded protein can then be used for selection against an immobilized target. In this work, biotinylated lysozyme was immobilized on streptavidin coated microtiter plates and incubated with the ternary complexes. Weakly bound mutants were removed by stringent washes. Surviving library members were recovered by dissociating the ribosomal proteins thereby releasing the mRNA into solution. mRNA stands coding for surviving mutants were reverse transcribed into cDNA and amplified by PCR for ligation back into pRDV for a subsequent round of selection. Library diversity can be conveniently introduced at this step by error-prone PCR, DNA shuffling, or some other mutagenesis technique. These cyclic processes, both ribosome display and directed evolution, can be repeated as necessary until the desired phenotype is achieved.

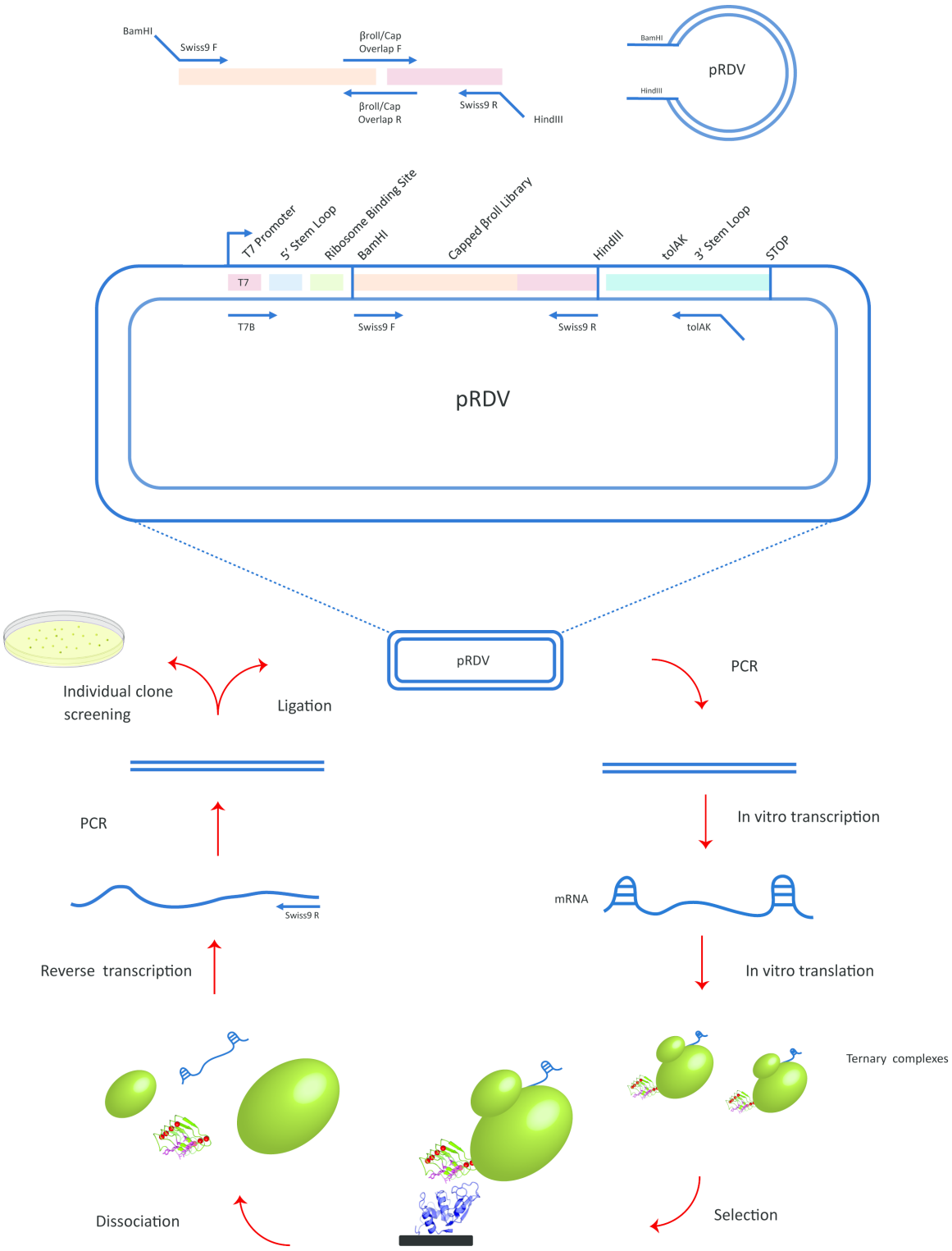

Figure 5.3: Ribosome display vector map and selection process.

5.2.3 Isothermal Titration Calorimetry

In this work, we hope to evolve a folded RTX mutant with the ability to bind lysozyme. Following the directed evolution process, the phenotypes of surviving mutants must be assessed. Most methods of evaluating molecular recognition, including ELISA and IC_{50}, do so indirectly and depend on other chemical reactions or binding interactions concomitantly. Isothermal titration calorimetry (ITC) experimetns can be perfomed on spectrophotometrically silent reactants, in turbid or hetrogeneous solutions, and over a wide range of biologically relavent environemtns (pH, ionic strength, temperature) [48]. ITC can provide a complete thermodynamic analysis of binding energetics between two molecules without the need for extraneous reactions or labeling reagents. Molecular recognition events are invariably associated with energetic changes in the system. These small amounts of heat evolved from the formation/breaking of interactions can be detected accurately to approximately $\pm$ 0.1 μcal with current calorimeters [50]. In a typical experiment, a concentrated solution of ligand is titrated isothermally into a cell containing a dilute solution of its binding partner, usually referred to as the macromolecule. A schematic of the instrument is provided in Figure 5.4. A reference cell is held at a constant temperature. Any energy released to or absorbed by the system upon the formation of macromolecule-ligand complexes in the sample cell are detected in a feedback loop. A compensatory amount of power is delivered to the sample cell to maintain a constant temperature difference with the reference cell (ideally $\Delta T = 0$). The differential power applied to the sample cell is recorded for each injection of ligand and integrated with respect to time. From these integrated power plots, a quantitative analysis of binding affinity and thermodynamic driving forces for molecular association

can be performed.

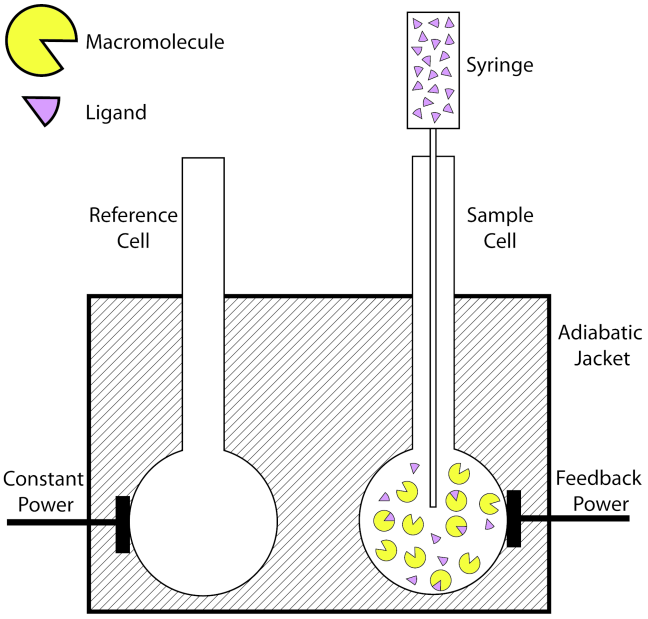

Figure 5.4: ITC schematic. Two cells, a reference and sample, are maintained at a constant temperature. Ligand is titrated into the sample cell containing macromolecule. Energy absorbed by or released to the system upon macromolecule-ligand complex formation is detected by a feedback control loop in the sample cell. The system either lowers or raises the thermal power applied to the sample cell to restore the temperature balance between the two cells.

For a simple molecular binding model consisting of a macromolecule (M) and ligand (X), the reversible binding interaction can be written as [50]:

$$M + X \rightleftharpoons MX \tag{5.1}$$

The change in Gibbs free energy (ΔG) upon the formation of the MX complex can be related to the standard Gibbs free energy (ΔG^0) through the equations:

$$\Delta G = \Delta G^0 + RTlnK_a \tag{5.2}$$

and

$$K_a = \frac{[MX]}{[M][X]} \tag{5.3}$$

where K_a represents the association binding constant. At equilibrium, $\Delta G = 0$ and the following substitution can be made:

$$\Delta G^0 = -RTln\left(\frac{[MX]}{[M][X]}\right) \tag{5.4}$$

Additionally, the molar ratio between the concentration of bound ligand (X_b) and the concentration of total macromolecule (M_t) in the system can be calculated. This parameter, ν, is given by:

$$\nu = \frac{[X]_b}{[M]_t} = \frac{[MX]}{[M]_t} = \frac{[MX]}{[MX] + [M]} = \frac{K_a[X]}{1 + K_a[X]} \tag{5.5}$$

Since the calorimeter measures the enthalpic contributions directly, the entropic changes can be calculated by using the standard form of the overall Gibbs free energy change.

$$\Delta G^0 = \Delta H^0 - T\Delta S^0 \tag{5.6}$$

By substitution:

$$\Delta H^0 - T\Delta S^0 = -RTln\left(\frac{[MX]}{[M][X]}\right) \tag{5.7}$$

In one ITC experiment, using this relatively simple analysis, a complete energetic profile of binding as well the affinity and stoichiometry can be calculated.

5.3 Materials & Methods

5.3.1 Materials

The maltose binding protein (MBP) expression kit, amylose resin, and all cloning enzymes were purchased from New England Biolabs (Ipswich, MA). Isopropyl β-D-1-thiogalactopyranoside (IPTG) and ampicillin sodium salt were obtained from Gold Biotechnology (St. Louis, MO). Amicon centrifugal filters were purchased from Millipore (Billerica, MA). Native PAGE gels, running buffer, protein ladder, and SimplyBlue SafeStain were obtained from Life Technologies (Grand Island, NY). All DNA oligonucleotides were synthesized by Integrated DNA Technologies (Coralville, IA). All chemicals and other reagents were purchased from Sigma-Aldrich (St. Louis, MO) unless otherwise specified.

5.3.2 Library Construction

The randomized β-roll library was constructed using two, long, overlapping oligonucleotides encoding for the entire gene. Randomized positions were created at the DNA level using mixed codons. At the eight selected positions, NNK degenerate codons were inserted. N represents any base, A, T, C or G. K represents the keto-containing bases, G or T. This codon stretch can represent all 20 common amino acids while simultaneously knocking out two *E. coli* RNA stop codons, ochre (UAA) and umber (UGA). The

library oligonucleotides were annealed and extended creating full-length, hybridized library. The C-terminal capping region was added by overlap extension PCR. Please refer to Appendix A for oligonucleotide sequences and PCR conditions.

5.3.3 Ribosome Display

The ribosome display method is thoroughly outlined in Appendix A. It was modeled after previously published protocols from Pluckthun and coworkers [39,40,93]. Instructions for preparing *E. coli* extracts and translational premix can be found in these protocols as well.

5.3.4 Cloning into the pMAL Vector

The consensus β-roll selected from the ribosome display experiments was cloned into the pMAL vector and an intein-modified pMAL construct described previously [35]. Both cloning experiments were designed identically. The gene was amplified out of pRDV using the following forward and reverse primers with KpnI and HindIII restriction sites, respectively.

5'-AATAATGGTAACGGGTTCTGCACGCGACGATGTGC-3'
5'-TAATAAAAGCTTTTAGTCCGGATACTGCGCCATTGCC-3'

Following purification, the PCR product was digested and ligated into the appropriate vector with T4 DNA ligase yielding pMAL-B1β and pMAL-intein-B1β. The constructs were then transformed into *E. coli* for expression.

5.3.5 Expression & Purification of B1β Constructs

All pMAL constructs were expressed identically. 1 L cultures of sterilized TB media supplemented with 2 g/L D-glucose and 100 μg/mL ampicillin were inoculated with saturated 10 mL cultures of *E. coli* harboring the appropriate plasmid. Cell growth was carried out at 37 °C and 220 RPM until $OD_{600} = 0.6$. At this point, expression was induced by adding IPTG to a final concentration of 0.3 mM. Expression was carried out for 5 h at 37 °C and 220 RPM after which the cells were harvested by centrifugation at 3,000 x g for 10 min. Cell pellets were resuspended in 50 mL of MBP column buffer (20 mM Tris-HCl, 200 mM NaCl, 1 mM EDTA, pH 7.4) and lysed via microtip sonication for 6 min on ice (Sonicator 3000, QSonica, Newtown, CT). Cell debris and insoluble protein were pelleted by centrifugation at 15,000 x g for 30 min. Soluble fractions were pooled and diluted in 250 mL MBP column buffer. The clarified lysate was then loaded onto amylose resin drip columns. Host cell proteins in the flow through were discarded and captured MBP-tagged constructs were washed with 50 mL of MBP column buffer. Immobilized MBP-B1β was then used for chromatography experiments as described below. Intein containing constructs were washed with intein cleaving buffer (137 mM NaCl, 2.7 mM KCl, 8.1 mM Na_2HPO_4, 1.76 mM KH_2PO_4, 40 mM bis-Tris, 2 mM EDTA, pH6.2), capped, and allowed to cleave for 12-16 h at 37 °C. Cleaved constructs were eluted with 25 mL MBP column buffer and concentrated in 10 kDa MWCO centrifugal filters. Anion exchange chromatography (AEC) was used as a polishing step to remove any residual MBP-intein. Samples were buffer exchanged into a low salt AEC buffer (20 mM bis-Tris, 25 mM NaCl, pH 6.0) and loaded onto a 16/10 Q FF ion-exchange column using an $AKTA_{FPLC}$ (GE Healthcare). Samples

were washed with low salt AEC buffer and eluted on a 20 column volume gradient with a high salt AEC buffer (20 mM bis-Tris, 500 mM NaCl, pH 6.0). Untagged B1β fractions were pooled, concentrated and buffer exchanged into an appropriate assay buffer. Purity levels were confirmed by SDS-PAGE analysis. Protein concentrations were determined by absorbance at 280 nm using a calculated extinction coefficient (ε_{280} = 22,190 $M^{-1}cm^{-1}$)

5.3.6 Circular Dichroism Spectroscopy

Circular dichroism experiments were performed as previously described [19,35]. Briefly, 100 μM samples were analyzed on a Jasco J-815 CD spectrometer (Jasco, Easton, MD) in 50 mM Tris pH 7.4. Samples were incubated with increasing amounts of $CaCl_2$ for titration experiments. The temperature was held constant at 25 °C by a Peltier junction temperature controller and all experiments were performed in triplicate. Titration data were fit to the Hill equation using SigmaPlot nonlinear regression software (Systat Software, San Jose, CA).

5.3.7 Fluorescence Resonance Energy Transfer (FRET)

1 μM protein samples were titrated with increasing concentration of terbium chloride. Changes in fluorescence emission from bound terbium ions were tracked at 545 nm following the excitation of a proximal tyrosine residue at 282 nm. All experiments are performed in 96 well microtiter plates in 20 mM PIPES pH 6.8, 120 mM NaCl, 10 mM KCl. Terbium was incubated with the protein samples for 30 min at 25°C prior to reading. All data were collected in triplicate and analyzed using SigmaPlot nonlinear

regression software (Systat Software, San Jose, CA).

5.3.8 Bis-ANS Binding

Bis-ANS dye binding experiments were performed in 1 cm path length UV cuvettes on a Spectramax M2 spectrophotometer (Molecular Devices, Sunnyvale, CA). 1 µM β-roll samples were incubated in the presence or absence of 50 mM $CaCl_2$. 5 µg/mL bis-ANS dye was added following equilibration. Fluorescence emission was measured from 420 nm to 600 nm following excitation at 390 nm. All measurements were made in triplicate in 50 mM Tris pH 7.4.

5.3.9 Isothermal Titration Calorimetry (ITC)

ITC experiments were performed on a MicroCal Auto-iTC_{200} system (GE Healthcare) in 50 mM Tris pH 7.4. 3.5 mM lysozyme in this same buffer was used in the syringe and 150 µM of purified B1β was used in the cell. A series of 18 2 µL injections were made over the course of a 50 min run. The resultant changes in differential power upon injection were recorded. These peaks were integrated and fit using Origin data analysis and graphic software (Northampton, MA). Kinetic and thermodynamic properties of binding were calculated.

5.3.10 Immobilized β-roll Chromatography

B1 β-roll was expressed as a fusion to MBP and lysed using the conditions described above. MBP-B1β fusions were immobilized in amylose-charged drip columns while host cell contamination was removed with 50 mL of MBP column buffer. The columns

were then equilibrated with a modified MBP column buffer without EDTA and supplemented with either 50 mM $CaCl_2$ or $MgCl_2$. A concentrated bolus of lysozyme in the appropriate modified MBP column buffer was injected to the top the column. Syringe pumps supplied modified buffer to the top of the columns at 1 mL/min. Fractions were collected in 1 min intervals and analyzed on a spectrophotometer for total protein content by absorbance at 280 nm.

5.4 Results

5.4.1 Ribosome Display

A randomized β-roll library was subjected to several rounds of selection against immobilized lysozyme via ribosome display in the presence of calcium. Detailed procedural notes on the ribosome display cycle can be found in Appendix A. Throughout the selection process, the amount of recovered mRNA after each round was tabulated and can be found in Table 5.1. During the first 4 rounds, as the number of washes per round slowly increased, the mRNA recovery levels steadily increased. When the stringency was ramped up in round 5, a marked drop in recovery was observed. The recovery levels were found to increase four-fold in the following round, while maintaining the same number of washes. While mRNA recovery levels do not directly report molecular recognition, the resultant trend is interesting. It is also important to note here that the amount of lysozyme immobilized in each round remained constant throughout the entire experiment.

Following each round of selection, the recovered genetic information was cloned

Round	Washes	mRNA (ng/μL)	Full Length Recovery
1	1	12	50%
2	2	20	63%
3	3	36	38%
4	5	40	25%
5	8	4	13%
6	8	16	60%

Table 5.1: mRNA & full length β-roll clone recoveries. Recovered mRNA concentrations for all rounds of selection are given. The percentage of full-length β-roll genes without stop codons recovered after each round is given in the last column.

Clone	Randomized Residues
B1	WF LE AT DA
B2	WF LE AT DA
B3	WF LE AT DA
B4	WF LE AT DA
B5	LY RQ AT DA
B6	VP EG SP VP

Table 5.2: Randomized positions for selected clones. The eight randomized spots for each full-length selected β-roll mutant after the 6th round are given.

back into the ribosome display vector for subsequent rounds. At this point, some of the DNA was transformed into *E. coli* and 8-10 individual colonies were screened to ensure the integrity of the library and to determine if a convergent sequence emerged. The percentage of recovered full-length β-roll genes without stop codons is provided in Table 5.1. Of the 10 clones sequenced following the 6th round of selection, 6 contained full-length β-roll genes without stop codons. The randomized positions of these 6 clones are given in Table 5.2. At this point, a consensus sequence emerged and no further selections were carried out. The B1 β-roll mutant (B1β) was cloned into an expression vector for analysis.

5.4.2 B1β Preliminary Characterization

B1β was expressed and purified using the pMAL-intein system described above. The structural response of the mutant peptide to calcium was analyzed by far UV circular dichroism (CD). Spectra were obtained for 100 μM samples in the presence and absence of 10 mM calcium and are given in Figure 5.5a. The peptide was highly disordered in the calcium-free environment evidenced by the large negative peak at 198 nm. Upon calcium addition, a negative peak emerged at 218 nm, indicative of β-sheet formation. These spectra are characteristic of the disordered to β-roll structural transition for RTX domains, as discussed in Chapters 2 and 3. A calcium titration was performed and the resultant data were fit to the Hill equation (Figure 5.5b). B1β bound calcium cooperatively with an affinity of 2.7 ± 0.1 mM and a Hill coefficient of 4.4 ± 0.4. To further characterize the B1 clone, a bis-ANS dye binding experiment was performed (Figure 5.5c). Bis-ANS binds non-specifically to surface exposed hydrophobic patches and can be used to evaluate β-roll conformation [19, 35, 56]. 1 mM β-roll samples were tested in the presence and absence of 50 mM calcium. A large increase in bis-ANS fluorescence was observed in the calcium-rich environment indicating a more structured conformation. A terbium chloride titration was also performed to evaluate B1β. This lanthanide ion is commonly used as a calcium analog and was shown to trigger β-roll folding in previous studies [19, 35]. Terbium will participate in fluorescence resonance energy transfer with a tyrosine residue in the 7th repeat of the β-roll. Tyrosine can be excited at 282 nm and the subsequent emission from the bound terbium ion can be tracked at 545 nm. The results from this experiment are given in Figure 5.5d. A typical hyperbolic response to increasing terbium concentration was observed and

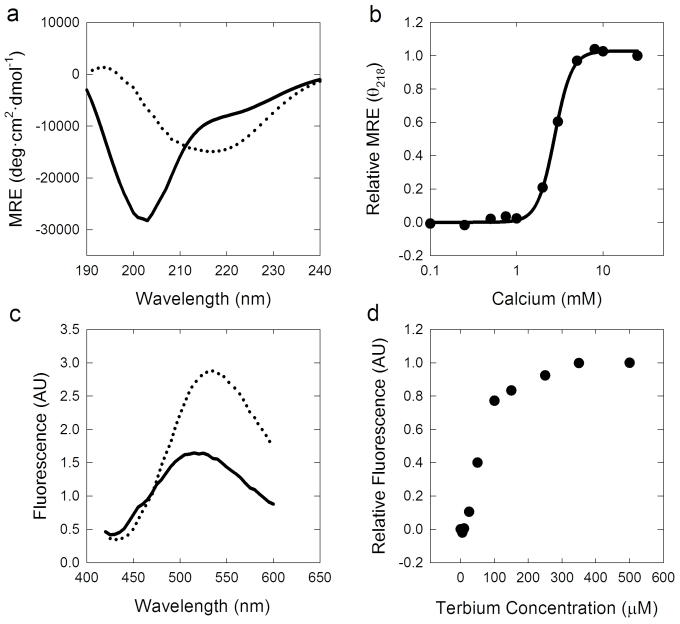

Figure 5.5: Preliminary B1β characterization. (a) Far UV CD spectra for B1β in the presence (• • •) and absence (—) of 10 mM $CaCl_2$. (b) Calcium titration for B1β by monitoring MRE at 218 nm from 0-10 mM $CaCl_2$. (c) bis-ANS dye binding spectra for B1β in the presence (• • •) and absence (—) of 50 mM $CaCl_2$. (d) Terbium titration for B1β by monitoring emission at 545 nm from bound terbium ions.

agrees with other mutant β-roll domains characterized. These data all suggest that B1β behaves similarly to the wild type β-roll (WTβ) and retained the intrinsic calcium-induced structural rearrangement.

5.4.3 B1β Binding Characterization

Following the preliminary analysis of B1β, the affinity of the mutant β-roll for lysozyme was characterized by isothermal titration calorimetry (ITC). 3.5 mM lysozyme was titrated into the experimental cell containing 150 μM purified B1β. The resulting heats generated are given in Figure 5.6a. A control experiment that accounts for any buffer

mismatch effects was performed and the resulting titration is given in Figure 5.6b. Here, 3.5 mM lysozyme was titrated into the cell which contained only buffer. Despite the large background heats, a clear difference is observed between these experiments. In the titration containing the evolved β-roll (Figure 5.6a), a considerably larger differential power was observed for the first several injections. The peak areas were integrated and plotted against the molar ratio of lysozyme to β-roll, given in Figure 5.6c. A control experiment where 3.5 mM lysozyme was titrated into the cell containing the wild type β-roll was also performed. The integrated heats from this experiment are plotted in Figure 5.6d. While the wild type control experiment shows no evidence of binding, the B1β titration fits the typical sigmoidal response, indicative of molecular interaction. These data were fit to an iterated equation of the form [122]:

$$Q = \frac{nM_t\Delta HV_o}{2}\left[1 + \frac{X_t}{nM_t} + \frac{1}{nK_aM_t} - \sqrt{\left(1 + \frac{X_t}{nM_t} + \frac{1}{nKM_t}\right)^2 - \frac{4X_t}{nM_t}}\right] \tag{5.8}$$

where:

Q	= total heat content	K_a	= equilbrium association constant
ΔH	= molar heat of ligand binding	M_t	= macromolecule bulk concentration
V_o	= active cell volume	X_t	= ligand bulk concentration
n	= number of sites		

with inital guesses for K_a, ΔH and n. The derivation for this formula can be found in the Supplemental Information. From these fits an equilibrium dissociation constant, binding stoichiometry, and thermodynamic binding contributions were extracted and

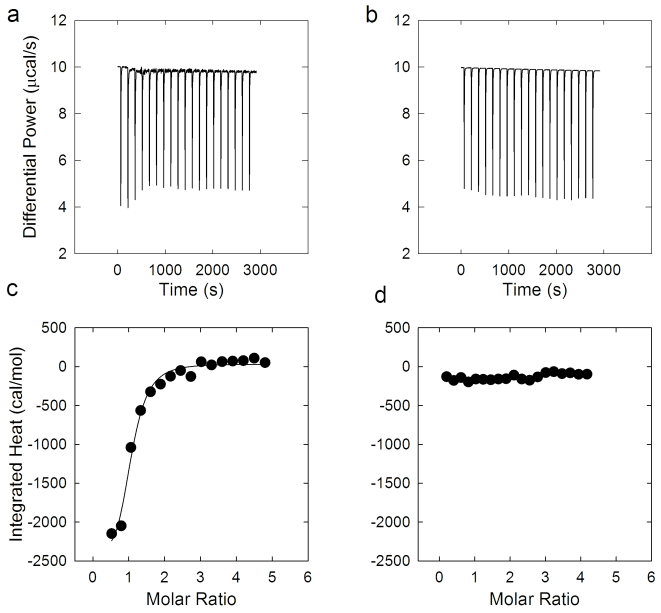

Figure 5.6: B1β binding characterization. (a) Raw ITC data showing changes in differential power in response to a lysozyme titration into B1β. (b) Raw ITC data showing the buffer contribution to the released heats. (c) Integrated heats from the lysozyme titration into B1β. (d) Integrated heats from the lysozyme titration into WTβ control experiment. Non-linear fits were made using Origin data analysis and graphic software.

summarized in Table 5.3. B1β binds to lysozyme in a 1:1 fashion with low micromolar affinity. The binding was shown to be exothermic as evidenced by the calculated change in enthalpy.

In order to assess the practical utility of the mutant β-roll and allosteric regulation of the binding interface, we conducted a chromatographic residence time assay. The B1β clone was expressed as a fusion to MBP and captured on amylose resin drip columns. The columns were then equilibrated with 50 mM $CaCl_2$ or $MgCl_2$. A concentrated bolus of lysozyme was introduced to the top of the column while under 1 mL/min flow of MBP column buffer supplemented with the appropriate salt. Fractions were

n	0.942 ± 0.04	
K_D	6.21 ± 2.3	(μM)
ΔH	-2,549 ± 190	(cal/mol)
ΔS	15.3	(cal/mol/deg)

Table 5.3: B1β binding parameters.

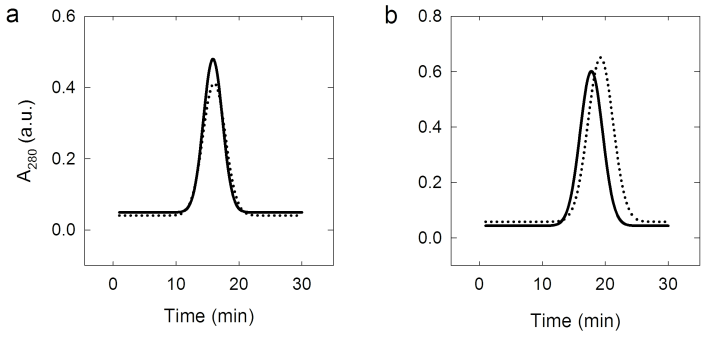

Figure 5.7: Lysozyme elution plots. Absorbance at 280 nm was tracked over the elution in 50 mM $CaCl_2$ (• • •) and 50 mM $MgCl_2$ (—) for WTβ (a) and B1β (b).

collected from the eluate and analyzed for total protein content. Elution plots for B1β and WTβ are given in Figure 5.7 in the presence of calcium and magnesium. The data were fit to a Gaussian distribution and the peak residence times are given in Table 5.4. The data demonstrated that in the presence of calcium, the B1β mutant significantly increased the residence time of lysozyme in the amylose columns. Lysozyme incubated with immobilized WTβ eluted at the same time regardless of the magnesium or calcium concentration.

Construct	Peak Residence Time (min)
WTβ + $MgCl_2$	15.9
WTβ + $CaCl_2$	16.0
B1β + $MgCl_2$	17.6
B1β + $CaCl_2$	19.2

Table 5.4: Lysozyme peak residence times for the WTβ and B1β constructs in magnesium and calcium.

5.5 Discussion

In this work, we have evolved a mutant β-roll domain with affinity for lysozyme from a randomized library using ribosome display technology. This cyclic process maintains the critical linkage between genotype and phenotype, necessary for any directed evolution experiment, through ternary complexes composed of the nascent translated protein, the cognate mRNA coding for that protein, and the ribosomal complex responsible for translation. Following each round of selection, the mRNA from surviving clones was recovered and moved back into the ribosome display plasmid for subsequent rounds of selection. The total mRNA recovery for each round was tabulated and provided in Table 5.1. As the selection process progressed, mRNA recovery levels steadily increased. This is most likely due to the increased recovery of β-roll clones with affinity for the immobilized target. When the selections became more stringent in the 5th round, the mRNA recovery dropped by an order of magnitude suggesting clones with low affinity for the target or clones non-specifically bound to the blocking proteins or polystyrene plate were removed from the library. In the following round the recovery levels quadrupled while maintaining high stringency, suggesting the library was enriched with target-binding β-roll domains. A strong parallel can be drawn between

the mRNA recovery data and the sequencing results from full-length β-roll clones. A marked increase in full-length recovery was observed between rounds 5 and 6 (Table 5.1). Increased washing stringency in the 5th round may have also helped remove some of the frame shifted, truncated, or otherwise disrupted β-roll mutants with non-specific affinity or transcriptional advantages from the library.

Following the 6th round of selection, 67% of the full-length genes sequenced contained identical residues at the 8 randomized positions indicating the emergence of a consensus sequence (Table 5.2). Additionally, clone B5 contained identical residues at positions 5-8 with the consensus B1 β-roll. A homology model of the B1β binding interface was generated and compared to WTβ in Figure 5.8. The evolved binding interface topology is considerably different from the relatively flat surface of WTβ. Tryptophan and phenylalanine, two bulky amino acids, occupy the first two randomized positions and extend outward into the solvent creating a cleft. Two negatively charged residues occupy the 4th and 7th positions and may provide some electrostatic stabilization of the B1β-lysozyme complex.

The consensus B1β was extensively characterized using several biophysical techniques to ensure retention of the intrinsic calcium-responsive behavior. Far UV circular dichroism analysis in Figure 5.5a indicated a similar disordered to β-sheet transition as seen with other mutant β-roll domains previously evaluated in Chapters 2 and 3. B1β was shown to bind calcium ions cooperatively and with similar affinity as WTβ, Leuβ, and DLeuβ (Figure 5.5b). Increases in bis-ANS fluorescence in the presence of calcium indicated the formation of a partially hydrophobic surface amenable to dye binding (Figure 5.5c). Terbium chloride titrations showed near identical responses to all other

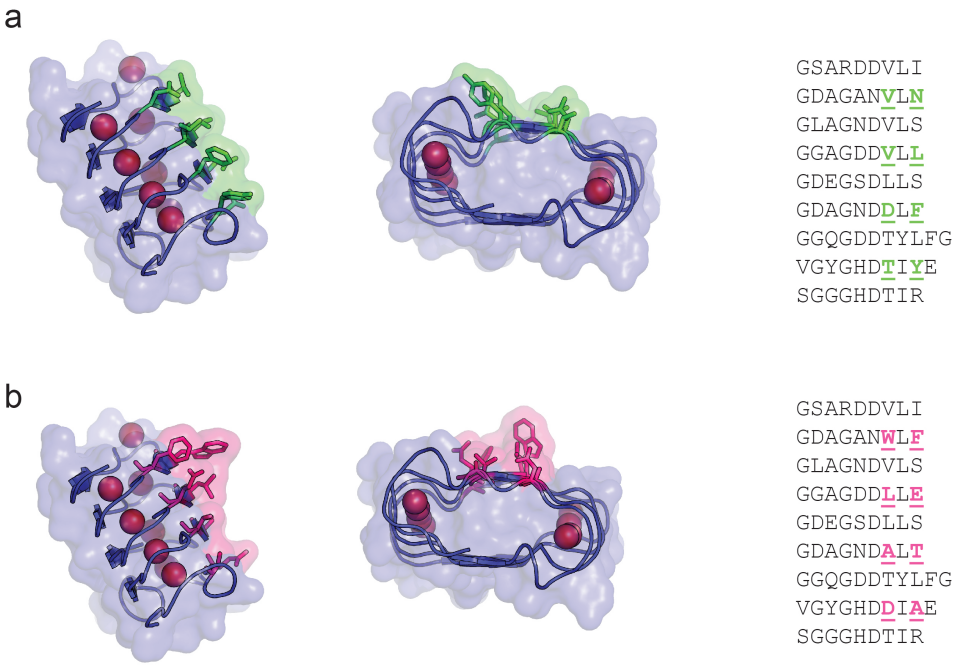

Figure 5.8: WTβ and B1β surface topology. Homology models are given for WTβ (a) and B1β (b) in the calcium-bound conformation highlighting the evolved binding interface. The spheres represent bound calcium ions. The primary sequences for each domain are given on the right. Both models were generated using SWISS-MODEL (Swiss Institute of Bioinformatics) and rendered in PyMOL.

β-roll domains analyzed previously (Figure 5.5d). The initial characterization of B1β determined that the mutant binds calcium and undergoes a structural transition into a stable β-roll secondary structure similar to that of the WT domain.

B1β was selected from the randomized library in the presence of calcium and therefore was most likely in the folded conformation during the selection process. To assess the affinity of B1β for lysozyme, isothermal titration calorimetry (ITC) experiments were performed. Small amounts of heat released to or absorbed by the system upon ligand binding can be detected and analyzed. B1β titrations with lysozyme in the presence of calcium produced changes in differential power when compared to lysozyme titrations into buffer alone (Figure 5.6a, b). The titration data was analyzed and the integrated heats for the lysozyme-B1β titration are given in Figure 5.6c. Identical experiments were conducted using the unmodified WTβ as a control. Integrated heats for this titration are given in Figure 5.6d (raw data not shown).

The data were fit using the equation provided in the previous section and several binding parameters were extracted (Table 5.3). B1β bound lysozyme at 1:1 stoichiometry with low micromolar affinity, while the WTβ had no affinity for the target whatsoever under identical conditions. Since both lysozyme and the β-roll are of similar size (lysozyme 14.7 kDa, β-roll 15.9 kDa), and monomeric, a 1:1 binding ratio was expected. Thermodynamic contributions to the Gibbs free energy of association were also calculated from the data. A modest enthalpy change of -2.5 kcal/mol indicated an exothermic binding process. The magnitude and sign of the enthalpic contribution represent the global heat effects on the system during the titration. However, a favorable reorganization of the hydrogen bonding network between the macromolecule, ligand

and solvent is typically the largest contributor to a negative change in enthalpy [50]. The entropic contributions were also indirectly measured and determined to be 15.3 cal/mol/deg. This increase is most likely caused by the exclusion of water molecules previously arranged on the lysozyme-B1β interface [47, 79].

An affinity of 6.21 ± 2.3 µM of B1β for lysozyme was determined by preliminary ITC experiments. To investigate the possible utility of evolved β-roll domains in smart chromatography applications, we attempted to capture lysozyme using immobilized B1β. We hypothesized that we can use the intrinsic calcium-induced conformational response of the β-roll to selectively modulate the designed binding interface. After capturing the target protein, it can be released by chelating the calcium ions out of solution thereby delocalized the evolved binding surface and returning the β-roll to its disordered state. MBP-B1β fusions were prepared and immobilized in amylose resin columns equilibrated with $CaCl_2$. Initial attempts to capture injected lysozyme on B1β packed columns proved unsuccessful. SDS-PAGE analysis confirmed lysozyme was not retained in the column but rather eluted upon washing the column with calcium-rich buffer (data not shown). It was determined that the affinity of B1β was simply too weak to successfully capture the target protein on column.

Alternatively, a column residence time assay was performed to investigate the effects, if any, B1β had on lysozyme retention inside the packed columns. This assay also provided insight into the allosteric regulation of lysozyme binding. A concentrated dose of lysozyme was injected on to a B1β immobilized column equilibrated with $CaCl_2$ or $MgCl_2$, and the eluate was evaluated for total protein content. Additional control experiments were completed with immobilized WTβ and the elution plots are given in

Figure 5.7. The residence times for the lysozyme peaks were calculated and are given in Table 5.4. Lysozyme eluted from the WTβ packed column at approximately 16 minutes regardless of β-roll conformation. Columns packed with B1β in the presence of calcium showed significant retention of lysozyme with a peak elution time of 19.2 minutes as compared to 17.6 minutes in $MgCl_2$. B1β bound to lysozyme sufficiently well enough to slow its elution from the column by 3.2 minutes when compared to WTβ in the presence of calcium. An intermediate residence time of 17.6 minutes for B1β in $MgCl_2$ is an interesting result. This indicates that either the unstructured version of B1β has some affinity for lysozyme or that some fraction of B1β is actually folded despite $MgCl_2$ saturation, perhaps due to molecular crowding.

Some considerations need to be taken into account in order to successfully implement an evolved β-roll domain into a stimulus-responsive chromatography system. First, and most importantly, β-roll peptides with sub-micromolar affinities for desired targets need to be isolated. Following 6 rounds of fairly stringent selection, we were able to evolve a β-roll with low micromolar affinity, which is significantly weaker binding when compared to antibodies with typical affinities in the mid to low nanomolar range. Affinity maturation strategies such as error-prone PCR and DNA shuffling can be used to add diversity to selected libraries and explore more of the possible sequence space [11]. The ribosome display cycle requires a PCR step where these strategies can be conveniently introduced. Also, selecting for smaller dissociation rate constants directly can be used to evolve higher affinity variants [93]. An alternative strategy to immobilize evolved β-roll clones on a solid chromatography support will be required. We have previously shown that β-roll domains tolerate C-terminal cysteine mutations, which can

be used to conjugate β-rolls to sulfhydrl agarose resins via covalent thioether linkages [105]. Once an immobilization strategy is optimized, β-roll packed columns can be tested for capture efficiency, durability, shelf-life, and tolerance to harsh buffering conditions.

5.6 Conclusions

We have successfully developed a platform to select RTX binding domains from a randomized library via ribosome display. By conducting rounds of panning against an immobilized model protein lysozyme, we selected an RTX variant, B1β, with low micromolar affinity in the calcium-bound conformation. This task was particularly challenging when compared to most work in this field as the RTX domain does not naturally participate in biomolecular recognition. A full energetic profile of B1β –lysozyme binding was elucidated through isothermal titration calorimetry. We were unable to successfully capture the target protein on a B1β packed column, but we were able to observe substantial shifts in lysozyme residence time when compared to the WTβ. Our inability to capture the target on column can most likely be attributed to the relatively weak dissociation constant. However, there are several strategies available to select for the tightest binders possible including affinity maturation and off-rate selection. These methods are currently being explored to select against other interesting target proteins including maltose binding protein, green fluorescent protein, and the Fc domain of antibodies.

5.7 Supplemental Information

5.7.1 Fitting ITC Data to a Single Binding Site

This derivation has been taken from the ITC Data Analysis in Origin Tutorial Guide, version 7.0.

K_a = association binding constant

n = number of binding sites

V_o = active cell volume

Mt, M = bulk and free concentrations of macromolecule

Xt, X = bulk and free concentrations of ligand

Θ = fraction of sites occupied by the ligand, X

The association binding constant can be defined as:

$$K_a = \frac{\Theta}{(1-\Theta)[X]} \tag{5.9}$$

The bulk concentration of ligand in the cell can be defined as:

$$X_t = [X] + n\Theta M_t \tag{5.10}$$

Combining the two above equations yields:

$$\Theta^2 - \Theta\left[1 + \frac{X_t}{nM_t} + \frac{1}{nK_aM_t}\right] + \frac{X_t}{nM_t} = 0 \tag{5.11}$$

Solving this quadratic expression for Θ gives only one root:

$$\Theta = \frac{1}{2}\left[1 + \frac{X_t}{nM_t} + \frac{1}{nK_aM_t} - \sqrt{\left(1 + \frac{X_t}{nM_t} + \frac{1}{nK_aM_t}\right)^2 - \frac{4X_t}{nM_t}}\right] \tag{5.12}$$

The total heat content of the solution of volume V_o can be written as:

$$Q = n\Theta M_t \Delta H V_o \tag{5.13}$$

Substitution for Θ gives:

$$Q = \frac{nM_t\Delta HV_o}{2}\left[1 + \frac{X_t}{nM_t} + \frac{1}{nK_aM_t} - \sqrt{\left(1 + \frac{X_t}{nM_t} + \frac{1}{nK_aM_t}\right)^2 - \frac{4X_t}{nM_t}}\right] \tag{5.14}$$

This value of Q describes the total heat content in the system at any particular injection with volume V_o. However, the parameter of interest is the change of heat between injections. Since the volume changes incrementally with each injection of ligand, a small volume correction must be included to calculate the difference in heats between each injection. The correct expression to calculate the heat releasted between injections is therefore:

$$\Delta Q(i) = Q(i) + \frac{dV_i}{V_o}\left[\frac{Q(i) + Q(i-1)}{2}\right] - Q(i-1) \tag{5.15}$$

Initial guess are typically made by Origin for n, K_a, and ΔH with reasonable accuracty. The calculated heat is compared to the measured heat for each injection and improvemnts to the inital guesses are made. This process is iterated until no significant

improvment in the fit can be made.

Chapter 6

Summary & Future Directions

6.1 Summary & Future Directions

6.1.1 Summary

In this work, we describe our efforts to engineer the calcium-responsive RTX domain for use in various biotechnology applications. Chapter 1 provides a broad strokes overview of protein engineering theory and techniques. The success of engineered antibodies is discussed along with many of the difficulties associated with their production and purification. Engineers are beginning to investigate alternative protein scaffolds to circumvent these issues. Several of these domains are identified and discussed including repeat scaffolds composed of short, repeating motifs. We then provide an in-depth review of the RTX domain including biological relevance and structural characterization. The block V RTX from *B. pertussis* was shown to undergo a disordered to β-roll transition in response to calcium binding independently from the other blocks, providing and interesting calcium-responsive scaffold akin to other antibody mimetic proteins. Several studies characterizing the block V domain and evaluating its potential as a scaffold for protein engineering are discussed. A large majority of the initial characterization focused on identifying the minimum capping requirements for calcium-induced folding and exploring the tolerance to concatenation and immobilization. It was determined that only a C-terminal flanking region is required for calcium-dependent β-roll formation which impacted the design of the constructs presented in this work. These extensive studies performed by coworkers Blenner, Shur, and Szilvay provided the necessary foundations to actually engineer the RTX domain for specific purposes [19, 104, 105, 111].

Chapter 2 focuses on rationally engineering the block V RTX protein for use in

calcium-responsive hydrogel systems. We identified 8 residues in the folded β-roll conformation suitable for mutation. These positions form a stacked β-sheet face with the side chains projecting radially into the solvent. By changing these positions to leucine, we created a hydrophobic sticky patch that is present only in the calcium-bound conformation. A robust analysis of the mutant construct ensured retention of the calcium-responsive properties intrinsic to the wild type domain. In the absence of calcium, the leucine-rich patch is delocalized thus mitigating the driving force for self-assembly. Alpha-helical leucine zipper domains capable of forming tetrameric coiled-coil bundles were appended to the N-terminus of the leucine β-roll mutants to provide additional means of cross-linking. The constructs were evaluated by microrheology in calcium or magnesium rich buffer. The rheological analysis confirmed our hypothesis that self-assembly is calcium-dependent and the resulting hydrogels can be allosterically regulated by adjusting the calcium concentration.

Chapter 3 expands on the platform discussed in Chapter 2. The folded β-roll structure is composed of two parallel β-sheet faces separated by flexible turning regions. Here we deigned a "double-face" leucine β-roll where both β-sheet faces are rationally mutated to contain leucine residues. Again, this construct was extensively characterized to ensure β-roll formation in response to calcium. Despite the hydrophobicity of the surface exposed residues on both faces, the double mutant responded to calcium in a similar manner as the wild type protein. Constructs were prepared with alpha helical leucine zippers as before and microrheology was used to confirm the formation of a hydrogel in the presence of calcium. Self-assembly was observed at considerably lower protein concentrations due to the higher cross-linking content and oligomeriza-

tion state. We also confirmed the potential of the double leucine β-roll to function as a stand-alone cross-linking domain. Concatemers of maltose binding protein and the double leucine mutant were constructed and analyzed. Self-assembly in response to calcium was observed without the aid of additional cross-linking moieties. This is an exciting result that opens the door to a host of biomaterials applications.

In Chapter 4, we explored a consensus design strategy for the RTX domain. Consensus design is used to identify the minimal requirements for a single unit in repeat proteins, often times resulting in higher stability and recombinant expression levels. We searched the UniProt data base and examined approximately 250 RTX containing proteins to identify a consensus sequence. Concatemers of 5, 9, 13, and 17 repeats were constructed and analyzed. Unexpectedly, these consensus constructs underwent a reversible phase change in response to calcium. Instead of abandoning these designed β-roll domains, we tried to use this inducible phase change for something useful. By appending the 17 repeat β-roll tag (BRT) to proteins of interest, we were able to rapidly and efficiently separate target proteins from host cell proteins by precipitation cycling. The precipitation mechanism was shown to be calcium-specific as other ions did not induce a phase change. This system worked remarkably well even with highly soluble proteins such as maltose binding protein. In addition to MBP, we were able to purify fusions to green fluorescent protein, β-lactamase and alcohol dehydrogenase D from *Pyrococcus furiosus*. The precipitation process had no adverse effects on protein structure or activity. To further improve the utility of the tag, we engineered a protease cleavage site between the BRT and protein of interest. Using this cleavage mechanism and re-precipitating the tag, we were able to purify significant amounts of pure, ac-

tive, untagged protein of interest. Our system offers a fast and reliable method to purify recombinant proteins without using time consuming and costly chromatographic purification.

Chapter 5 describes our last study in which we evaluated the RTX domain as a suitable scaffold for evolving molecular recognition. We planned to use the calcium-induced conformational change as a peptide switch to mediate an evolved binding interface, thus creating an allosterically regulated binding domain. We hoped to use this mutant RTX domain for capture and release smart chromatography. The same 8 positions that were shown to tolerate mutations in Chapter 2 were randomized for this work. An RTX library was generated by inserting randomized codons at these positions in two, long oligonucleotides. The gene was hybridized and cloned into a plasmid for directed evolution experiments via ribosome display. Ternary complexes of the ribosomal subunits, mRNA, and translated protein maintained a linkage between genotype and phenotype and were used for biopanning experiments. Following 6 rounds of selection against immobilized lysozyme, a consensus β-roll variant emerged, B1β. This mutant was characterized and was shown to undergo a disordered to β-roll transition in response to calcium. The thermodynamics and binding affinity between B1β and lysozyme were examined by isothermal titration calorimetry. B1β had relatively weak affinity for lysozyme at 6.2 μM. Due to this low affinity, we were unable to capture lysozyme on B1β packed columns. However, substantial increases in lysozyme residence time were observed. Strategies to evolve mutants with higher affinity and other considerations for implementation into a chromatographic system are discussed.

6.1.2 Future Work

While the work presented here is relatively extensive, there is always room for optimization and innovation. The biomaterials work in Chapters 2 and 3 describe the rational engineering approach taken to develop a calcium-responsive protein cross-linking domain suitable for hydrogel formation. This works clearly demonstrates the ability of the mutant RTX domain to self-assemble into protein hydrogels. However, further characterization of the resultant materials, including properties such as erosion rate, mesh size, precise oligomerization state, and aggregate structure would be beneficial prior to implementation into engineered systems.

The BRT system outlined in Chapter 4 demonstrates a useful method for purifying recombinantly expressed proteins. A few improvements can be made to increase its utility and make it more marketable commercially. First, the vector can be optimized to create a convenient multiple cloning site to allow researchers to easily swap out proteins of interest. Next, the mechanism by which proteins of interest are separated from the BRT can be optimized. Currently enterokinase must be used to proteolytically cleave off the tag and cannot be conveniently recovered after cleavage. Perhaps a more economically fruitful strategy would be to genetically fuse the BRT to the protease directly for expression in *E. coli*. BRT-enterokianse could be easily purified using precipitation cycling. This fusion could then be added directly to precipitation purified proteins of interest. After cleavage, BRT-enterokinase could be recovered along with the remaining BRT by re-precipitation. Alternatively, including a self-cleaving intein to remove the tag instead of a protease may help cut costs.

Strategies to improve evolved RTX binding domains as well as future directions were

discussed at the end of Chapter 5. Another interesting consideration worth mentioning is exploring the second face of the folded β-roll. Similar to the approach taken to double the cross-linking potential of the leucine β-roll, the second face could be evolved for molecular recognition. This could be used to simply increase avidity or to bring to proteins of interest in close proximity in a calcium-dependent manner.

These future experiments constitute only a few of the possible directions for this body of work. The β-roll domain has proven to be a versatile scaffold for calcium-responsive bio-based engineering applications.

Bibliography

[1] Michael D Abràmoff, Paulo J Magalhães, and Sunanda J Ram. Image processing with imagej. *Biophotonics international*, 11(7):36–43, 2004. 3.3.8

[2] Souhaila Al-Khodor, Christopher T Price, Awdhesh Kalia, and Yousef Abu Kwaik. Functional diversity of ankyrin repeats in microbial proteins. *Trends in microbiology*, 18(3):132–139, 2010. 1.2

[3] Matthew N Alder, Igor B Rogozin, Lakshminarayan M Iyer, Galina V Glazko, Max D Cooper, and Zeev Pancer. Diversity and function of adaptive immune receptors in a jawless vertebrate. *Science*, 310(5756):1970–1973, 2005. 1.2

[4] John E Allen and George L McLendon. Tryptophan and tyrosine to terbium fluorescence resonance energy transfer as a method to map aromatic residues and monitor docking. *Biochemical and biophysical research communications*, 349(4):1264–1268, 2006. 3.4.1

[5] Patrick Amstutz, H Kaspar Binz, Petra Parizek, Michael T Stumpp, Andreas Kohl, Markus G Grütter, Patrik Forrer, and Andreas Plückthun. Intracellular kinase inhibitors selected from combinatorial libraries of designed ankyrin repeat proteins. *Journal of Biological Chemistry*, 280(26):24715–24722, 2005. 1.2

[6] Patrick Amstutz, Holger Koch, H Kaspar Binz, Stefan A Deuber, and Andreas Plückthun. Rapid selection of specific map kinase-binders from designed ankyrin repeat protein libraries. *Protein Engineering Design and Selection*, 19(5):219–229, 2006. 1.2

[7] L Andrew Lyon. Bioresponsive hydrogels for sensing applications. *Soft Matter*, 5(1):29–35, 2009. 3.2

[8] Clement Angkawidjaja, Aditya Paul, Yuichi Koga, Kazufumi Takano, and Shigenori Kanaya. Importance of a repetitive nine-residue sequence motif for

intracellular stability and functional structure of a family i. 3 lipase. *FEBS letters*, 579(21):4707–4712, 2005. 2.2, 2.5

[9] Sindhu Balan, Jason Murphy, Igor Galaev, Ashok Kumar, George E Fox, Bo Mattiasson, and Richard C Willson. Metal chelate affinity precipitation of rna and purification of plasmid dna. *Biotechnology letters*, 25(13):1111–1116, 2003. 4.2

[10] Mahmoud Reza Banki, Liang Feng, and David W Wood. Simple bioseparations using self-cleaving elastin-like polypeptide tags. *Nature methods*, 2(9):659, 2005. 4.2

[11] Scott Banta, Kevin Dooley, and Oren Shur. Replacing antibodies: engineering new binding proteins. *Annual review of biomedical engineering*, 15:93–113, 2013. 1.1, 5.2, 5.5

[12] Scott Banta, Ian R Wheeldon, and Mark Blenner. Protein engineering in the development of functional hydrogels. *Annual review of biomedical engineering*, 12:167–186, 2010. 2.2, 3.2

[13] Cécile Bauche, Alexandre Chenal, Oliver Knapp, Christophe Bodenreider, Roland Benz, Alain Chaffotte, and Daniel Ladant. Structural and functional characterization of an essential rtx subdomain of bordetella pertussis adenylate cyclase toxin. *Journal of Biological Chemistry*, 281(25):16914–16926, 2006. 1.3, 2.2, 2.3.2, 3.2, 3.3.2, 4.2

[14] Richard P Baum, Vikas Prasad, Dirk Müller, Christiane Schuchardt, Anna Orlova, Anders Wennborg, Vladimir Tolmachev, and Joachim Feldwisch. Molecular imaging of her2-expressing malignant tumors in breast cancer patients using synthetic 111in-or 68ga-labeled affibody molecules. *Journal of Nuclear Medicine*, 51(6):892–897, 2010. 5.2

[15] Gene L Bidwell III and Drazen Raucher. Cell penetrating elastin-like polypeptides for therapeutic peptide delivery. *Advanced drug delivery reviews*, 62(15):1486–1496, 2010. 1.2

[16] H Kaspar Binz, Patrick Amstutz, Andreas Kohl, Michael T Stumpp, Christophe Briand, Patrik Forrer, Markus G Grütter, and Andreas Plückthun. High-affinity binders selected from designed ankyrin repeat protein libraries. *Nature biotechnology*, 22(5):575–582, 2004. 4.2

[17] H Kaspar Binz, Patrick Amstutz, and Andreas Plückthun. Engineering novel binding proteins from nonimmunoglobulin domains. *Nature biotechnology*, 23(10):1257–1268, 2005. 1.1, 5.2

[18] H Kaspar Binz, Michael T Stumpp, Patrik Forrer, Patrick Amstutz, and Andreas Plückthun. Designing repeat proteins: well-expressed, soluble and stable proteins from combinatorial libraries of consensus ankyrin repeat proteins. *Journal of molecular biology*, 332(2):489–503, 2003. 4.2

[19] Mark A Blenner, Oren Shur, Géza R Szilvay, Donald M Cropek, and Scott Banta. Calcium-induced folding of a beta roll motif requires c-terminal entropic stabilization. *Journal of molecular biology*, 400(2):244–256, 2010. 1.4, 2.2, 2.3.5, 2.4.1, 2.5, 3.2, 3.4.1, 3.4.1, 3.5, 4.2, 4.3.3, 5.3.6, 5.4.2, 6.1.1

[20] Ykelien L Boersma and Andreas Plückthun. Darpins and other repeat protein scaffolds: advances in engineering and applications. *Current opinion in biotechnology*, 22(6):849–857, 2011. 1.2

[21] J Brange, U Ribel, JF Hansen, G Dodson, MT Hansen, S Havelund, SG Melberg, F Norris, K Norris, L Snel, et al. Monomeric insulins obtained by protein engineering and their medical implications. 1988. 1.1

[22] Richard R Burgess and Nancy E Thompson. Advances in gentle immunoaffinity chromatography. *Current opinion in biotechnology*, 13(4):304–308, 2002. 5.2

[23] Helena Bysell, Ronja Månsson, Per Hansson, and Martin Malmsten. Microgels and microcapsules in peptide and protein drug delivery. *Advanced drug delivery reviews*, 63(13):1172–1185, 2011. 3.2

[24] Elliot Campbell, Ian R Wheeldon, and Scott Banta. Broadening the cofactor specificity of a thermostable alcohol dehydrogenase using rational protein design introduces novel kinetic transient behavior. *Biotechnology and bioengineering*, 107(5):763–774, 2010. 4.3.2, 4.3.3, 4.3.4, 4.4

[25] Alexandre Chenal, J Iñaki Guijarro, Bertrand Raynal, Muriel Delepierre, and Daniel Ladant. Rtx calcium binding motifs are intrinsically disordered in the absence of calcium implication for protein secretion. *Journal of Biological Chemistry*, 284(3):1781–1789, 2009. 1.3, 2.2, 3.2, 4.2

[26] Alexandre Chenal, Johanna C Karst, Ana Cristina Sotomayor Pérez, Anna Katarzyna Wozniak, Bruno Baron, Patrick England, and Daniel Ladant.

Calcium-induced folding and stabilization of the intrinsically disordered rtx domain of the cyaa toxin. *Biophysical journal*, 99(11):3744–3753, 2010. 1.3

[27] Ashutosh Chilkoti, Matthew R Dreher, Dan E Meyer, and Drazen Raucher. Targeted drug delivery by thermally responsive polymers. *Advanced drug delivery reviews*, 54(5):613–630, 2002. 1.2

[28] Karuppiah Chockalingam, Mark Blenner, and Scott Banta. Design and application of stimulus-responsive peptide systems. *Protein Engineering Design and Selection*, 20(4):155–161, 2007. 2.2

[29] Pietro Cicuta and Athene M Donald. Microrheology: a review of the method and applications. *Soft Matter*, 3(12):1449–1455, 2007. 2.3.10

[30] Matthew A Cooper and Victoria T Singleton. A survey of the 2001 to 2005 quartz crystal microbalance biosensor literature: applications of acoustic physics to the analysis of biomolecular interactions. *Journal of Molecular Recognition*, 20(3):154–184, 2007. 1.4

[31] Naomi Courtemanche and Doug Barrick. The leucine-rich repeat domain of internalin b folds along a polarized n-terminal pathway. *Structure*, 16(5):705–714, 2008. 4.2

[32] John C Crocker, Megan T Valentine, Eric R Weeks, Thomas Gisler, Peter D Kaplan, Arjun G Yodh, and David A Weitz. Two-point microrheology of inhomogeneous soft materials. *Physical Review Letters*, 85(4):888, 2000. 2.3.10, 3.3.8, 3.4.2

[33] Luca D D'Andrea and Lynne Regan. Tpr proteins: the versatile helix. *Trends in biochemical sciences*, 28(12):655–662, 2003. 1.2

[34] Fei-Xiang Ding, Hong-Li Yan, Qian Mei, Geng Xue, Yu-Zhao Wang, Yuan-Jian Gao, and Shu-Han Sun. A novel, cheap and effective fusion expression system for the production of recombinant proteins. *Applied microbiology and biotechnology*, 77(2):483–488, 2007. 4.2

[35] Kevin Dooley, Yang Hee Kim, Hoang D Lu, Raymond Tu, and Scott Banta. Engineering of an environmentally responsive beta roll peptide for use as a calcium-dependent cross-linking domain for peptide hydrogel formation. *Biomacromolecules*, 13(6):1758–1764, 2012. 3.2, 3.2, 3.2, 3.3.8, 3.4.1, 3.4.1, 3.4.2, 3.5, 4.2, 5.3.4, 5.3.6, 5.4.2

[36] Matthew R Dreher, Drazen Raucher, Narayanan Balu, O Michael Colvin, Susan M Ludeman, and Ashutosh Chilkoti. Evaluation of an elastin-like polypeptide–doxorubicin conjugate for cancer therapy. *Journal of Controlled Release*, 91(1):31–43, 2003. 1.2

[37] Matthew R Dreher, Andrew J Simnick, Karl Fischer, Richard J Smith, Anand Patel, Manfred Schmidt, and Ashutosh Chilkoti. Temperature triggered self-assembly of polypeptides into multivalent spherical micelles. *Journal of the American Chemical Society*, 130(2):687–694, 2008. 1.2

[38] Birgit Dreier, Galina Mikheeva, Natalya Belousova, Petra Parizek, Edgar Boczek, Ilian Jelesarov, Patrik Forrer, Andreas Plückthun, and Victor Krasnykh. Her2-specific multivalent adapters confer designed tropism to adenovirus for gene targeting. *Journal of molecular biology*, 405(2):410–426, 2011. 1.2

[39] Birgit Dreier and Andreas Plückthun. Ribosome display: a technology for selecting and evolving proteins from large libraries. In *PCR Protocols*, pages 283–306. Springer, 2011. 5.2.1, 5.2.2, 5.3.3

[40] Birgit Dreier and Andreas Plückthun. Rapid selection of high-affinity binders using ribosome display. In *Ribosome Display and Related Technologies*, pages 261–286. Springer, 2012. 5.2.1, 5.2.2, 5.3.3

[41] Jason D Ehrick, Sapna K Deo, Tyler W Browning, Leonidas G Bachas, Marc J Madou, and Sylvia Daunert. Genetically engineered protein in hydrogels tailors stimuli-responsive characteristics. *Nature materials*, 4(4):298–302, 2005. 2.2, 3.2

[42] John G Elvin, Ruairidh G Couston, and Christopher F van der Walle. Therapeutic antibodies: market considerations, disease targets and bioprocessing. *International journal of pharmaceutics*, 440(1):83–98, 2013. 1.1, 5.2

[43] Tatsuro Endo, Ryuzoh Ikeda, Yasuko Yanagida, and Takeshi Hatsuzawa. Stimuli-responsive hydrogel–silver nanoparticles composite for development of localized surface plasmon resonance-based optical biosensor. *Analytica chimica acta*, 611(2):205–211, 2008. 2.2

[44] Jenny Fitzgerald, Paul Leonard, Elaine Darcy, and Richard OKennedy. Immunoaffinity chromatography. In *Protein Chromatography*, pages 35–59. Springer, 2011. 5.2

[45] Baley A Fong, Wan-Yi Wu, and David W Wood. Optimization of elp-intein mediated protein purification by salt substitution. *Protein expression and purification*, 66(2):198–202, 2009. 4.2

[46] Baley A Fong, Wan-Yi Wu, and David W Wood. The potential role of self-cleaving purification tags in commercial-scale processes. *Trends in biotechnology*, 28(5):272–279, 2010. 2.3.2, 3.3.2

[47] Kendra King Frederick, Michael S Marlow, Kathleen G Valentine, and A Joshua Wand. Conformational entropy in molecular recognition by proteins. *Nature*, 448(7151):325–329, 2007. 5.5

[48] Matthew W Freyer and Edwin A Lewis. Isothermal titration calorimetry: experimental design, data analysis, and probing macromolecule/ligand binding and kinetic interactions. *Methods in cell biology*, 84:79–113, 2008. 5.2.3

[49] S Annie Gai and K Dane Wittrup. Yeast surface display for protein engineering and characterization. *Current opinion in structural biology*, 17(4):467–473, 2007. 5.2.1

[50] Luis García-Fuentes, Téllez-Sanz Ramiro, Indalecio Quesada-Soriano, and Carmen Barón. Thermodynamics of molecular recognition by calorimetry. 2011. 5.2.3, 5.2.3, 5.5

[51] Michaela Gebauer and Arne Skerra. Engineered protein scaffolds as next-generation antibody therapeutics. *Current opinion in chemical biology*, 13(3):245–255, 2009. 1.1, 5.2

[52] Matthew J Glassman, Jacqueline Chan, and Bradley D Olsen. Reinforcement of shear thinning protein hydrogels by responsive block copolymer self-assembly. *Advanced Functional Materials*, 23(9):1182–1193, 2013. 3.2

[53] Tijana Z Grove, Aitziber L Cortajarena, and Lynne Regan. Ligand binding by repeat proteins: natural and designed. *Current opinion in structural biology*, 18(4):507–515, 2008. 4.2

[54] Wafa Hassouneh, Trine Christensen, and Ashutosh Chilkoti. Elastin-like polypeptides as a purification tag for recombinant proteins. *Current Protocols in Protein Science*, pages 6–11, 2010. 1.2

[55] Wafa Hassouneh, Karl Fischer, Sarah R MacEwan, Robert Branscheid, Chuan Lawrence Fu, Rihe Liu, Manfred Schmidt, and Ashutosh Chilkoti. Unexpected multivalent display of proteins by temperature triggered self-assembly of elastin-like polypeptide block copolymers. *Biomacromolecules*, 13(5):1598–1605, 2012. 1.2

[56] Andrea Hawe, Marc Sutter, and Wim Jiskoot. Extrinsic fluorescent dyes as tools for protein characterization. *Pharmaceutical research*, 25(7):1487–1499, 2008. 3.4.1, 5.4.2

[57] Chaoliang He, Sung Wan Kim, and Doo Sung Lee. ¡ i¿ in situ¡/i¿ gelling stimuli-sensitive block copolymer hydrogels for drug delivery. *Journal of controlled release*, 127(3):189–207, 2008. 2.2

[58] Thomas Hey, Erik Fiedler, Rainer Rudolph, and Markus Fiedler. Artificial, non-antibody binding proteins for pharmaceutical and industrial applications. *TRENDS in Biotechnology*, 23(10):514–522, 2005. 1.1, 5.2

[59] I Barry Holland, Lutz Schmitt, and Joanne Young. Type 1 protein secretion in bacteria, the abc-transporter dependent pathway (review). *Molecular membrane biology*, 22(1-2):29–39, 2005. 4.2

[60] Philipp Holliger and Peter J Hudson. Engineered antibody fragments and the rise of single domains. *Nature biotechnology*, 23(9):1126–1136, 2005. 1.1

[61] Yun Huang, Yubin Zhou, Adriana Castiblanco, Wei Yang, Edward M Brown, and Jenny J Yang. Multiple ca2+-binding sites in the extracellular domain of the ca2+-sensing receptor corresponding to cooperative ca2+ response. *Biochemistry*, 48(2):388–398, 2008. 2.4.1

[62] Anika M Jonker, Dennis WPM Lo?wik, and Jan CM van Hest. Peptide-and protein-based hydrogels. *Chemistry of Materials*, 24(5):759–773, 2012. 3.2

[63] Brian D Kelley, Molly Tannatt, Robert Magnusson, Sigrid Hagelberg, and James Booth. Development and validation of an affinity chromatography step using a peptide ligand for cgmp production of factor viii. *Biotechnology and bioengineering*, 87(3):400–412, 2004. 5.2

[64] Scott B Kennedy, Kenneth Littrell, P Thiyagarajan, David A Tirrell, and Thomas P Russell. Controlled structure in artificial protein hydrogels. *Macromolecules*, 38(17):7470–7475, 2005. 2.2

[65] Minkyu Kim, Shengchang Tang, and Bradley D Olsen. Physics of engineered protein hydrogels. *Journal of Polymer Science Part B: Polymer Physics*, 51(7):587–601, 2013. 3.2

[66] Bostjan Kobe and Andrey V Kajava. The leucine-rich repeat as a protein recognition motif. *Current opinion in structural biology*, 11(6):725–732, 2001. 1.2

[67] Andreas Kohl, H Kaspar Binz, Patrik Forrer, Michael T Stumpp, Andreas Plückthun, and Markus G Grütter. Designed to be stable: crystal structure of a consensus ankyrin repeat protein. *Proceedings of the National Academy of Sciences*, 100(4):1700–1705, 2003. 1.2

[68] Jindřich Kopeček. Hydrogel biomaterials: a smart future? *Biomaterials*, 28(34):5185–5192, 2007. 2.2

[69] Piyush Koria, Hiroshi Yagi, Yuko Kitagawa, Zaki Megeed, Yaakov Nahmias, Robert Sheridan, and Martin L Yarmush. Self-assembling elastin-like peptides growth factor chimeric nanoparticles for the treatment of chronic wounds. *Proceedings of the National Academy of Sciences*, 108(3):1034–1039, 2011. 1.2

[70] Ashok Kumar, Per-Olof Wahlund, Cecilia Kepka, Igor Yu Galaev, and Bo Mattiasson. Purification of histidine-tagged single-chain fv-antibody fragments by metal chelate affinity precipitation using thermoresponsive copolymers. *Biotechnology and bioengineering*, 84(4):494–503, 2003. 4.2

[71] Kuen Yong Lee and David J Mooney. Hydrogels for tissue engineering. *Chemical reviews*, 101(7):1869–1880, 2001. 2.2

[72] Hauke Lilie, Wolfgang Haehnel, Rainer Rudolph, and Ulrich Baumann. Folding of a synthetic parallel β-roll protein. *FEBS letters*, 470(2):173–177, 2000. 1.5, 4.2, 4.4

[73] Irena Linhartová, Ladislav Bumba, Jiří Mašín, Marek Basler, Radim Osička, Jana Kamanová, Kateřina Procházková, Irena Adkins, Jana Hejnová-Holubová, Lenka Sadílková, et al. Rtx proteins: a highly diverse family secreted by a common mechanism. *FEMS microbiology reviews*, 34(6):1076–1112, 2010. 1.3

[74] John Löfblom. Bacterial display in combinatorial protein engineering. *Biotechnology journal*, 6(9):1115–1129, 2011. 5.2.1

[75] John Löfblom, Fredrik Y Frejd, and Stefan Ståhl. Non-immunoglobulin based protein scaffolds. *Current opinion in biotechnology*, 22(6):843–848, 2011. 1.1, 5.2

[76] Hoang D Lu, Ian R Wheeldon, and Scott Banta. Catalytic biomaterials: engineering organophosphate hydrolase to form self-assembling enzymatic hydrogels. *Protein Engineering Design and Selection*, 23(7):559–566, 2010. 2.2

[77] Sarah R MacEwan and Ashutosh Chilkoti. Elastin-like polypeptides: Biomedical applications of tunable biopolymers. *Peptide Science*, 94(1):60–77, 2010. 1.2

[78] E. R. Main, Y. Xiong, M.J. Cocco, L. D'Andrea, and L. Regan. Design of stable alpha-helical arrays from an idealized tpr motif. *Structure*, 11(5):497–508, 2003. 1.2, 4.2

[79] Michael S Marlow, Jakob Dogan, Kendra K Frederick, Kathleen G Valentine, and A Joshua Wand. The role of conformational entropy in molecular recognition by calmodulin. *Nature chemical biology*, 6(5):352–358, 2010. 5.5

[80] TG Mason, K Ganesan, JH Van Zanten, D Wirtz, and SC Kuo. Particle tracking microrheology of complex fluids. *Physical Review Letters*, 79(17):3282, 1997. 2.3.10

[81] Thomas G Mason and DA Weitz. Optical measurements of frequency-dependent linear viscoelastic moduli of complex fluids. *Physical review letters*, 74(7):1250, 1995. 2.3.10, 2.4.3

[82] Jonathan R McDaniel, J Andrew MacKay, Felipe García Quiroz, and Ashutosh Chilkoti. Recursive directional ligation by plasmid reconstruction allows rapid and seamless cloning of oligomeric genes. *Biomacromolecules*, 11(4):944–952, 2010. 4.3.2

[83] David T McPherson, Jie Xu, and Dan W Urry. Product purification by reversible phase transition following¡ i¿ escherichia coli¡/i¿ expression of genes encoding up to 251 repeats of the elastomeric pentapeptide gvgvp. *Protein expression and purification*, 7(1):51–57, 1996. 4.2

[84] Dan E Meyer and Ashutosh Chilkoti. Purification of recombinant proteins by fusion with thermally-responsive polypeptides. *Nature biotechnology*, 17(11):1112–1115, 1999. 4.2

[85] Dan E Meyer and Ashutosh Chilkoti. Genetically encoded synthesis of protein-based polymers with precisely specified molecular weight and sequence by recursive directional ligation: examples from the elastin-like polypeptide system. *Biomacromolecules*, 3(2):357–367, 2002. 4.3.2

[86] Leila K Mosavi, Tobin J Cammett, Daniel C Desrosiers, and Zheng-yu Peng. The ankyrin repeat as molecular architecture for protein recognition. *Protein Science*, 13(6):1435–1448, 2004. 4.2

[87] Dana L Nettles, Kenichi Kitaoka, Neil A Hanson, Charlene M Flahiff, Brian A Mata, Edward W Hsu, Ashutosh Chilkoti, and Lori A Setton. In situ crosslinking elastin-like polypeptide gels for application to articular cartilage repair in a goat osteochondral defect model. *Tissue Engineering Part A*, 14(7):1133–1140, 2008. 2.2

[88] Stewart D Nuttall and Renae B Walsh. Display scaffolds: protein engineering for novel therapeutics. *Current opinion in pharmacology*, 8(5):609–615, 2008. 1.1, 5.2

[89] Zeev Pancer and Max D Cooper. The evolution of adaptive immunity. *Annu. Rev. Immunol.*, 24:497–518, 2006. 1.2

[90] Zeev Pancer, Nil Ratan Saha, Jun Kasamatsu, Takashi Suzuki, Chris T Amemiya, Masanori Kasahara, and Max D Cooper. Variable lymphocyte receptors in hagfish. *Proceedings of the National Academy of Sciences of the United States of America*, 102(26):9224–9229, 2005. 1.2

[91] Fabio Parmeggiani, Riccardo Pellarin, Anders Peter Larsen, Gautham Varadamsetty, Michael T Stumpp, Oliver Zerbe, Amedeo Caflisch, and Andreas Plückthun. Designed armadillo repeat proteins as general peptide-binding scaffolds: consensus design and computational optimization of the hydrophobic core. *Journal of molecular biology*, 376(5):1282–1304, 2008. 4.2

[92] Ana-Cristina Sotomayor Pérez, Johanna C Karst, Marilyne Davi, J Iñaki Guijarro, Daniel Ladant, and Alexandre Chenal. Characterization of the regions involved in the calcium-induced folding of the intrinsically disordered rtx motifs from the¡ i¿ bordetella pertussis¡/i¿ adenylate cyclase toxin. *Journal of molecular biology*, 397(2):534–549, 2010. 1.3

[93] Andreas Plückthun. Ribosome display: a perspective. In *Ribosome Display and Related Technologies*, pages 3–28. Springer, 2012. 5.2.2, 5.3.3, 5.5

[94] Todd M Przybycien, Narahari S Pujar, and Landon M Steele. Alternative bioseparation operations: life beyond packed-bed chromatography. *Current opinion in biotechnology*, 15(5):469–478, 2004. 4.2

[95] Huan Qi, Haiqin Lu, Hua-Ji Qiu, Valery Petrenko, and Aihua Liu. Phagemid vectors for phage display: properties, characteristics and construction. *Journal of molecular biology*, 417(3):129–143, 2012. 5.2.1

[96] Yong Qiu and Kinam Park. Environment-sensitive hydrogels for drug delivery. *Advanced drug delivery reviews*, 53(3):321–339, 2001. 2.2

[97] Jasna Rakonjac. Filamentous bacteriophages: Biology and applications. *eLS*, 2011. 5.2.1

[98] J.S. Richardson and D.C. Richardson. Natural beta-sheet proteins use negative design to avoid edge-to-edge aggregation. *Proceedings of the National Academy of Sciences of the United States of America*, 99(5):2754–2759, 2002. 4.4

[99] Philippe Ringler and Georg E Schulz. Self-assembly of proteins into designed networks. *Science*, 302(5642):106–109, 2003. 4.2

[100] Theo Rispens, Pleuni Ooijevaar-de Heer, Ninotska IL Derksen, Gertjan Wolbink, Pauline A van Schouwenburg, Simone Kruithof, and Rob C Aalberse. Nanomolar to sub-picomolar affinity measurements of antibody–antigen interactions and protein multimerizations: Fluorescence-assisted high-performance liquid chromatography. *Analytical biochemistry*, 437(2):118–122, 2013. 5.2

[101] Andrew J Scotter, Meng Guo, Melanie M Tomczak, Margaret E Daley, Robert L Campbell, Richard J Oko, David A Bateman, Avijit Chakrabartty, Brian D Sykes, and Peter L Davies. Metal ion-dependent, reversible, protein filament formation by designed beta-roll polypeptides. *BMC structural biology*, 7(1):63, 2007. 1.5, 4.2, 4.4

[102] Wei Shen, Rob GH Lammertink, Jill K Sakata, Julia A Kornfield, and David A Tirrell. Assembly of an artificial protein hydrogel through leucine zipper aggregation and disulfide bond formation. *Macromolecules*, 38(9):3909–3916, 2005. 2.2, 2.3.2, 3.2, 3.3.2

[103] Wei Shen, Kechun Zhang, Julia A Kornfield, and David A Tirrell. Tuning the erosion rate of artificial protein hydrogels through control of network topology. *Nature materials*, 5(2):153–158, 2006. 2.2, 3.2

[104] Oren Shur and Scott Banta. Rearranging and concatenating a native rtx domain to understand sequence modularity. *Protein Engineering Design and Selection*, pages 1–10, 2012. 1.4, 4.4, 6.1.1

[105] Oren Shur, Jun Wu, Donald M Cropek, and Scott Banta. Monitoring the conformational changes of an intrinsically disordered peptide using a quartz crystal microbalance. *Protein Science*, 20(5):925–930, 2011. 1.4, 2.2, 5.5, 6.1.1

[106] Roland J Siezen, William M de Vos, Jack AM Leunissen, and Bauke W Dijkstra. Homology modelling and protein engineering strategy of subtilases, the family of subtilisin-like serine proteinases. *Protein Engineering*, 4(7):719–737, 1991. 1.1

[107] Arne Skerra. Alternative non-antibody scaffolds for molecular recognition. *Current opinion in biotechnology*, 18(4):295–304, 2007. 1.1, 5.2

[108] Ana-Cristina Sotomayor-Pe?rez, Orso Subrini, Audrey Hessel, Daniel Ladant, and Alexandre Chenal. Molecular crowding stabilizes both the intrinsically disordered calcium-free state and the folded calcium-bound state of a repeat in toxin (rtx) protein. *Journal of the American Chemical Society*, 135(32):11929–11934, 2013. 1.3

[109] Michael T Stumpp, Patrik Forrer, H Kaspar Binz, and Andreas Plückthun. Designing repeat proteins: modular leucine-rich repeat protein libraries based on the mammalian ribonuclease inhibitor family. *Journal of molecular biology*, 332(2):471–487, 2003. 1.2

[110] Zhijie Sui, William J King, and William L Murphy. Protein-based hydrogels with tunable dynamic responses. *Advanced Functional Materials*, 18(12):1824–1831, 2008. 3.2

[111] Géza R Szilvay, Mark A Blenner, Oren Shur, Donald M Cropek, and Scott Banta. A fret-based method for probing the conformational behavior of an intrinsically disordered repeat domain from bordetella pertussis adenylate cyclase. *Biochemistry*, 48(47):11273–11282, 2009. 1.4, 2.2, 3.2, 4.4, 6.1.1

[112] Reiji Takashi, Yuji Tonomura, and Manuel F Morales. 4, 4'-bis (1-anilinonaphthalene 8-sulfonate)(bis-ans): a new probe of the active site of myosin. *Proceedings of the National Academy of Sciences*, 74(6):2334–2338, 1977. 2.4.1

[113] Tsutomu Tanaka, Ryosuke Yamada, Chiaki Ogino, and Akihiko Kondo. Recent developments in yeast cell surface display toward extended applications in biotechnology. *Applied microbiology and biotechnology*, 95(3):577–591, 2012. 5.2.1

[114] Nancy E Thompson, Katherine M Foley, Elizabeth S Stalder, and Richard R Burgess. Identification, production, and use of polyol-responsive monoclonal antibodies for immunoaffinity chromatography. *Methods in enzymology*, 463:475–494, 2009. 5.2

[115] Shana Topp, V Prasad, Gianguido C Cianci, Eric R Weeks, and Justin P Gallivan. A genetic toolbox for creating reversible ca2+-sensitive materials. *Journal of the American Chemical Society*, 128(43):13994–13995, 2006. 2.2

[116] Michael W Traxlmayr and Christian Obinger. Directed evolution of proteins for increased stability and expression using yeast display. *Archives of biochemistry and biophysics*, 526(2):174–180, 2012. 5.2.1

[117] Kevin M Ulmer. Protein engineering. *Science*, 219(4585):666–671, 1983. 1.1

[118] Agathe Urvoas, Asma Guellouz, Marie Valerio-Lepiniec, Marc Graille, Dominique Durand, Danielle C Desravines, Herman van Tilbeurgh, Michel Desmadril, and Philippe Minard. Design, production and molecular structure of a new family of artificial alpha-helicoidal repeat proteins (αrep) based on thermostable heat-like repeats. *Journal of molecular biology*, 404(2):307–327, 2010. 1.2

[119] Ian Wheeldon. Protein engineering strategies for modular, responsive, and spatially organized biomaterials. *Tissue and Organ Regeneration: Advances in Micro-and Nanotechnology*, page 265, 2014. 3.2

[120] Ian R Wheeldon, Scott Calabrese Barton, and Scott Banta. Bioactive proteinaceous hydrogels from designed bifunctional building blocks. *Biomacromolecules*, 8(10):2990–2994, 2007. 2.2, 2.3.9

[121] Ian R Wheeldon, Joshua W Gallaway, Scott Calabrese Barton, and Scott Banta. Bioelectrocatalytic hydrogels from electron-conducting metallopolypeptides coassembled with bifunctional enzymatic building blocks. *Proceedings of the National Academy of Sciences*, 105(40):15275–15280, 2008. 2.2

[122] Thomas Wiseman, Samuel Williston, John F Brandts, and Lung-Nan Lin. Rapid measurement of binding constants and heats of binding using a new titration calorimeter. *Analytical biochemistry*, 179(1):131–137, 1989. 5.4.3

[123] David W Wood, Wei Wu, Georges Belfort, Victoria Derbyshire, and Marlene Belfort. A genetic system yields self-cleaving inteins for bioseparations. *Nature biotechnology*, 17(9):889–892, 1999. 4.2

[124] Jun Wu, Donald M Cropek, Alan C West, and Scott Banta. Development of a troponin i biosensor using a peptide obtained through phage display. *Analytical chemistry*, 82(19):8235–8243, 2010. 1.4

[125] Jun Wu, Jong Pil Park, Kevin Dooley, Donald M Cropek, Alan C West, and Scott Banta. Rapid development of new protein biosensors utilizing peptides obtained via phage display. *PloS one*, 6(10):e24948, 2011. 1.4

[126] T Wurch, P Lowe, V Caussanel, C Bes, A Beck, and N Corvaia. Development of novel protein scaffolds as alternatives to whole antibodies for imaging and therapy: status on discovery research and clinical validation. *Current pharmaceutical biotechnology*, 9(6):502–509, 2008. 5.2

[127] Thierry Wurch, Alain Pierré, and Stéphane Depil. Novel protein scaffolds as emerging therapeutic proteins: from discovery to clinical proof-of-concept. *Trends in biotechnology*, 30(11):575–582, 2012. 5.2

[128] Chunyu Xu, Victor Breedveld, and Jindrich Kopecek. Reversible hydrogels from self-assembling genetically engineered protein block copolymers. *Biomacromolecules*, 6(3):1739–1749, 2005. 2.2, 2.2, 2.3.10, 2.4.3, 3.2, 3.2

[129] Tetsuji Yamaoka, Takumi Tamura, Yuuki Seto, Tomoko Tada, Shigeru Kunugi, and David A Tirrell. Mechanism for the phase transition of a genetically engineered elastin model peptide (vpgig) 40 in aqueous solution. *Biomacromolecules*, 4(6):1680–1685, 2003. 4.2

[130] Wei Yang, Lisa M Jones, Leanne Isley, Yiming Ye, Hsiau-Wei Lee, Anna Wilkins, Zhi-ren Liu, Homme W Hellinga, Russell Malchow, Mohammed Ghazi, et al. Rational design of a calcium-binding protein. *Journal of the American Chemical Society*, 125(20):6165–6171, 2003. 2.4.1

[131] Christian Zahnd, Emanuel Wyler, Jochen M Schwenk, Daniel Steiner, Michael C Lawrence, Neil M McKern, Frédéric Pecorari, Colin W Ward, Thomas O Joos, and Andreas Plückthun. A designed ankyrin repeat protein evolved to picomolar affinity to her2. *Journal of molecular biology*, 369(4):1015–1028, 2007. 1.2

Appendix A

RTX Ribosome Display

A.1 Introduction

Ribosome display is a proven *in vitro* selection technique that is commonly used to evolve new high-affinity protein binders. Engineered antibody fragments as well as other alternative protein scaffolds, including designed ankyrin repeat proteins (DARPins), have been successfully evolved. This protocol aims to outline the necessary steps to obtain a high-affinity RTX binding domain using this technology.

A.2 Materials

A.2.1 General

- 96-well streptavidin coated plates, pre-blocked (Pierce 15501)
- RNeasy RNA purification mini kit (QIAGEN 74104)
- QIAquick PCR purification kit (QIAGEN 28104)
- RNaseZAP (Sigma R2020-250ML)
- MEGAScript T7 in vitro transcription kit (Life Technologies AM1334)
- Sterilized pipette tips and centrifuge tubes

A.2.2 Buffers

- TBS - 50 mM Tris, 150 mM NaCl pH 7.5 sterile filtered
- TBST - 50 mM Tris, 150 mM NaCl, 0.05% (v/v) Tween 20 pH 7.5 sterile filtered

- WBT - 50 mM Tris acetate, 150 mM NaCl, 50 mM magnesium, 0.05% (v/v) Tween 20 pH 7.5 sterile filtered
- WB-BSA - 50 mM Tris acetate, 150 mM NaCl, 50 mM magnesium, 0.5% (w/v) BSA pH 7.5
- EB - 50 mM Tris acetate, 150 mM NaCl, 25 mM EDTA pH 7.5 sterile filtered
- *Saccharomyces cerevisiae* RNA (Sigma R6750-100MG), 25 µg/µL in H_2O. Aliquot and store at -20C
- 200 mg/mL heparin in H_2O, store 20 µL aliquots at -20C, do not filter
- 2M $CaCl_2$ in TBS
- 2M $MgCl_2$ in TBS

A.2.3 Library Oligonucleotides and Primers

Swiss9 Library F

5'-TCGCGGCCCAGCCGGCCATGGCGGGTTCTGCACGCGACGATGTGCTGA-
TCGGCGACGCGGGTGCGAATNNKCTGNNKGGCCTGGCTGGTAACGACGT-
CTTGTCTGGTGGTGCGGGCGATGATNNKCTGNNKGGTGACGAGGGCTCC-
GATCTGCTGAGCGGTGATGCCGGCAACGAC-3'

Swiss9 Library R

5'-TTCGGCCCCCGAGGCCCCGCCACGGATCGTGTCATGGCCACCACCGGAC-
TCMNNAATMNNGTCGTGACCATAACCAACACCGAACAGGTAGGTATCGTC-

GCCCTGACCGCCMNNCAAMNNGTCGTTGCCGGCATCACCGCTCAGCAGAT-
CGGAGCCCTCGTCACC-3’

Swiss9 pRDV F (BamHI)

5’-AATAATGGATCCGGTTCTGCACGCGACGATGTGC-3’

Swiss9 pRDV R (HindIII)

5’-TAATAAAAGCTTGTCCGGATACTGCGCCATTGCCTC-3’

β-roll/Cap Overlap F

5’-GTGGCCATGACACGATCCGTATCAACGCGGGGGCGGACCA-3’

β-roll/Cap Overlap R

5’-TGGTCCGCCCCCGCGTTGATACGGATCGTGTCATGGCCAC-3’

T7B

5’-ATACGAAATTAATACGACTCACTATAGGGAGACCACAACGG-3’

tolAK

5’-CCGCACACCAGTAAGGTGTGCGGTTTCAGTTGCCGCTTTCTTTCT-3’

Anti-ssRA

5’-TTAAGCTGCTAAAGCGTAGTTTTCGTCGTTTGCGACTA-3’

Swiss9 pMAL F (KpnI)

5'-AATAATGGTACCGGGTTCTGCACGCGACGATGTGC-3'

Swiss9 pMAL R (HindIII)

5'-TAATAAAAGCTTTTAGTCCGGATACTGCGCCATTGCC-3'

A.3 Ribosome Display Cycle

A.3.1 Library Construction

The β-roll library is constructed by annealing and extending the library oligonucleotides Swiss9 Library F and Swiss9 Library R. Since the library oligonucleotides are so large, touchdown PCR is used to avoid any non-specific annealing. Prepare reactions on ice and add components in the following order:

Volume	*Component*
36 µL	H_2O
10 µL	HF Buffer
1 µL	Swiss9 Library F
1 µL	Swiss9 Library R
1 µL	dNTPs
1 µL	Phusion

and use the following PCR protocol:

PCR Conditions		
98C	Hold	
98C	5:00	
98C	0:15	x7
72C*	0:20	x7
72C	1:30	
4C	Hold	

*Annealing temperature is decreased by 2C each cycle until 60C is reached.

Run 5µL of this product on an agarose gel. The gel may appear smeared, but there should be a bright band around 250bp. Pool all reactions and purify using the QIAGEN PCR cleanup kit. The C-terminal capping group can now be added by overlap extension PCR. Prepare reactions on ice and add components in the following order:

Library

Volume	*Component*
35 µL	H_2O
10 µL	HF Buffer
1 µL	Swiss9 pRDV F (BamHI)
1 µL	β-roll/Cap Overlap R
1 µL	dNTPs
1 µL	Swiss9 Library
1 µL	Phusion

C-terminal Cap

Volume	*Component*
35 µL	H_2O
10 µL	HF Buffer
1 µL	β-roll/Cap Overlap F
1 µL	Swiss9 pRDV R (HindIII)
1 µL	dNTPs
1 µL	pMAL-WTβ-roll*
1 µL	Phusion

*Any construct containing the C-terminal cap can be used as template here.

The same PCR conditions can be used to amplify both the library and the C-terminal capping group. The primers have been designed with a Tm of 69C enabling the use of two-step PCR.

PCR Conditions		
98C	Hold	
98C	2:00	
98C	0:15	x30
72C	0:05	x30
72C	4:00	
4C	Hold	

The resulting gels are shown below with the library on the left and the C-terminal cap on the right.

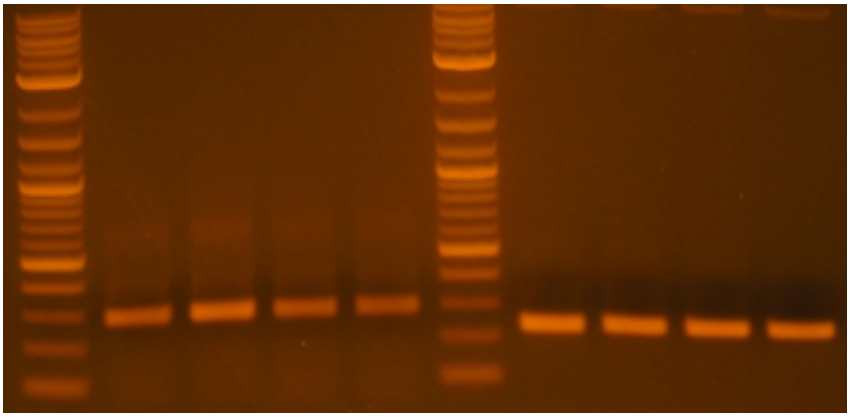

All library and C-terminal cap reactions should be pooled and purified separately. The library and C-terminal cap are now prepared to be fused by overlap extension PCR. Prepare reactions on ice and add components in the following order:

Volume	*Component*
34 µL	H_2O
10 µL	HF Buffer
1 µL	Swiss9 pRDV F (BamHI)
1 µL	Swiss9 pRDV R (HindIII)
1 µL	Swiss9 Library OE
1 µL	C-terminal Cap OE
1 µL	dNTPs
1 µL	Phusion

PCR	*Conditions*	
98C	Hold	
98C	2:00	
98C	0:15	x30
72C	0:08	x30
72C	4:00	
4C	Hold	

Capped Swiss9 Library

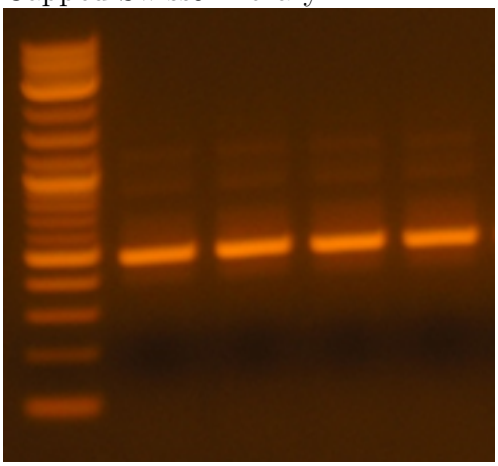

Pool all reactions and purify using the QIAGEN PCR cleanup kit. If there are multiple non-specific bands, use the QIAGEN gel extraction kit instead. The library is now prepared for cloning into pRDV. Digest both the library and pRDV with BamHI-HF and HindIII-HF using the following procedure:

Digestion	*Conditions*
42 µL	DNA
5 µL	Cut Smart Buffer
1.5 µL	BamHI
1.5 µL	HindIII

Mix well by pipetting up and down and incubate at 37C for 1 h. For the digested library, remove enzymes and DNA fragments by purifying on the QIAGEN PCR cleanup kit. Elute the cleaned DNA into 30 µL of H_2O. Run the entire pRDV digestion on an 80 mL agarose gel. Excise the digested vector backbone and purify using the QIAGEN gel extraction kit. Combine 2 lanes of digested vector on a single spin column and elute in 50 µL of H_2O.

Digested pRDV

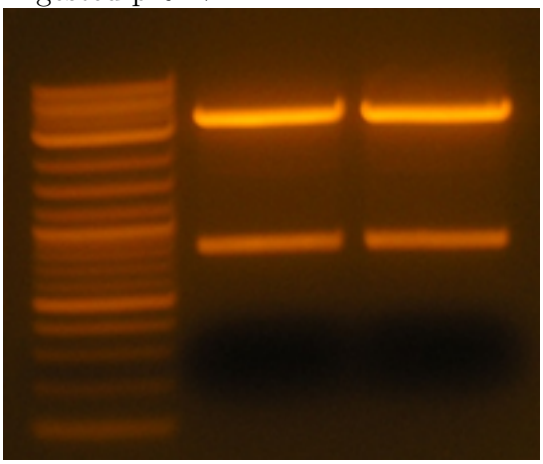

The digested vector and library are now ready to be ligated. For the initial library ligation, several ratios should be investigated. For later rounds of cloning after selections, only the most efficient ratio should be used (5:1 worked the best for lysozyme work). Incubate the ligation reactions at 16C for 16-24 hours. Clean up the ligation reactions using the QIAGEN PCR clean up kit and elute into 10 µL of water. Transform 0.8 µL of the ligation reaction into 25 µL of 5α electrocompetent cells. Plate 100 µL of the transformants on LB-AMP plates and pick several colonies for sequencing analysis to ensure the library is intact.

A.3.2 Preparing DNA for *in vitro* Transcription

Once the library has been successfully ligated into pRDV, the DNA required for in vitro translation can be amplified directly off of the ligation reactions. Prepare reactions on ice and add components in the following order:

Volume	*Component*
35 µL	H_2O
10 µL	HF Buffer
1 µL	T7B
1 µL	tolAK
1 µL	dNTPs
1 µL	pRDV-Swiss9 Ligation
1 µL	Phusion

PCR	*Conditions*	
98C	Hold	
98C	2:00	
98C	0:15	x30
65C	0:15	x30
72C	0:20	x30
72C	5:00	
4C	Hold	

T7B/tolAK PCR

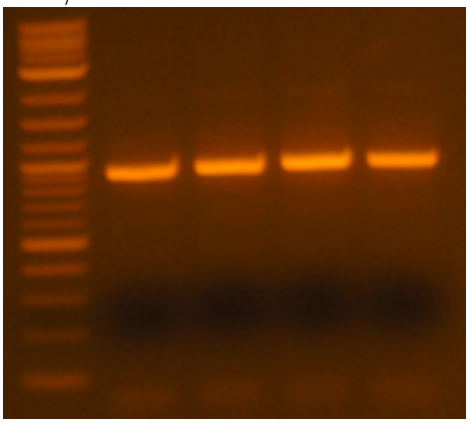

Pool all reactions and purify on the QIAGEN PCR cleanup kit. Record the concentration by A_{260}. This will be used as the template DNA for in vitro transcription. Excess DNA can be stored at -20C indefinitely.

A.3.3 *In vitro* Transcription

Care needs to be taken when handling RNA. It is very temperamental and degrades very easily. Spray all pipettes and bench space down with RNaseZAP. Wear gloves at all times when handling reagents, pipettes, and tubes. Remove the MEGAscript T7 transcription kit from the -20C and keep the enzyme mix on ice. Vortex the ribonucleotides and reaction buffer until they are completely in solution. Briefly centrifuge all reagents before opening them. Keep the 10X reaction buffer at room temperature. Assemble the reaction at room temperature, **not on ice**. The 10X reaction buffer can co-precipitate the template DNA if the reaction is assembled on ice. Prepare the reactions in the following order:

Volume	*Component*
to 20 µL	Nuclease-free H_2O
2 µL	ATP
2 µL	CTP
2 µL	GTP
2 µL	UTP
2 µL	10X Reaction Buffer
0.1 µg	PCR product
2 µL	Enzyme Mix

For convenience, mix all ribonucleotides together first, and add 8 µL if setting up more than one reaction. Gently flick the tube to mix the reagents and briefly centrifuge to collect the reaction mixture at the bottom of the tube. Incubate the reaction mix at 37C for 4.5 hours. Both the transcription time and amount of PCR product have been optimized for the Swiss9 library.

After 4.5 hours, the reaction should be complete. Use the QIAGEN RNeasy RNA

purification mini kit to isolate the mRNA. The on-column DNase digestion is not necessary. Elute once with 50 µL of RNase free H_2O. Use the A_{260} measurement to estimate the RNA concentration.

A_{260} x dilution factor x 40 = µg/mL RNA

Typically yields are approximately 2.5-3 µg/µL. 10 µg are required for *in vitro* translation. Transcriptional efficiency can also be evaluated by gel electrophoresis. On a 1% TBE agarose gel, load approximately 1 µg of RNA mixed with an equal volume of Gel Loading Buffer II. Be sure to denature the mRNA prior to loading. Incubate the mRNA with the loading buffer at 80-90C for 3-5 minutes. Run the gel under standard conditions (150 V, 25 minutes). Save transcribed mRNA for future use at -80C

A.3.4 *In vitro* Translation

The purified mRNA from the previous section will be used as template for the *in vitro* translation reaction. Prepare reactions on ice and add components in the following order:

Volume	*Component*	*Stock Conc.*	*Final Conc.*
to 110 µL	Nuclease-free H_2O	-	-
24 µL	mRNA	2.5 µg/µL	10 µg
50 µL	S12 Extract	-	-
41 µL	Translational Premix	-	-
3.3 µL	Anti-ssRA Oligo	100 µM	3 µM

If the mRNA concentration is below 2.5 µg/µL, up to 15.7 µL can be added. Compensate by adding less nuclease-free water. Mix carefully in the tube by pipetting up and down. Incubate at 37C for 12.5 minutes. Stop the reactions by transferring 100

µL of the reaction into 400 µL of ice-cold WBT containing 0.5% BSA and 12.5 µL/mL heparin (200 mg/mL stock). Place the stopped reaction on ice for 1-2 minutes. Centrifuge for 5 minutes at 14,000 x g at 4C and transfer to an ice-cold tube. Use 150 µL of this translated mix for the selection experiments. Discard the remaining solution.

A.3.5 Target Immobilization

The most efficient way to complete rounds of selections is against an immobilized target. Biotinylated targets can easily be immobilized on streptavidin coated plates. Kits are available to chemically biotinylate a protein of interest (Pierce 21338). Alternatively, and more conveniently, biotinylated targets may be available directly from vendors (Lysozyme – GeneTex GTX82960, GST – Perkin Elmer 6760305M).

Wash a streptavidin coated plate with ice cold TBST once. Add a molar excess of biotinylated target (usually 100 µL of 100-200 µM solution) in TBST to the pre-blocked plate. Two wells will be needed per round of selection (folded/unfolded). Cover with parafilm and allow the target to incubate for 1 h at 4C on an orbital shaker. Wash the wells three times with ice cold TBST, slapping the wells face-down each time on a paper towel. Wash once with ice cold WBT and do not remove until the ternary complexes are ready to be added for selection.

A.3.6 Selection

Add 150 µL of the translated mix to the wells containing the immobilized target. Add 1.9 µL of 2 M $CaCl_2$ or $MgCl_2$ to the well to a final concentration of 25 mM for folded and unfolded selections, respectively. *Gently* pipette up and down to mix. Cover the wells with parafilm and incubate for 1 h at 4C on an orbital shaker.

A.3.7 Washing

After an h of binding, non-specifically bound clones must be washed off. Wells should be washed with 300 µL ice cold WBT containing 0.1% BSA, slapping the well face-down on a clean paper towel each time. For initial rounds of selection, fewer washes should be used (1-3 washes). The stringency should be increased for later rounds of selection (5-10 washes). Off-rate selections can also be used by simply incubating with WBT for 5-10 minutes on an orbital shaker instead of immediately removing the buffer. The Tween 20 percentage can also be increased for more stringent washes.

A.3.8 Elution

After the final wash, the bound complexes can be eluted by simply adding a chelator. This will cause the ribosomes to dissociate and release the captured mRNA. To each well, add 100 µL EB (containing 25 mM EDTA) and let stand for 1-2 minutes. Transfer the eluate to a fresh microcentrifuge tube containing 1 µL of 1mg/mL *S. cerevisiae* RNA solution. Add 100 µL EB a second time to the same well, let sand, and transfer to the same microcentrifuge tube. Additional *S. cerevisiae* RNA is not needed. Incubate the tube on ice for 10 minutes. Purify the recovered mRNA using the QIAGEN RNeasy RNA purification mini kit. Double all required buffer volumes since the starting volume is 200 µL. Elute once into 30 µL of RNase free H_2O. Obtain the RNA concentration at store at -80C.

A.3.9 Reverse Transcription

Once the recovered mRNA has been purified, it must be transcribed back to cDNA for subsequent cloning into pRDV. Prepare the following mixes on ice and add the reagents in the order listed.

Volume	*Component*	*Stock Conc.*	*Final Conc.*
10.3 µL	Recovered mRNA	-	-
2.5 µL	Swiss9 pRDV R (HindIII)	10 µM	2.5 µM

To denature mRNA, heat Mix 1 in the thermocycler to 70C for 5 minutes, then chill on ice for at least 5 minutes.

Volume	*Component*	*Stock Conc.*	*Final Conc.*
4 µL	Reaction Buffer	5x	1x
1.2 µL	$MgCl_2$	25 mM	1.5 mM
1 µL	dNTP Mix	0.5 mM	10 mM
1 µL	Reverse Transciptase	20x	1x

Combine the denatured Mix 1 with Mix 2. Use the following procedure in the thermocycler:

RT Conditions	
25C	Hold
25C	5:00
42C	60:00
4C	Hold

After completion, the reaction can be stored in the -20C. No further treatment/purification is necessary.

A.3.10 Amplifying the cDNA

Once the cDNA is synthesized, it needs to be hybridized and amplified to be cloned back into pRDV. Prepare the following mixes on ice and add the reagents in the order listed.

Volume	*Component*
34 µL	H_2O
10 µL	HF Buffer
1 µL	Swiss9 pRDV F (BamHI)
1 µL	Swiss9 pRDV R (HindIII)
1 µL	dNTPs
1 µL	cDNA
1 µL	Phusion

PCR Conditions		
98C	Hold	
98C	2:00	
98C	0:15	x30
72C	0:08	x30
72C	4:00	
4C	Hold	

PCR from cDNA

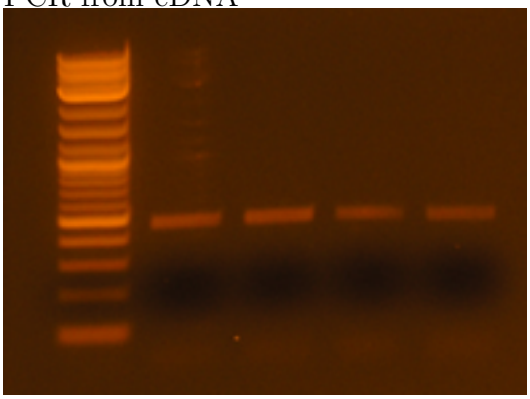

The DNA should be clean and should not require gel extraction, especially in the first few rounds. Clone this DNA back into pRDV as recommended in the previous section.